National Library of Canada
Bibliothèque nationale du Canada

Canadian Theses Service
Service des thèses canadiennes

Ottawa, Canada
K1A 0N4

NOTICE

The quality of this microform is heavily dependent upon the quality of the original thesis submitted for microfilming. Every effort has been made to ensure the highest quality of reproduction possible.

If pages are missing, contact the university which granted the degree.

Some pages may have indistinct print especially if the original pages were typed with a poor typewriter ribbon or if the university sent us an inferior photocopy.

Reproduction in full or in part of this microform is governed by the Canadian Copyright Act, R.S.C. 1970, c. C-30, and subsequent amendments.

AVIS

La qualité de cette microforme dépend grandement de la qualité de la thèse soumise au microfilmage. Nous avons tout fait pour assurer une qualité supérieure de reproduction.

S'il manque des pages, veuillez communiquer avec l'université qui a conféré le grade.

La qualité d'impression de certaines pages peut laisser à désirer, surtout si les pages originales ont été dactylographiées à l'aide d'un ruban usé ou si l'université nous a fait parvenir une photocopie de qualité inférieure.

La reproduction, même partielle, de cette microforme est soumise à la Loi canadienne sur le droit d'auteur, SRC 1970, c. C-30, et ses amendements subséquents.

NL-339 (r. 88/04) c

Canada

NEW DEVELOPMENTS IN THE TRANSMISSION LINE MATRIX AND THE FINITE ELEMENT METHODS FOR NUMERICAL MODELING OF MICROWAVE AND MILLIMETER-WAVE STRUCTURES

by

ESWARAPPA

A Doctoral Dissertation
Submitted to the School of Graduate Studies and Research
of the University of Ottawa
in partial fulfillment of the requirements
for the Degree of

DOCTOR OF PHILOSOPHY

in

Electrical Engineering

Ottawa-Carleton Institute
for Electrical Engineering
Department of Electrical Engineering
University of Ottawa

National Library of Canada
Canadian Theses Service

Ottawa, Canada
K1A 0N4

Bibliothèque nationale du Canada
Service des thèses canadiennes

ISBN 0-315-60109-4

UNIVERSITÉ D'OTTAWA
UNIVERSITY OF OTTAWA

To my mother, to the memory of my father,
and to my uncle and aunt.

I hereby declare that I am the sole author of this thesis. I authorize the University of Ottawa to lend this thesis to other institutions or individuals for the purpose of scholarly research.

Eswarappa

I further authorize the University of Ottawa to reproduce this thesis by photocopying or by other means, in total or in part, at the request of other institutions or individuals for the purpose of scholarly research.

Eswarappa

ACKNOWLEDGEMENTS

It is a pleasure to express the author's sincere gratitude to his supervisors Dr. Wolfgang J. R. Hoefer and Dr. George I. Costache for their constant encouragement and expert guidance throughout this work. It has been an honor and a privilege to work with them.

The author would also like to thank the advisory committee members Dr. M. Ney and Dr. J. Wight for their many useful suggestions and discussions.

The author is indebted to his colleagues Adiseshu Nyshadham and Chris Sibbald who contributed their time and energy to read the manuscript and gave fine and constructive comments.

The author wishes to thank J. Uher for computing the characteristics of the E-plane filter with his mode-matching program.

The author would like to thank all the members of Microwave Group for their help and encouragement. A special note of thanks is due to Ihn Kim for his splendid company.

The author would like to thank Dr. Rajeswari Chattopadhyaya for her encouragement to do Ph.D. The author would also like to thank Management of M/S Indian Telephone Industries Limited, Bangalore for granting me study leave.

The author wishes to acknowledge the financial assistance from the Canadian Commonwealth Scholarship and Fellowship Administration.

Lastly, but by no means least, the author would like to express his sincere thanks to his wife Shaila and his parents. It would not have been possible to finish this long-term work without their support.

ABSTRACT

New and efficient numerical modeling concepts and procedures based on Transmission Line Matrix and Finite Element methods have been developed for the analysis of generalized microwave and millimeter-wave structures.

An algorithm, based on a vectorial Finite Element approach, has been developed to determine the dispersion characteristics, field distributions, pseudo-impedances and, losses of shielded transmission media of arbitrary cross-section. The structures analysed with this algorithm include dielectrically loaded ridged waveguides, bilateral finlines in rectangular and circular waveguide enclosures and ridged finlines. The major contributions to the literature are the estimation of losses of bilateral finlines in rectangular waveguide enclosures, the effect of substrate bending and mounting grooves on the dispersion characteristics, the study of finlines in circular waveguide enclosures, and, the analysis of a new modified finline structure called " Ridged Finline ".

New algorithms to apply the principles of Diakoptics to the TLM method for field partitioning in large structures have been developed. Diakoptics leads to considerable reduction in memory and CPU requirements for large structures since it allows numerical preprocessing of parts of a large electromagnetic structure which remain unchanged during an analysis and optimization procedure. A space interpolation technique based on the transverse field distribution of the propagating mode has been proposed for efficient field partitioning in single-mode structures. Frequency dispersive boundaries are represented in the time domain by their characteristic impulse response or numerical/discrete Green's function. This discrete Green's function has been named the " Johns matrix " in honour of the late P. B. Johns, pioneer of TLM and time domain Diakoptics. The parasitic

reflections from the absorbing boundaries in 3-D structures, due to the finite space and time discretization have been reduced to less than one percent by exponentially tapering the impulse response, or Johns Matrix, of frequency dispersive boundaries. This allows wideband S - parameter extraction of waveguide discontinuities and components from a single impulsive TLM simulation. This tapered impulse response has been named the " Tapered Johns Matrix ".

CONTENTS

ACKNOWLEDGEMENTS ii

ABSTRACT iii

CONTENTS v

LIST OF FIGURES ix

LIST OF TABLES xiv

CHAPTER PAGE

I. INTRODUCTION 1

1.1 Motivation 1

1.2 State of the Art and Original Contributions 5

1.3 Organisation of this Thesis 10

II. PRELIMINARIES 12

2.1 Introduction 12

2.2 Finite Element Method 12

  2.2.1 Quasi-static Problems 13

  2.2.2 Waveguide Problems 18

  2.2.3 Inhomogeneous Waveguide Problems 19

2.3 Transmission Line Matrix Method 20

  2.3.1 The Two-dimensional TLM Models 20

  2.3.2 The Two-dimensional Graded TLM Models 25

  2.3.3 The Three-dimensional TLM Models 29

2.3.4 Applictions of the TLM Method 36

2.4 Discussion 37

III. NUMERICAL MODELING OF TRANSMISSION LINES 38

3.1 Introduction 38

3.2 The Finite Element Analysis 39

3.2.1 Theory 39

3.2.2 Interpolation Functions, Discretization and Global Matrix Formulation 41

3.2.3 Computation of Propagation constant and Field Distribution 42

3.2.4 Spurious Mode Detection 43

3.2.5 Computation of Conductor and Dielectric Losses 44

3.2.6 Computation of Characteristic Impedance 47

3.3 Applications of the Finite Element Method 48

3.3.1 Dielectrically Loaded Ridged Waveguides 48

3.3.2 Bilateral Finlines in Rectangular Waveguide Enclosures 51

3.3.3 Effect of Substrate Bending 57

3.3.4 Bilateral Finlines in Circular Waveguide Enclosures 57

3.3.5 Ridged Bilateral Finlines in Rectangular Waveguide Enclosures 59

3.4 Study of Bilateral Finlines in Rectangular and Circular Waveguide Enclosures with 2D-Graded Mesh TLM Method 68

3.5 Conclusion 68

IV. DIAKOPTICS FOR MICROWAVE STRUCTURES 72

4.1 Introduction 72

4.2 Steady-state Solution using Diakoptics 73
4.3 Segmentation for Planar Circuits 77
4.4 Time Domain Diakoptics for 2-D TLM Method 78
  4.4.1 Computation of the Numerical Green's Function of S_{super} 79
  4.4.2 Analysis of the Overall Structure by Discretizing only the Structure S_{sub} and Using the Johns Matrix 82
4.5 Discussion 87
V. 2-D TLM MODELING OF DISPERSIVE WIDEBAND ABSORBING BOUNDARIES WITH TIME DOMAIN DIAKOPTICS 89
5.1 Introduction 89
5.2 TEM Absorbing Boundaries 90
5.3 Narrow-band Non-TEM absorbing Boundaries 92
5.4 Wideband Absorbing Boundaries 93
  5.4.1 Modeling of a Waveguide Termination with Gradually Increasing Losses 95
  5.4.2 Modeling of a Very Long Uniform Waveguide Section 100
  5.4.3 Implementation of Wideband Absorbing Boundary Conditions with Time Domain Diakoptics approach 102
5.5 Extraction of Scattering Parameters 104
5.6 Applications 106
  5.6.1 Inductive Waveguide Iris Discontinuity 106
  5.6.2 E-Plane Filter 109
  5.6.3 Iris-Coupled Waveguide Bandpass Filter 109
5.7 Conclusions 112

VI. DIAKOPTICS AND WIDEBAND ABSORBING BOUNDARIES IN THE 3-D TLM METHOD WITH SYMMETRICAL CONDENSED NODES 113

6.1 Introduction 113

6.2 Time Domain Diakoptics 114

6.3 Modeling of Absorbing Boundary Conditions 117

6.3.1 Computation of Impulse Response or Johns Matrix of a Long Waveguide .. 119

6.3.2 Convolution with Impulse Response or Johns Matrix 119

6.4 Tapered Impulse Response or Johns Matrix 120

6.5 Conclusions 131

VII. DISCUSSION AND CONCLUSIONS 132

REFERENCES 136

LIST OF FIGURES

FIG. NO. PAGE

2.1 Finite element discretization of a quasi-static structure 14

2.2 Nodes for a second-order triangular element and local (or simplex) coordinates for a point P 14

2.3 a) Junction between transmission lines, b) Equivalent circuit of a transmission line junction, c) Transmission line matrix in x-z plane 22

2.4 Graded mesh (for N = 3) and a unit element by Saguet 26

2.5 3-D expanded TLM node consisting of three shunt and three series connected 2-D nodes 30

2.6 A 3-D node equipped with reactive and dissipative stubs for the modeling of permittivity, permeability and losses 31

2.7 Asymmetrical condensed TLM node by Saguet 32

2.8 Symmetrical condensed TLM node by P. B. Johns 34

3.1 a) Dispersion characteristics of a dielectrically loaded ridge waveguide (dimensions are in millimeters) 49

b) Characteristic impedance and losses of a dielectrically loaded ridge waveguide, $tan\delta = .0002$, $\rho = 3 * 10^{-8}$ Ohm m 50

3.2 Dispersion characteristics of a bilateral finline in rectangular waveguide (WR28) housing. $\epsilon_r = 3.0$, h = 0.125 mm, w = 0.5 mm, — HE1 and HE7 modes for t = 0 and g = 0; .... HE1 and HE7 modes for t = 35 μ m and g = 0; ---HE2 mode for t = 0 and g = 0; -·-HE2 mode for t = 0 and g = 0.5 mm 52

3.3 a) Conductor and dielectric losses as function of gapwidth (w) of a bilateral finline in rectangular waveguide housing (WR28). h = 0.254 mm, $\epsilon_r = 2.22$, $tan\delta = 0.0002$, $\rho = 3 * 10^{-8}$ Ohm m 55

b) Conductor loss per wavelength as function of frequency of a bilateral finline in rectangular waveguide housing (WR28). h = 0.254 mm, $\epsilon_r = 2.22$, $tan\delta = 0.0002$, $\rho = 3 * 10^{-8}$ Ohm m 56

3.4 Dispersion characteristics of a bilateral finline in rectangular waveguide housing (WR28) with bent substrate for different values of deflection d. $\epsilon_r = 3.0$, h = 0.125 mm, w = 0.5 mm 58

3.5 Dispersion characteristics of a bilateral finline in circular waveguide housing (WC 33). a = 4.165 mm, h = 0.254 mm, w = 0.3 mm, $\epsilon_r = 2.2$. — Magnetic wall along YY, Electric wall along XX; --- Electric wall along YY, Magnetic wall along XX; ...... Electric wall along YY, Electric wall along XX; -.- Magnetic wall along YY, Magnetic wall along XX 60

3.6 Electric field lines of the dominant mode and higher order modes at cutoff in a bilateral finline in circular waveguide housing (WC 33). a = 4.165 mm, h = 0.254 mm, w = 0.3 mm, $\epsilon_r = 2.2$. a) Field in the slot region, b) Field in the air region (only one quarter of cross-section shown) 61-64

3.7 Dispersion characteristics of a ridged bilateral finline (dimensions in millimeters) 65

3.8 Electric field lines of the dominant mode at cutoff in a bilateral ridged finline (only the upper right quadrant of the cross-section is shown). a) Enlarged region around the edge, b) Remaining air-filled region 66

3.9 Average power ($Watts/mt^2$) distribution around the fin for the fundamental mode of ridged bilateral finline 67

3.10 Bilateral finlines in rectangular and circular waveguide enclosures 69

4.1 Network substructures connected by removed branches 74

4.2 Segmentation of planar elements 74

4.3 Segmentation of a large network for Diakoptics 80

4.4 a) g(1,1,k) term of Johns Matrix 83

b) g(2,1,k) and g(3,1,k) terms of Johns Matrix 84

4.5 TLM algorithms with and without Diakoptics 86

4.6 Frequency response of a bilateral finline computed using Diakoptics. —w = 0.7112 mm, ... w = 0.8534 mm 88

5.1 Modeling of general boundaries in a 2-D shunt connected TLM mesh 91

5.2 A comparison of the return loss characteristics of absorbing waveguide boundaries obtained by two different methods. ···· termination with wave impedance and 1500 iterations,--- termination with wave impedance and 2500 iterations, — termination with Johns Matrix 94

5.3 a) Modeling of a wideband absorbing waveguide termination by a cascade of nine lossy line sections b) Optimized lengths and dielectric loss tangents for a matched WR28 load (TE_{10}-mode) 96

5.4 Return loss of the lossy waveguide termination. — Simulation using Touchstone, ... Simulation using TLM method 97

5.5 Configuration for computing the discrete numerical Green's function or Johns Matrix of a lossy waveguide matched termination. 101

5.6 Convolution of the Johns Matrices of wideband matched terminations with the impulse response of the circuit 101

5.7 Return loss of back-to-back waveguide absorbing boundaries computed with Diakoptics ..... Lossy waveguide termination, — Long uniform waveguide termination 105

5.8 S-parameters of an inductive iris. — computed with Diakoptics, o □△◇ computed using Marcuvitz's formulas [86] 107

5.9 Electric field variation along the length of a waveguide containing the inductive iris discontinuity at 40 Δl 108

5.10 a) The geometry of a two-section maximum flat E-plane filter. 110

b) Transmission characteristics of a E-plane filter. —|S21| computed with Diakoptics, ...|S21 computed with Diakoptics, △ |S21| computed with mode matching technique, o |S21 computed with mode matching technique 110

5.11 a) The geometry of a four-section waveguide iris-coupled bandpass filter 111

b) A comparison of the return loss and insertion loss characteristics, obtained by lumped element model and Diakoptics, of a waveguide iris-coupled bandpass filter. — Diakoptics, --- Super-Compact 111

6.1 Separation of a large network for diakoptics 115

6.2 Discontinuity in a waveguide section 118

6.3 S-parameter extraction using Diakoptics 118

6.4 Reflection characteristics of absorbing boundaries (WR28) represented by regular and tapered Johns Matrices 121

6.5 S-parameters of an inductive iris computed with regular Johns Matrix absorbing boundaries 122

6.6 S-parameters of an inductive iris computed with tapered Johns Matrix absorbing boundaries 125

6.7 S-parameters of a capacitive iris computed with tapered Johns Matrix absorbing boundaries 126

6.8 The axial strip in a rectangular waveguide 127

6.9 S-parameters of a non-touching axial strip computed with tapered Johns Matrix absorbing boundaries 128

a) Magnitude of S-parameters 128

b) Phase of S-parameters 129

6.10 S-parameters of a metallic post computed with tapered Johns Matrix absorbing boundaries 130

LIST OF TABLES

TABLE NO. PAGE

3.1 Effect of slot height on the guide parameters of dielectrically loaded ridge waveguides (dimensions are defined in Fig. 3.1 (a)). 51

3.2 Losses in homogeneously filled waveguide. a = 10 mm, b = 5 mm, $tan\delta = 2 \times 10^{-4}$, $\rho = 3 \times 10^{-8}$ Ohm m, $\epsilon_r = 1.0$ 54

3.3 Measured losses of bilateral finlines in $WR28$ waveguide enclosures. w = 0.4 mm 54

3.4 Cutoff frequencies of a bilateral finline in rectangular waveguide housing ($WR28$), computed with the TLM method. a = 7.112 mm, $\epsilon_r = 2.2$. (a), (b) : w = h = 0.7112 mm, (c): w = h = 0.688 mm 69

3.5 Comparison of computer run time for different grading ratios (TLM) 69

3.6 Cutoff frequencies of a bilateral finline in circular waveguide housing (WC 33) (TLM) $\epsilon_r = 2.2$, w = h = 1.53 mm 70

3.7 Higher order mode cutoff frequencies of a bilateral finline in circular waveguide housing (WC 33). Comparison between TLM and Finite Element methods 70

Chapter I

INTRODUCTION

1.1 MOTIVATION

Numerical models for microwave structures consisting of various transmission media and their discontinuities are needed for computer simulation of circuits in communication systems. The most commonly used transmission media at microwave and millimeter-wave frequencies are waveguides, microstrip lines, coplanar lines, slot lines, finlines, and various forms of dielectric waveguides. The parameters which characterize these transmission lines are the propagation constant, the characteristic impedance, the conductor and dielectric losses, the power handling capacity and the monomode bandwidth. Discontinuities in the transmission lines are characterized by their scattering parameters.

In the past, various analytical methods such as Green's function techniques [1]-[5], Conformal mapping [6]-[7], Variational methods [8]-[9], Fourier transform method [10], Fourier integral method [11], Spectral domain method [12]-[14], and Mode matching techniques [15]-[19] have been used to obtain the above design data. However, these methods cannot be applied to transmission lines and discontinuities of arbitrary cross-section. Furthermore, the realistic features such as finite metallization thickness, substrate mounting grooves, irregularities in the structures caused during manufacturing, etc., cannot be easily accounted for. Many planar integrated circuits are not easily amenable to closed form analytical expressions because of the associated singularities. Moreover in the case of microwave and millimeter-wave monolithic integrated circuits, it is very difficult and almost impossible to adjust the circuit characteristics once they are fabricated. Therefore, very accurate characterization numerical techniques are essential to model the structures.

Numerical techniques such as the Finite Element Method [20]-[21], the Moment Method [22], the Boundary Element Method [23]-[24], the Finite-Difference Frequency-Domain (FD-FD) Method [25]-[26], the Transmission Line Matrix (TLM) Method [27]-[30], and the Finite-Difference Time-Domain (FD-TD) Method [31]-[32] have evolved in the last two decades. Recent advances in modeling concepts and computer technology have expanded the scope, accuracy and speed of these methods. Generalized programs based on these techniques can be applied to design novel structures with the desired electrical characteristics, or to study second order effects on their characteristics. These methods are also suitable for lookup table generation for CAD applications [33]. To analyse a specific problem, the most appropriate numerical method should be chosen to obtain accurate results. To do this, awareness of the main advantages and basic limitations of each numerical method is a must.

Some of these methods are more versatile than others (in the sense that, formulation of the method to solve any kind of electromagnetic problem is almost same). For example, in time domain numerical methods such as TLM and FD-TD, the analytical pre-processing is almost negligible, and the basic algorithms are easily modified to solve any kind of electromagnetic problem, either bounded problems (microwave circuits, etc.,) or unbounded problems (Antennas, EMI/EMC problems). Whereas in methods such as Finite Element Method, the functional to be discretized will differ, depending upon the problem (static problems, eigenvalue problems, eddy current problems, etc.,). However, the Finite Element

Method is more versatile when compared to other frequency domain numerical methods such as the Moment Method and the Boundary Element Method.

In this thesis, new procedures and concepts have been developed to overcome the limitations of some existing numerical methods in analyzing microwave and millimeter-wave structures. To characterize uniform transmission lines of any arbitrary cross-section, i.e., to compute cutoff frequencies, dispersion characteristics, characteristic impedances, conductor and dielectric losses, etc., the Finite Element Method has been chosen, while the TLM mehtod has been chosen for computation of scattering parameters of the microwave circuits. The following considerations justify these choices.

In the Finite Element Method, the domain of interest is first divided into subdomains or elements, and the unknown electromagnetic fields are approximated by a linear combination of a complete set of interpolation polynomials (or other functions depending upon the nature of the field) over each element. Then an energy-based functional is minimized, leading to a system of equations. Upon solving this system, the field values at the designated nodes are obtained. Knowing these nodal values, and geometry of the elements, the field values at any other point can be calculated easily and accurately. This means the field, or potential, is defined explicitly everywhere. This simplifies further mathematical manipulation, such as evaluating spatial derivatives and integrals to obtain other fields and field related parameters such as characteristic impedances, conductor and dielectric losses, etc. Often, closed form expressions can be obtained, thus avoiding troublesome numerical integrations and differentiations. This is the main advantage of the Finite Element Method over the TLM and Finite Difference methods. Also altering the density of elements or the order of elements (matching according to the regions of rapid field variation) is easier. However, the time domain methods are also slowly attaining these features with the development of graded mesh schemes and algorithms in curvilinear coordinates [34], [35].

The most serious problem associated with the Finite Element Method is the appearance of so called " spurious modes ", the non-physical solutions. This spurious mode problem coupled with involved 3-D Finite Element formulation and programming, makes this method unsuitable for extraction of scattering parameters of microwave circuits. Moreover, to extract the scattering parameters of a general two port circuit, the Finite Element discretization should be carried out four times with four different pairs of inhomogeneous Dirichlet boundary conditions specified at the input and output reference planes [36]. These reference planes are placed sufficiently far away from the discontinuity to ensure that only the dominant mode exists at these planes. Keeping in mind that the above procedure must be repeated for each frequency, one can imagine the enormity of computations involved in the extraction of scattering parameters using the Finite Element Method.

The impulsive excitation capability of the TLM method can be exploited for computation of scattering parameters over a wide frequency range with only one simulation. Compare this with 100 Finite Element simulations to compute the scattering parameters (of a two port symmetrical and reciprocal circuit) at the 50 frequency points which are normally required to characterize the circuit over the operating frequency band (of the input/output). Computation of S-parameters does not involve the calculation of spatial derivatives or integrals. Hence there is no need to know the field values at points other than at the input and the output sampling points (these could be anywhere in the discretized domain, of course lying on the same axis). Also, the TLM method is so versatile that with one simulation, the scattering parameters of the discontinuities, the propagation constants and all six field components at the nodes can be obtained over a wide frequency range.

1.2 STATE OF THE ART AND ORIGINAL CONTRIBUTIONS

In this section, the current state of the Finite Element as well as TLM methods, and their major pitfalls which are to be overcome for efficient analysis of microwave and millimeter-wave structures are described. Also, the original contributions made in this thesis are mentioned.

Although the Finite Element Method has been in wide use for a long time in such diverse fields as Structural Analysis, Fluid Mechanics, Heat Transfer, etc., its potential applications in the field of Electrical Engineering are being realized only recently. Early applications of this method in the field of Electrical Engineering were mostly related to electrostatic and magnetostatic problems. In these applications, the final system of equations to be solved are of the deterministic type and, hence, computer run time and memory requirements are not so great. But in the case of waveguide problems, eigenvalue equations must be solved. Early eigen-solvers required enormous computer run time and memory. The newly developed methods, such as, Simultaneous Iteration Method [37], Subspace Iteration Method [38], Lanczos Method [39], and Conjugate Gradient Method [40] are very efficient and exploit the sparseness of the matrices by storing and processing them in variable bandwidth form. This will further enhance the applications of the Finite Element Method. For instance, large-scale configuration iteration calculations of electronic wave functions of atoms and molecules have become practical and increasingly common in recent years (order of matrices - a few hundred or a few thousand).

Many researchers [41]-[48] have reported applications of the Finite Element Method to waveguide problems. Their applications, however, were not rigorous, and limited only to computation of cutoff frequencies and dispersion characteristics of some standard, simple structures (Waveguides, Dielectric Loaded Waveguides and Dielectric Waveguides, etc.,).

To the author's knowledge, there has been no effort to compute the field related parameters such as pseudo-characteristic impedances and conductor and dielectric losses using Finite Element Method for inhomogeneous complicated structures like finlines (except for P. Daly [49] and, Zorica Pantic and Raj Mittra's [50] work based on quasi-TEM analysis).

In this thesis, new algorithm containing special computational matrices based on a vectorial Finite Element approach is presented to analyse any shielded, inhomogeneous transmission line structure of arbitrary cross-section [90]. In addition, with the help of this new algorithm, new millimeter-wave structures like " finlines in circular waveguide enclosures " and " ridged bilateral finlines " have been proposed and analyzed [90]-[92]. The "ridged finlines" have large monomode bandwidth and less dispersion. Also, the dielectric and conductor losses of bilateral finlines and the effect of substrate bending and mounting grooves on the dispersion characteristics have been studied with this algorithm.

The TLM method is a numerical time domain technique, first described by Johns and Beurle [27], in which both space and time are discretized. Unlike other time domain methods which are based on the discretization of Maxwell's or Helmholtz's time-dependent equations, the TLM method embodies Huygens's principle in discretized form. The details of this method and an extensive list of references on this subject can be found in a Chapter on TLM [29] by Hoefer. It uses an equivalent network of ideal two-wire transmission lines to implement Huygens's principle in discretized form. Either shunt or series connection of transmission lines can be used for 2-D analysis. Attached to the nodes are a number of stubs whose electrical properties are used to represent the electrical characteristics of the propagation space. Analysis of the transmission line matrix leads to a system of equations which can be identified with Maxwell's equations by drawing equivalences between voltages, currents, line constants, and stub parameters in the TLM model, and the field quantities in the propagating medium. The numerical procedure then entails determining the impulse response of this equivalent network and taking the Fourier transform of the output response function to obtain the spectral domain solution. To analyse 3-D problems, three different types of nodes, namely the expanded node [51], the asymmetrical condensed node [52] and the symmetrical condensed node [53] exist.

The earlier applications of the TLM method have concentrated mainly on finding the cutoff frequencies and the propagation characteristics of transmission lines and the resonant frequencies of cavities. Few attempts have been made to compute the scattering parameters with this method, since wideband absorbing boundaries could not be modeled in the time domain, particularly in structures supporting non-TEM modes of propagation. However, in the absence of a wideband absorbing termination, the impulse excitation capability, which is one of the main assets of the TLM method, cannot be exploited. There will rarely be any use in obtaining the time-domain solutions if they are needed only at one frequency, or even two. Furthermore, the wideband absorbing boundaries must be of high quality since the Fourier transform of time domain results is very sensitive to imperfect boundary treatment. Small errors in the time domain may produce fairly large errors in the frequency domain. Thus, even though the time domain results may be reasonably accurate, the frequency domain results obtained from their Fourier transform may not be acceptable. Therefore, simulation of good absorbing boundary conditions is crucial for computation of S-parameters.

In this thesis, efficient algorithms for the simulation of dispersive wideband absorbing boundaries for use with 2-D and 3-D TLM algorithms are presented [93]-[94]. Johns's Time Domain Diakoptics approach [58]-[59] has been used to implement them. Reflections of less than one percent have been achieved, enabling accurate characterization of waveguide discontinuities over a wide frequency range with a single TLM simulation.

The Diakoptics technique is ideal for solving large field problems. It is a method of partitioning large structures into substructures which are solved independently and later reassembled. It is very attractive for the repeated analysis of large structures in which only a small portion is changed from one problem to another. For example, during the optimization of planar and quasi-planar circuits, the metallization in a restricted part may only be varied and the homogeneous dielectric regions remain unchanged. It is wasteful to analyze the entire structure every time a small change is made. The iteration time required for accurate analysis depends upon the complexity of the problem. Suppose a large network has a few highly non-uniform field areas (it takes more computer run time to analyse the whole network). If the network can be split into substructures, then those with complex fields can be analysed with a large number of iterations, while those with nearly uniform fields can be analysed with fewer iterations. These substructures are then connected together, saving computer time.

The method was originated by Kron [54] and has since been applied extensively in conjunction with frequency domain methods [55] - [57]. For example, irregular two - dimensional planar components can be analyzed by segmenting them into regular shapes for which the analytical Green's functions are known. However, there are only a few regular shapes, and these applications are thus limited to some standard regular geometries. The technique has been extended to the time domain for 2-D TLM modeling by Johns and Akhtarzad in 1981 [58] - [59]. They have shown how the substructures may be solved in the time domain using the TLM method and how the reconnection is made. Recently, Hoefer has generalized these concepts and proposed the discrete time Green's function or Johns Matrix to represent the impulse response of any structure [60].

In this thesis, the Diakoptics technique has successfully been extended to 3-D TLM method with symmetrical condensed nodes [94]-[95]. A 3-D Johns Matrix has been proposed for the characteristic impulse response of dispersive absorbing boundaries in 3-D structures. A Tapered Johns Matrix has been proposed to reduce the parasitic reflections from the absorbing boundaries due to finite space and time units, thus achieving less than one percent reflections [94].

Since the characteristic impulse response or Johns Matrix of the substructures must be computed and stored, the extra dimension of time associated with the TLM method vastly increases the computer storage (when compared with steady state problems). To reduce the computational effort, Johns and Akhtarzad [58] have proposed space approximations along the connecting interface: they connect only a fraction of the TLM branches in the interface and a polynomial approximationship (linear if only two branches are connected, quadratic if only three branches are connected, etc.,) is assumed for the remaining branches. Using this space interpolation technique they computed the cutoff frequencies of simple waveguides and ridged waveguides. Although the computed values compared reasonably well with analytical values, the frequency response curve was no longer of standard $\frac{\sin(x)}{x}$ shape but was distorted because of loss/gain of power during the approximate connection process. This shows that, even though the above space approximated Diakoptics may work reasonably well to compute eigenvalues, it may introduce considerable errors in the computation of scattering parameters.

In this thesis, the space interpolation techniques based on the dominant mode field distribution are proposed [93], [96]. This speeds extraction of scattering parameters of waveguide discontinuities by several orders of magnitude.

1.3 ORGANISATION OF THIS THESIS

This thesis is divided into six chapters which are outlined below:

Chapter II reviews in brief the Finite Element and TLM methods. The basics of these methods are introduced.

Chapter III deals with the application of the Finite Element Method to eigenvalue problems. Formulation of the Finite Element Method to compute the dispersion characteristics, pseudo characteristic impedances and, conductor and dielectric losses of any hybrid mode is presented. The results obtained with this algorithm for standard finlines are given. Some novel finline structures, such as " ridged finlines " and " finlines in circular waveguides " are proposed. The two-dimensional graded mesh TLM technique is also applied to analyze some structures, and the results are compared with those obtained with the Finite Element Method.

Chapter IV describes steady-state network Diakoptics, Segmentation approach for planar components, and time domain Diakoptics for the 2-D TLM method. It has been shown how a microwave structure can be partitioned into substructures which are solved independently and later reassembled. The Johns Matrix is proposed for representing the discrete impulse response of a microwave structure.

In Chapter V, the TLM modeling of dispersive, wideband, absorbing boundaries is described. A space interpolation technique, in accordance with the spatial distribution of the dominant mode, is proposed for efficient analysis. Two ways of modeling frequency dispersive boundaries are presented. Some typical applications of these procedures to two-dimensional waveguide discontinuities and circuits are given.

Chapter VI describes the application of the Diakoptics technique to the 3-D TLM method using symmetrical condensed nodes. A 3-D " Johns Matrix " is proposed to represent wideband non-TEM absorbing boundary conditions. A " Tapered Johns Matrix " is introduced, which eliminates parasitic reflections due to finite space and time discretization. The results of some 3-D waveguide discontinuities computed with these techniques are presented.

The Chapter VII contains an overall review and conclusions.

Chapter II

PRELIMINARIES

2.1 INTRODUCTION

The principles involved in the Finite Element analysis are described in a book by P. Silvester [21]. The theory and applications of the TLM method are described in a review paper [28] and a Chapter on TLM by Hoefer [29]. The relevance of the fundamental principles of the Finite Element and the TLM methods to the work presented in the following chapters warrants a discussion of these methods, and hence a brief description and a review of these methods is presented in the following sections.

2.2 FINITE ELEMENT METHOD

A variational principle is an alternative way of expressing the physical content of a set of differential equations. It is an assertion that the solution to the original differential equation is that function which renders the associated functional (which usually is proportional to the energy) stationary. For example, according to Thomson's theorem [61], when a voltage is applied between two conductors, the fields distribute themselves in such a way that the energy in the system is a minimum.

The Finite Element Method is based on this variational principle. However it differs from the other classical variational methods (e.g., Rayleigh-Ritz, Galerkin and Least Squares methods) in two respects: First, the domain of the problem is represented as a collection of several simple elements; second, the approximating functions are algebraic polynomials which are derived systematically for each element using ideas from interpolation theory. The essence of this method is illustrated below for quasi-static and waveguide problems.

2.2.1 QUASI-STATIC PROBLEMS

For a general 2-D quasi-static problem shown in Fig. 2. 1, the equation to be solved is a Laplacian equation with associated Dirichlet and Neumann boundary conditions:

$$\frac{\partial^2\Phi(x,y)}{\partial x^2}+\frac{\partial^2\Phi(x,y)}{\partial y^2}=0 \tag{2.2.1}$$

$\phi = V_0$ on boundary b_1

$\phi = 0$ on boundary b_2

$\frac{\partial\phi}{\partial n} = 0$ on boundary b_3

The problem is to find the electric potential for an inhomogeneous region, where the permittivity ϵ(x,y) is a function of position. The appropriate energy-based functional to be minimized in this situation is given by:

$$F(\phi)=\frac{1}{2}\int_D \epsilon(x,y)(\nabla\phi(x,y))^2\,dx\,dy \tag{2.2.2}$$

where the domain D is the cross-section of the problem, and is divided into a large number of subregions or elements in an arbitrary manner, provided that all the dielectric interfaces coincide with the element sides. Although a variety of different elements can be choosen, the triangular elements are most commonly used.

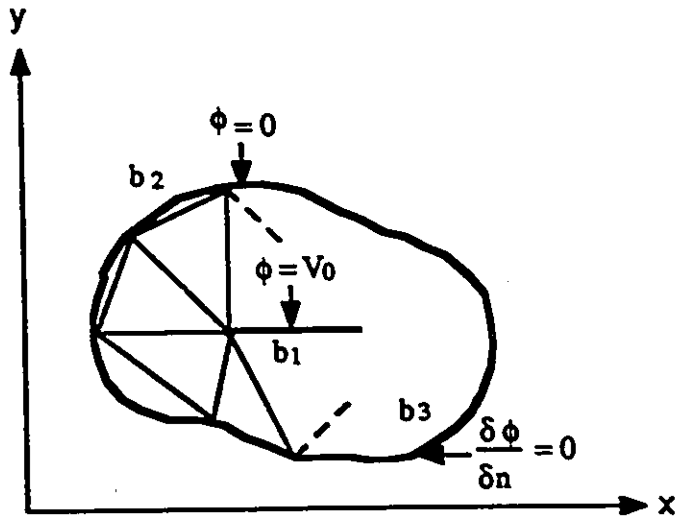

Fig. 2. 1 : Finite Element Discretization of a Quasi-static Structure

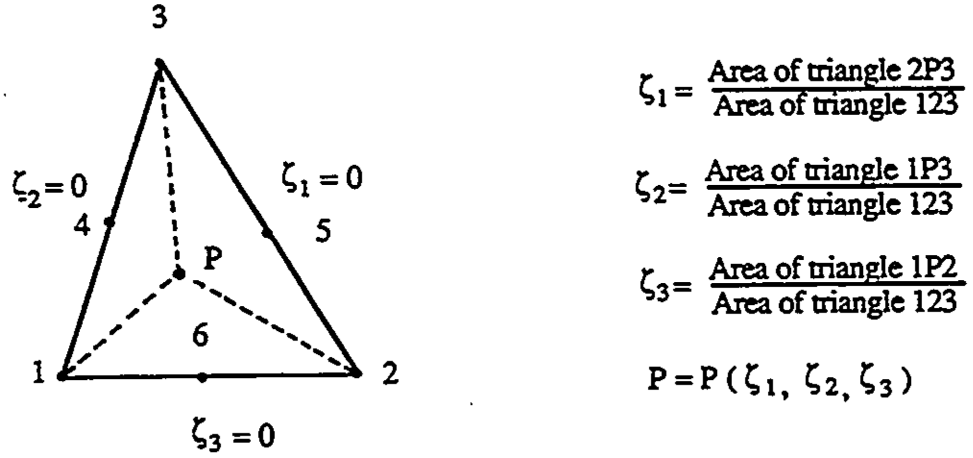

$\zeta_1 = \frac{\text{Area of triangle 2P3}}{\text{Area of triangle 123}}$

$\zeta_2 = \frac{\text{Area of triangle 1P3}}{\text{Area of triangle 123}}$

$\zeta_3 = \frac{\text{Area of triangle 1P2}}{\text{Area of triangle 123}}$

$P = P(\zeta_1, \zeta_2, \zeta_3)$

Fig. 2. 2 : Nodes for a Second-order Triangular Element and Local (or simplex) Coordinates for a Point P

In each triangle, the electric potential ϕ is approximated by a linear combination of a complete set of interpolation polynomials, each of degree 1, 2, or higher depending upon the complexity of the field distribution. For example,

$$\phi(x,y) = c_0 + c_1 x + c_2 y \tag{2.2.3}$$

for the first degree interpolation, and

$$\phi(x,y) = c_0 + c_1 x + c_2 y + c_3 x^2 + c_4 xy + c_5 y^2 \tag{2.2.4}$$

for the second degree interpolation, and so on.

The first-degree polynomial involves three coefficients and, hence, can be expressed in terms of three nodal potential values at the triangle vertices. The second-degree polynomial needs six coefficients and can similarly be expressed in terms of potential values of six nodes, located at the vertices and midpoints of the sides, as in Fig. 2. 2. Hence, the potential in a triangle can be written as

$$\phi(x,y) = \sum_{i=1}^{n} \phi_i \ \alpha_i(x,y) \tag{2.2.5}$$

where $n = (N+1)(N+2)/2$, N is the order of the triangle; and ϕ_1, ϕ_2, ... are the values of the potential at the interpolation nodes; α_i are the interpolatory functions.

Discretization of the functional is simplified if simplex or local coordinates are used. They are defined with respect to a typical point P in Fig. 2. 2. For the triangle, they are more natural, having no bias to any vertex. Hence a set of general coefficients for the integrals involved in the functional can be computed once and for all.

For first order triangular elements, the interpolatory functions α_i are the same as the triangular coordinates. i.e.,

$$\alpha_1 = \zeta_1, \quad \alpha_2 = \zeta_2, \quad \alpha_3 = \zeta_3 \tag{2.2.6}$$

Hence the equation (2.2.5) becomes

$$\phi(x,y) = \zeta_1\phi_1 + \zeta_2\phi_2 + \zeta_3\phi_3 \tag{2.2.7}$$

For second-order triangular elements, it can be written as

$$\begin{aligned}\phi(x,y) = {} & \zeta_1(2\zeta_1 - 1)\phi_1 + 4\zeta_1\zeta_2\phi_2 + 4\zeta_1\zeta_3\phi_3 \\ & + \zeta_2(2\zeta_2 - 1)\phi_4 + 64\zeta_2\zeta_3\phi_5 + \zeta_3(2\zeta_3 - 1)\phi_6\end{aligned} \tag{2.2.8}$$

After substituting the expression (2.2.5) for ϕ into (2.2.2), the contribution of one triangle (say pth) can be written as

$$F_p(\phi) = \frac{1}{2}\epsilon_p \sum_{i=1}^{n}\sum_{j=1}^{n} \phi_i\ \phi_j \int \nabla\alpha_i\ \nabla\alpha_j \tag{2.2.9}$$

This can be further written as follows:

$$F_p(\phi) = [\phi_p]^T[S][\phi_p] - [\phi_p]^T\bar{b} \tag{2.2.10}$$

where $[\phi_p]^T = [\phi_1, \phi_2, \phi_3, \phi_4, ..., \phi_n]$; $\bar{b}$ contains the information on the boundary condition; and S is a square matrix of order n [20]. The elements of S can be computed using the following equation:

$$S_{ij} = \sum_{k=1}^{3} Q_{ij}^{k}\ cot\ \theta_k \tag{2.2.11}$$

where θ_k is the included angle at vertex k. The three Q matrices are purely numeric, and are independent of size and shape of the triangles.

These base matrices S and b are successively applied to the total number of triangles to obtain the final global matrices A and B, thus summing the contributions F_p of all the triangles yields the following equation for F:

$$F(\phi) = [\phi]^T[A][\phi] - [\phi]^T B \tag{2.2.12}$$

where $[\phi]$ is an ordered array of potential nodal variables. Taking the first variation of (2.2.12) with respect to the these nodal variables leads to the following linear system of equations:

$$[A][\phi] = B \tag{2.2.13}$$

where $[A]$ is a symmetric matrix.

Once the potential distribution is obtained upon solving the above equation, the x and y components of electric field E can be computed from the following formula:

$$E = -\nabla\phi = -(\hat{x}\frac{\partial\phi}{\partial x} + \hat{y}\frac{\partial\phi}{\partial y}) \tag{2.2.14}$$

The per-unit length capacitance can be computed from its energy relation

$$C = \frac{2W_e}{V_o^2} \tag{2.2.15}$$

where

$$W_e = \sum_{p=1}^{NOTR} \epsilon_p[\phi_p]^T[S][\phi_p] \tag{2.2.16}$$

and $NOTR$ is the total number of triangles.

Since the computation of electric field components involves space derivatives, at least second-order elements should be used to avoid singularities.

2.2.2 WAVEGUIDE PROBLEMS

For homogeneously filled waveguides, the equations to be solved are Helmholtz's equations

$$\nabla_t^2 E_z + (k^2 - \beta^2) E_z = 0 \tag{2.2.17}$$

with Dirichlet boundary condition $E_z = 0$ on the waveguide boundary for TM modes, and

$$\nabla_t^2 H_z + (k^2 - \beta^2) H_z = 0 \tag{2.2.18}$$

with Neumann boundary condition $\frac{\partial H_z}{\partial n} = 0$ on the waveguide boundary for TE modes, where $\nabla_t^2 = \frac{\partial^2}{\partial x^2} + \frac{\partial^2}{\partial y^2}$ and β is the propagation constant.

The functional for TM modes can be written as

$$F(E_z) = \frac{1}{2}\int_D ((\nabla_t \, E_z)^2 - (k^2 - \beta^2) E_z^2) \; dx \, dy \tag{2.2.19}$$

subject to the Dirichlet boundary condition $E_z = 0$ on the waveguide boundary. A similar functional in H_z can be written for TE mode subject to the natural boundary condition.

Following the procedure described in the Section (2.2.1), the contribution of one triangle (say pth) to the functional can be written as

$$F_p(E_z) = \frac{1}{2}\sum_{i=1}^{n}\sum_{j=1}^{n} E_{zi}E_{zj}\int \nabla\alpha_i \; \nabla\alpha_j \, dx \, dy - (\frac{(k^2 - \beta^2)}{2})\sum_{i=1}^{n}\sum_{j=1}^{n} E_{zi}E_{zj}\int \alpha_i \; \alpha_j \; dx \; dy \tag{2.2.20}$$

where the coefficients E_{zi} represent the values of E_z at the interpolation nodes.

This can be further written as

$$F_p(E_z) = [E_{zp}]^T[S][E_{zp}] - (\frac{(k^2 - \beta^2)}{2})[E_{zp}]^T T[E_{zp}] \tag{2.2.21}$$

where S matrix is the same as discussed in the last section, and the T matrix is also independent of triangle shape and size [20], and hence needs to be evaluated only once.

Summing the contributions F_p of all the triangles and taking the variation with respect to the $[E_z]$ nodal values yields the following eigenvalue problem:

$$[A][E_z] = (\frac{(k^2 - \beta^2)}{2})[B][E_z] \qquad (2.2.22)$$

Upon solving this eigenvalue problem, the propagation constant β and the transversal dependence of the fields can be obtained.

2.2.3 INHOMOGENEOUS WAVEGUIDE PROBLEMS

The scalar variational formulation discussed above is not applicable for general inhomogeneous waveguide structures. Only cutoff frequencies of such structures can be computed because the hybrid modes are either TE or TM at cutoff. There are different types of vector variational formulations suitable for inhomogeneous and anisotropic waveguide problems. These are described below :

i) Variational expressions which are formulated in terms of the longitudinal components of the electric field (E_z) and the magnetic field (H_z) [45] and can be written as

$$\omega = functional\ (\beta, E_z, H_z) \qquad (2.2.23)$$

ii) Variational expressions employing all three components of electric field [46] and can be written as

$$\omega = functional\ (\beta, E_t, E_z) \qquad (2.2.24)$$

where E_t is the transverse electric field.

(iii) Variational expressions employing all three components of magnetic field [44], [47] and can be written as

$$\omega = functional\ (\beta, H_t, H_z) \qquad (2.2.25)$$

where H_t is the transverse magnetic field.

iv) Variational expressions employing the transverse electric and magnetic field [48] and can be written as

$$\beta = functional\ (\omega, E_t, H_t) \tag{2.2.26}$$

The above variational expressions have been applied to compute the propagation constants of some standard structures, such as dielectric loaded waveguides, ferrite loaded waveguides, microstrip lines and optical waveguides.

2.3 TRANSMISSION LINE MATRIX METHOD

2.3.1 THE TWO-DIMENSIONAL TLM MODELS

The TLM method was first described by Johns and Beurle [27] in 1971. The basis of this method has been established by adopting the wave propagation concept postulated by Huygens, who considered a wavefront to consist of a number of secondary radiators which give rise to spherical wavelets. To formulate Huygens's principle in discretized form, both the space and time are represented in terms of finite elementary units Δl and Δt, which are related by the velocity of light such that

$$\Delta t = \frac{\Delta l}{c} \tag{2.3.1}$$

The unit time Δt is then the time required for an electromagnetic pulse to travel from one node to the next.

Earlier network simulation techniques (for the solution of electromagnetic problems) developed by Kron [63], and Whinnery and Ramo [64] prompted the implementation of this discrete Huygens's model on a digital computer through a Cartesian mesh of open two-wire transmission lines. Each node in the mesh corresponds to a junction between a pair of transmission lines as shown in Fig. 2. 3(a).

In order to show how Maxwell's equations may be represented by the transmission-line matrix, the elementary length of the transmission line between two nodes of the mesh is represented by lumped inductors and capacitors. If the inductance and capacitance, per unit length for an individual line, are L and C, respectively, the junction between a pair of lines at a mesh node point can be represented by the basic elementary network of Fig. 2. 3(b). The complete network is made up of a large number of such building blocks, connected as a two-dimensional array (see Fig. 2. 3(c)).

The fundamental differential equations giving the voltage and current for the elementary network can be written as

$$\frac{\partial V_y}{\partial x} = -L\frac{\partial}{\partial t}(I_{x1} - I_{x3}) \qquad \frac{\partial V_y}{\partial z} = -L\frac{\partial}{\partial t}(I_{z2} - I_{z4}) \tag{2.3.2}$$

$$\frac{\partial}{\partial x}(I_{x1} - I_{x3}) + \frac{\partial}{\partial z}(I_{z2} - I_{z4}) = -2C\frac{\partial V_y}{\partial t} \tag{2.3.3}$$

These equations may be combined to give the following 2-D wave equation

$$\frac{\partial^2 V_y}{\partial x^2} + \frac{\partial^2 V_y}{\partial z^2} = 2LC\frac{\partial^2 V_y}{\partial t^2} \tag{2.3.4}$$

For a TE_{n0} mode with field components E_y, H_x and H_z, and $\partial/\partial y = 0$, the Maxwell's curl equations may be written as

$$\frac{\partial E_y}{\partial x} = -\mu\frac{\partial H_z}{\partial t} \qquad \frac{\partial E_y}{\partial z} = \mu\frac{\partial H_x}{\partial t} \tag{2.3.5}$$

$$\frac{\partial H_x}{\partial z} - \frac{\partial H_z}{\partial x} = \epsilon\frac{\partial E_y}{\partial t} \tag{2.3.6}$$

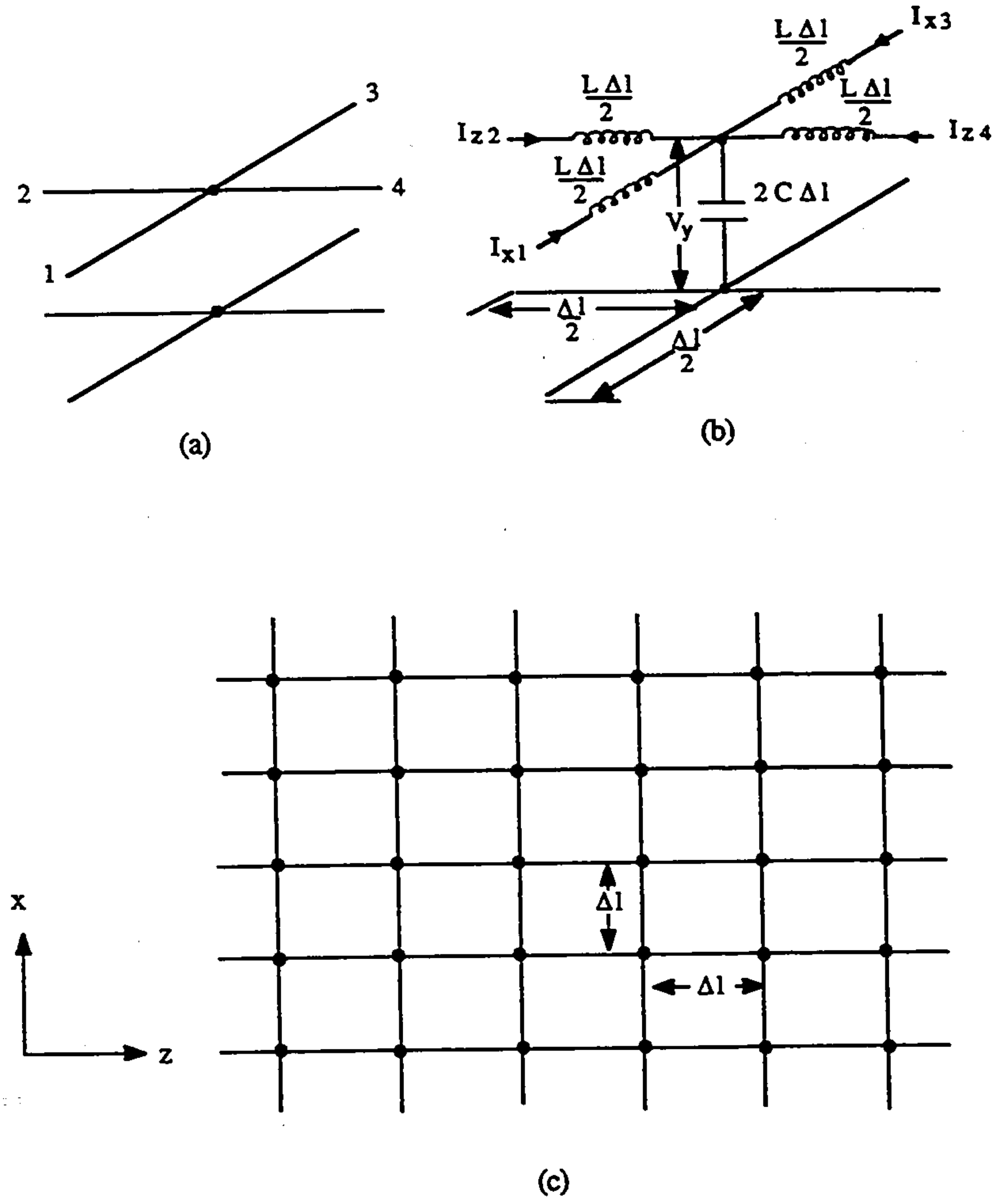

(a)

(b)

(c)

Fig. 2. 3 : a) Junction between Transmission Lines b) Equivalent Circuit of a Transmission Line Junction c) Transmission Line Matrix in x-z Plane

These combine to give the wave equation

$$\frac{\partial^2 E_y}{\partial x^2} + \frac{\partial^2 E_y}{\partial z^2} = \mu\epsilon \frac{\partial^2 E_y}{\partial t^2} \tag{2.3.7}$$

The equivalences between TLM mesh parameters and field parameters can be obtained by comparison between the equations (2.3.2)-(2.3.4) and (2.3.5)-(2.3.7):

$$E_y \equiv V_y \qquad H_z \equiv -(I_{x3} - I_{x1}) \tag{2.3.8}$$

$$-H_x \equiv (I_{z2} - I_{z4}) \qquad \mu \equiv L \qquad \epsilon \equiv 2C \tag{2.3.9}$$

If the voltage and current waves on each transmission line linking any two nodes travel at the speed of light, the complete network of intersecting transmission lines represents a medium of relative permittivity twice that of free space. This means that as long as the mesh parameter Δl is very small, the propagation velocity in the TLM mesh is $\frac{1}{\sqrt{2}}$ times the velocity of light and is independent of the direction of propagation. If Δl is comparable to the wavelength, the propagation velocity is space dispersive [29].

Having proved how Maxwell's equations can be represented by a Cartesian mesh of TEM transmission lines, the implementation of the TLM method on a digital computer will be described.

The numerical calculation usually starts by exciting the mesh at specific points by voltage or current impulses and follows the propagation of these impulses over the mesh as they are scattered by the nodes and boundaries. The scattering matrix equation relating the reflected voltage impulses at time (k + 1) Δt to the incident voltage impulses at the previous time step $k\Delta t$ for the node shown in Fig. 2. 3(a) can be written as

$$ {}_{k+1}\begin{pmatrix} V_1 \\ V_2 \\ V_3 \\ V_4 \end{pmatrix}^r = \frac{1}{2}\begin{pmatrix} -1 & 1 & 1 & 1 \\ 1 & -1 & 1 & 1 \\ 1 & 1 & -1 & 1 \\ 1 & 1 & 1 & -1 \end{pmatrix} {}_{k}\begin{pmatrix} V_1 \\ V_2 \\ V_3 \\ V_4 \end{pmatrix}^i \qquad (2.3.10) $$

Any impulse emerging from a node at position (z,x) in the mesh (reflected impulse) becomes automatically an incident impulse on the neighbouring node. This can be represented by the following equations:

$$ \begin{aligned} {}_kV_4^r(z,x) &= {}_{k+1}V_2^i(z+1,x) \qquad & {}_kV_3^r(z,x) &= {}_{k+1}V_1^i(z,x+1) \\ {}_kV_2^r(z,x) &= {}_{k+1}V_4^i(z-1,x) \qquad & {}_kV_1^r(z,x) &= {}_{k+1}V_3^i(z,x-1) \end{aligned} \qquad (2.3.11) $$

The TLM algorithm consists of applying equations 2.3.10 and 2.3.11 for each node in the network. The output which is taken from a chosen point is a series of discrete impulses of varying magnitudes separated by constant time intervals. At any node in the mesh, the discrete field components can be computed by storing the impulse values on the four branches for each iteration and performing the following operations:

$$ \begin{aligned} {}_kE_y \equiv {}_kV_y &= \frac{1}{2}\sum_{m=1}^{4} {}_kV_m^i \\ -{}_kH_x \equiv {}_kI_z &= ({}_kV_2^i - {}_kV_4^i) \\ {}_kH_z \equiv {}_kI_x &= ({}_kV_1^i - {}_kV_3^i) \end{aligned} \qquad (2.3.12) $$

The frequency response within any frequency range $\Delta l/\lambda \ll 1$ can be obtained by taking the discrete Fourier transform on the output function.

To represent a lossy inhomogeneous material, the TLM mesh can be loaded at the nodes situated inside the material with additional reactive and dissipative elements. The length of the stub is equal to the half the length of the link line to achieve time synchronism.

Due to the dual nature of the electric and magnetic fields, the same wave propagation can be modeled by a series connected mesh of transmission lines [29].

In order to ensure time synchronism, the conventional TLM network described above, uses a square mesh to model a given propagation space. This can lead to large computer run time and memory if the structure contains field singularities such as sharp corners or fins, where highly non-uniform fields require the use of a very fine mesh. Also in the fixed mesh schemes, the bigger dimensions of the structure must be an integer multiple of smaller dimension of the structure, putting constraints on dimensions of the structure. To overcome these problems, Saguet and Pic [65] and Al-Mukhtar and Sitch [66] have independently proposed ways to implement irregularly graded TLM meshes which allow the network to adapt its density to the local nonuniformity of the fields. These methods are briefly discussed and reviewed below.

2.3.2 THE TWO-DIMENSIONAL GRADED TLM MODELS

The graded mesh and a basic elementary network by Saguet [65] are shown in Fig. 2.4. The phase velocity is kept the same in all cells regardless of the mesh size. The time step Δt is taken as the time required to travel the length of the shortest link line. Therefore $\Delta t = \frac{\Delta l_1}{c}$, where Δl_1 is the length of the shortest link line and c is the velocity of light. To keep the phase velocities of travelling impulses the same in all cells regardless of the mesh size, one should have

$$\frac{1}{\sqrt{(L_2C_2)}} = \frac{1}{\sqrt{(L_1C_1)}} \tag{2.3.13}$$

where L_1, C_1, L_2, C_2 are the inductances and capacitances per unit length of the transmission lines. Then if

$$L_2 = NL_1, \quad then \quad C_2 = C_1/N \tag{2.3.14}$$

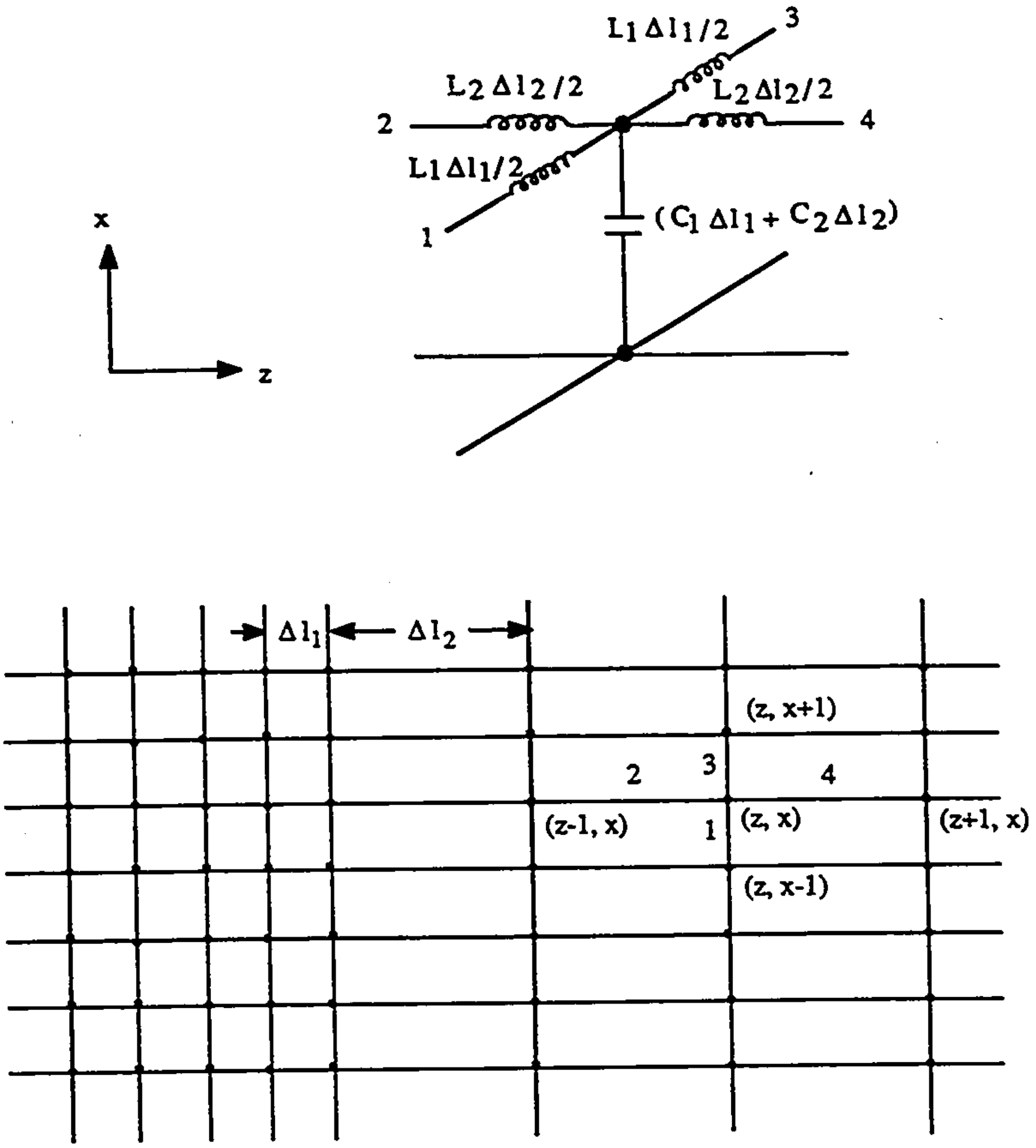

Fig. 2.4 : Graded Mesh (for N=3) and a Unit Element by Saguet [65]

where N = grading ratio. Thus the inductance per unit length of the longer mesh lines is increased by a factor N, while their capacitance per unit length is reduced by $1/N$.

The characteristic impedances of the two link transmission lines are related by

$$Z_2 = NZ_1 \tag{2.3.15}$$

Thus different branches (1,2,3,4) will have different characteristic impedances unlike the uniform mesh. The length of the permittivity stub is equal to the half the length of the shortest link line to achieve time synchronism. An impulse incident upon a stub loaded node is scattered into six lines. The loss stub absorbs all the incident power. On other five lines, the impulses are returned to the node after reflection at the other ends. The scattering matrix (for $N = 3$) for such a stub loaded shunt node can be written as follows:

$$
{}_{k+1}\begin{pmatrix} V_1 \\ V_2 \\ V_3 \\ V_4 \\ V_5 \end{pmatrix}^{r} = \frac{1}{y}\begin{pmatrix} (2Y_1 - y) & 2Y_2 & 2Y_3 & 2Y_4 & 2Y_5 \\ 2Y_1 & (2Y_2 - y) & 2Y_3 & 2Y_4 & 2Y_5 \\ 2Y_1 & 2Y_2 & (2Y_3 - y) & 2Y_4 & 2Y_5 \\ 2Y_1 & 2Y_2 & 2Y_3 & (2Y_4 - y) & 2Y_5 \\ 2Y_1 & 2Y_2 & 2Y_3 & 2Y_4 & (2Y_5 - y) \end{pmatrix} \begin{pmatrix} {}_{k}V_1 \\ {}_{k-2}V_2 \\ {}_{k}V_3 \\ {}_{k-2}V_4 \\ {}_{k}V_5 \end{pmatrix}^{i} \tag{2.3.16}
$$

where $y = Y_1 + Y_2 + Y_3 + Y_4 + Y_5 + g_o$; Y_1, Y_2, Y_3, Y_4 are the characteristic admittances of the four branches of a unit cell, Y_5 is the characteristic admittance of the open-ended stub of length $\Delta l_1/2$ (permittivity stub) and g_o is the characteristic admittance of the loss stub.

The equation (2.3.11) for this particular graded mesh becomes

$$
\begin{aligned}
{}_{k}V_4^r(z,x) &= {}_{k+3}V_2^i(z+1,x) \qquad & {}_{k}V_3^r(z,x) &= {}_{k+1}V_1^i(z,x+1) \\
{}_{k}V_2^r(z,x) &= {}_{k+3}V_4^i(z-1,x) \qquad & {}_{k}V_1^r(z,x) &= {}_{k+1}V_3^i(z,x-1)
\end{aligned}
\tag{2.3.17}
$$

The two scattering processes described above form the basic algorithm as in the conventional TLM model. In this case, to compute the reflected impulses on the branches at time $(k+1)\Delta t$, we should know the incident impulses on the branches at time $(k+1-N)\Delta t$ (in the case of longer branches). Hence the impulses travelling on the longer branches are kept in store for N iterations before being injected into the next node. The grading ratio N must be an odd integer to get time synchronism, otherwise at the transition from the dense mesh to the coarse mesh, the separation between adjacent elements is $\frac{\Delta l_1}{2}$.

To overcome these problems and to achieve time synchronism, Al-Mukhtar and Sitch [66] proposed two different approaches:

- In the first approach, the propagation velocity of the impulses is made proportional to the link transmission line length. That is, the impulses travel faster on long lines and slower on short lines, thus maintaining a constant time step. But the inductance and capacitance per unit length will be different for different branches.

- In the second approach, the shortest link line is taken to be of unit length. In areas where the link lines are longer than the unit length, additional series stubs between nodes and shunt stubs at the nodes are introduced to account for extra inductances and capacitances. This arrangement also makes it possible to represent inhomogeneous propagation space by making changes to the impedances of the stubs.

In these approaches, the grading ratio can be a real number. Hence they are quite useful especially when the geometry of the problem is large, and with dimensions that are not small integer multiples of a common length. The mesh, however, may be more dispersive due to the loading of the additional stubs.

2.3.3 THE THREE-DIMENSIONAL TLM MODELS

If the voltages of the 2-D TLM matrix represent E-fields in the medium, the shunt connected matrix provides a solution for TE_{no} modes while the series connected matrix provides a solution for TM_{no} modes [29]. Therefore, these two separate matrices will solve the Maxwell's equations in two dimensions. Hence to solve Maxwell's equations in three dimensions, there must be a parallel matrix and a series matrix in each plane.

Akhtarzad and Johns [51] built such a 3-D TLM node by interlacing shunt and series nodes in all three coordinate directions. The resulting unit element consists of three shunt and three series nodes. The three shunt nodes represent the E-field, and the three series nodes represent the H-field in the the coordinate directions as shown in Fig. 2.5. To account for dielectric and magnetic materials, open-circuited and short-circuited stubs are added to shunt and series nodes, respectively. The 3-D node is further equipped with stubs of infinite length at the shunt nodes to model dielectric losses. Fig. 2.6 shows schematically a 3-D unit cell with completely equipped nodes. It uses a total of 26 real memory stores per 3-D node. Since the six components of the electromagnetic field are available at the corners of the 3-D node cube (separated by a distance $\frac{\Delta l}{2}$), the network is called the "expanded-node".

Because of the spatial separation of the six field components, the description of the boundaries and the dielectric interfaces is difficult, and the problem is particularly acute when automatic data preparation schemes are implemented. The process of Diakoptics for forming structures is also difficult to organise because of the half-time steps and the spatial separation of different polarizations. This inconvenience lead to the development of a condensed node structure by Saguet and Pic [52]. This node, shown in Fig. 2.7, is a 3-D Cartesian mesh with two lines, corresponding to two polarizations, in each branch.

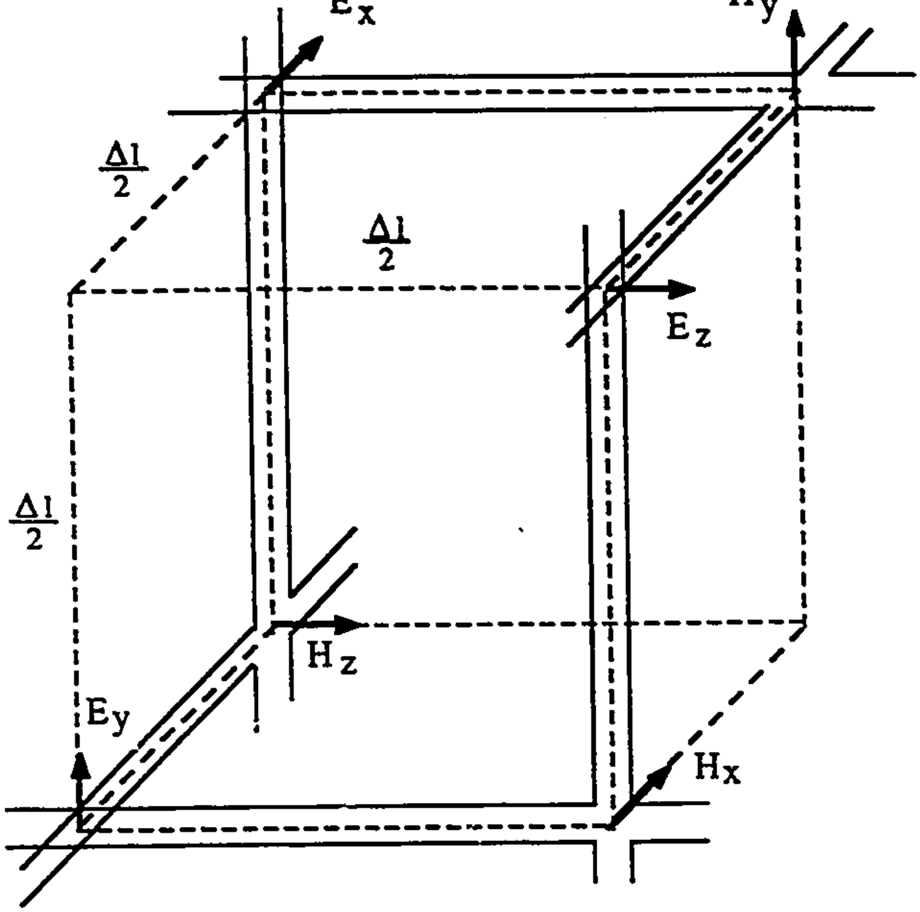

Fig. 2. 5 : 3-D Expanded TLM Node Consisting of Three Shunt and Three Series Connected 2-D Nodes.

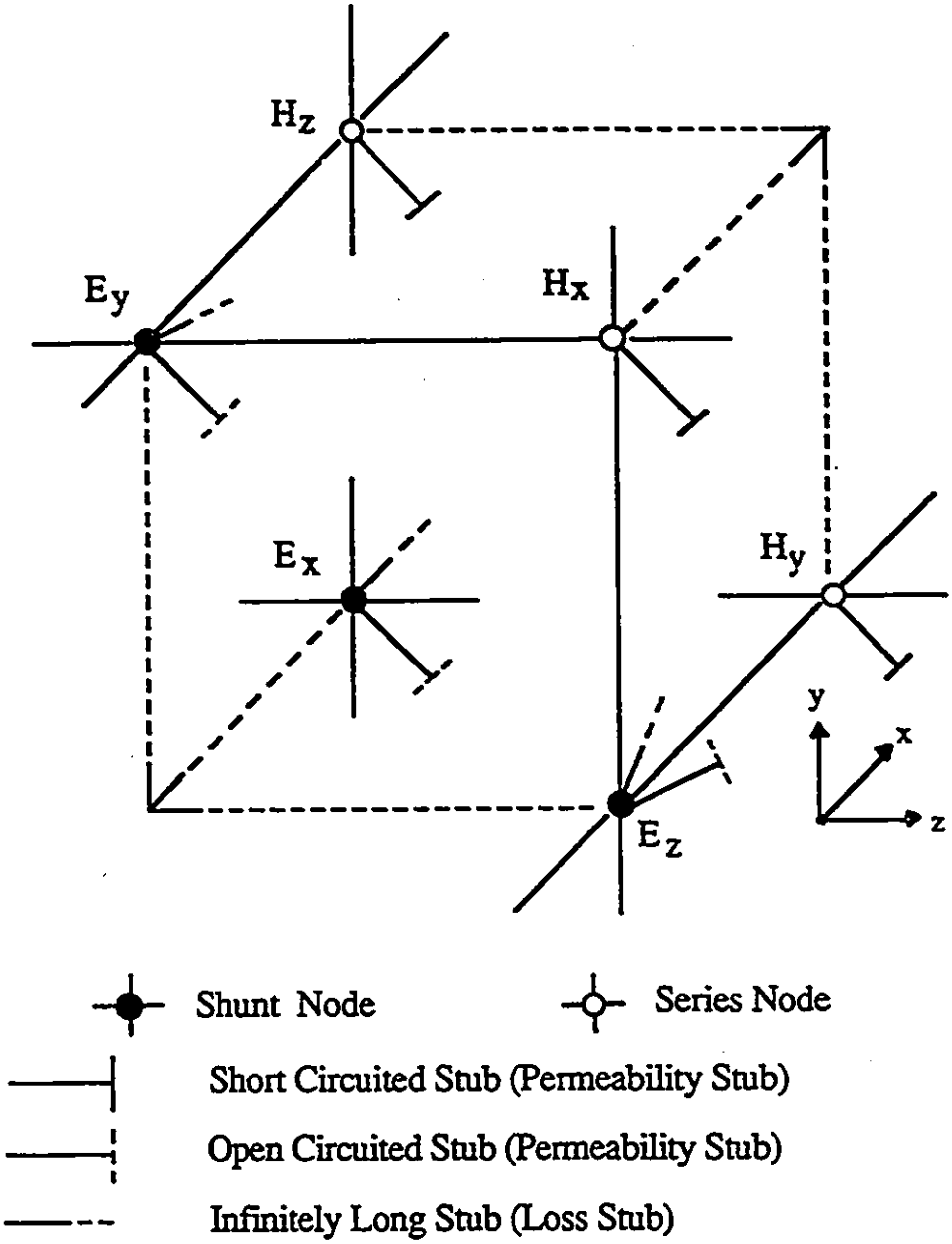

Fig. 2.6 : A 3-D Node Equipped with Reactive and Dissipative Stubs for the Modeling of Permittivity, Permeability and Losses.

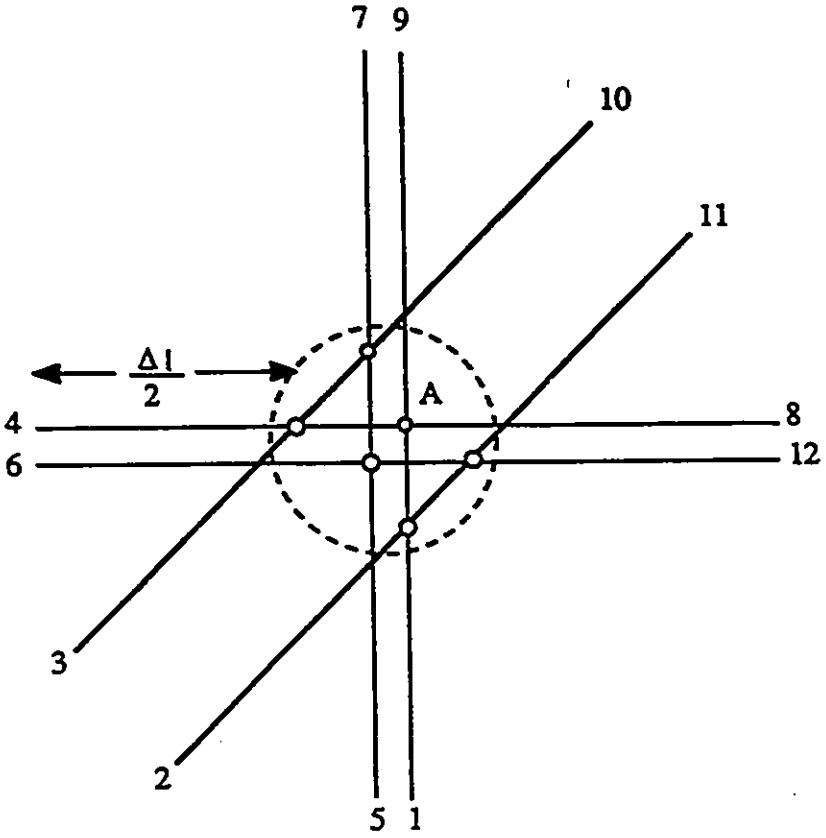

Fig. 2.7 : Asymmetrical Condensed TLM Node by Saguet [52]

All six field components are defined at one point in space, and boundary conditions can be applied at the node or halfway between the nodes. However, this node is asymmetrical because, depending upon the direction of view, the first connection in the node is either shunt or series. This implies that boundaries viewed in one direction have slightly different properties when viewed in another, especially at high frequencies.

Recently, a symmetrical 3-D condensed node has been developed by P. B. Johns [53]. The node, without any stubs, is shown in Fig. 2.8 and it avoids the above problems and is more accurate than the other mesh schemes. It can be used to represent a cubic block of homogeneous space by a Cartesian mesh.

The symmetrical condensed node has six branches, each branch consisting of two uncoupled two-wire transmission lines. The 12 transmission lines linking the Cartesian mesh of nodes together have the characteristic impedance of free-space. These lines are numbered and oriented according to the voltages shown in Fig. 2.8. Each line has two fields associated with it. For example, a voltage impulse incident upon port 1 has associated with it the field quantities E_x and H_z. A voltage impulse proceeding outwards at port 2 has associated with it the field quantities E_x and $-H_y$. Twelve impulses on the link transmission lines, incident upon the node, result in twelve scattered impulses. The scattering matrix S for the node has been derived by P. B. Johns by studying the behaviour of the electromagnetic fields (through Maxwell's equations) associated with impulses on various transmission lines. After applying the field continuity and energy conservation conditions, the following impulse scattering matrix is obtained.

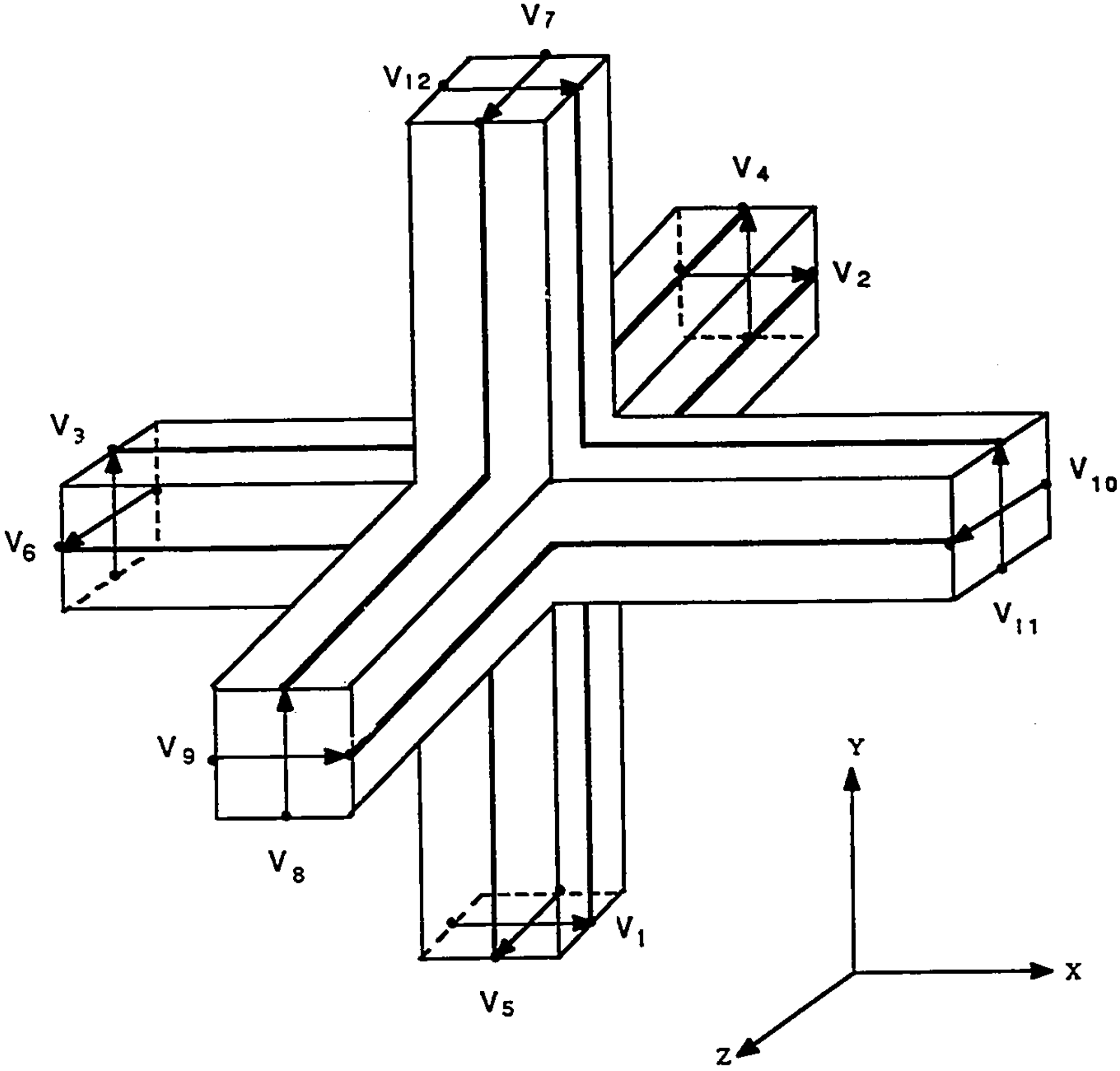

Fig. 2.8 : Symmetrical Condensed TLM Node by P. B. Johns [53]

$$S = \frac{1}{2}\begin{pmatrix} & 1 & 1 & & & & & & 1 & & -1 & \\ 1 & & & & & 1 & & & & -1 & & 1 \\ 1 & & & 1 & & & & 1 & & & & -1 \\ & & 1 & & 1 & & -1 & & & & 1 & \\ & & & 1 & & 1 & & -1 & & 1 & & \\ & 1 & & & 1 & & 1 & & -1 & & & \\ & & & -1 & & 1 & & 1 & & 1 & & \\ & & 1 & & -1 & & 1 & & & & 1 & \\ 1 & & & & & -1 & & & & 1 & & 1 \\ & -1 & & & 1 & & 1 & & 1 & & & \\ -1 & & & 1 & & & & 1 & & & & 1 \\ & 1 & -1 & & & & & & 1 & & 1 & \end{pmatrix} \qquad (2.3.18)$$

The six electromagnetic field quantities at any node can be calculated from the impulses on the twelve branches as follows:

$$\begin{aligned} E_x &= (V_1^i + V_2^i + V_9^i + V_{12}^i)/2, \\ E_y &= (V_3^i + V_4^i + V_8^i + V_{11}^i)/2, \\ E_z &= (V_5^i + V_6^i + V_7^i + V_{10}^i)/2, \\ H_x &= (V_4^i - V_5^i + V_7^i - V_8^i)/2, \\ H_y &= (-V_2^i + V_6^i + V_9^i - V_{10}^i)/2, \\ H_z &= (-V_3^i + V_1^i + V_{11}^i - V_{12}^i)/2, \end{aligned} \qquad (2.3.19)$$

The symmetrical condensed node has no dispersion in the coordinate directions (i.e., the velocity is constant at all frequencies and there is no cutoff of the waves in these directions), unlike the expanded node and asymmetrical condensed node which have no dispersionless direction of propagation. R. Allen, A. Mallik and P.B. Johns [67] have done numerical experiments which indicate that the velocity characteristics of the symmetrical condensed node are altogether better than the expanded node and the asymmetrical node. This means that, for a given problem, a coarse mesh can be used with symmetrical condensed nodes, saving computer run time and memory.

To use the node in inhomogeneous structures and in problems described by a completely general orthogonal mesh, six stubs should be used to add extra capacitance and inductance to the node locally. This is based on the technique developed by Al-Mukhtar and Sitch [66] described in section 2.3.2.

2.3.4 APPLICATIONS OF THE TLM METHOD

The TLM method has been widely used to compute the mode spectrum and propagation constants of uniform transmission lines such as microstrip lines on isotropic [68] and anisotropic [69] substrates, dielectric loaded waveguides, finlines [70], etc. Mariki and Yeh [69] have also computed the characteristic impedance of microstrip line on sapphire substrates using the TLM method. To obtain the propagation constants (or dispersion characteristics), a quarter wavelength section was usually considered, where different values of β and ω are simulated using different cavity lengths. To avoid discretizing quarter wavelength long sections, Sitch and P. B. Johns [71] have proposed a simple technique known as the " Stepped Impedance Approach ", which enables the length of the cavity to be no more than 2.5 mesh lengths. Recently, the scattering parameters of a bilateral finline T-junction have been computed by Saguet and Hoefer using the TLM method [72].

In all of the applications mentioned above, the most important characteristic of the TLM method, namely the impulsive excitation capability, was utilized only for the computation of the mode spectrum of uniform transmission lines. It is also possible, however, to extract the propagation constants, scattering parameters and field components over a wide frequency range from a single TLM simulation. Chapters V and VI deal with this aspect.

2.4 DISCUSSION

This chapter has introduced the principles and concepts involved in the Finite Element and TLM analysis. The variational principle, interpolation polynomials, triangular coordinates have been briefly discussed. The existing functionals for quasi-static, homogeneous and inhomogeneous waveguides have been reviewed.

2-D and 3-D TLM models have been briefly discussed. The condensed 3-D TLM node proposed by P. B. Johns is the most accurate and less dispersive model than the other 3-D nodes, and is also more appropriate for the application of Diakoptics. The main applications of the TLM method have been reviewed, and the need for wideband absorbing boundary conditions for exploitation of the impulsive excitation capability of the TLM method has been discussed.

Chapter III

NUMERICAL MODELING OF TRANSMISSION LINES

3.1 INTRODUCTION

As discussed in the Chapters I and II, the Finite Element method is the most appropriate technique for characterizing uniform transmission lines of arbitrary cross-section. In this chapter, the formulation of the algorithm based on this method for computing the dispersion characteristics, pseudo characteristic impedances, and conductor and dielectric losses is presented.

Ridged waveguides and finlines have been analysed with this algorithm. These transmission media have found many applications in microwave and millimeter-wave circuits, such as directional couplers, varactor-tuned oscillators, step transformers, filters, and PIN diode attenuators. The main advantages of these structures are large monomode bandwidth, small dispersion and high power handling capability. To the authors' knowledge, there is no data available on the losses of dielectrically loaded ridged waveguides, and no rigorous theoretical study of finlines in ridged waveguides (ridged finlines) and finlines in circular waveguide enclosures was done. Using the algorithm presented in this thesis, the above problems have been successfully tackled. Furthermore, the second-order effects, such as the effect of finite metallization thickness, substrate bending and mounting grooves, on the characteristics of the transmission lines have been studied.

The graded mesh TLM algorithm discussed in the Section (2.3.2) has also been applied to compute the cutoff frequencies of finlines in rectangular and circular waveguide enclosures. The results have been compared with those obtained with the Finite Element method.

3.2 THE FINITE ELEMENT ANALYSIS

3.2.1 THEORY

For the analysis of inhomogeneous waveguides, several variational formulations have been mentioned in the previous chapter. The variational formulation in terms of the longitudinal components of the electric and magnetic fields is chosen for our purpose because of its simplicity and small matrix size of the eigenvalue problem.

Consider an inhomogeneous waveguide of arbitrary cross section and uniform in the z direction, which consists of isotropic, lossless dielectric media. Assume that the cross-section can be divided into several subregions over which the relative permittivity is constant. Further, assume propagation along the z-axis of the form $\exp[j(\omega t - \beta z)]$ with longitudinal field components H_z and E_z. In a typical subregion (say the p^{th}), E_z and H_z satisfy the Helmholtz equations:

$$(\nabla_t^2 + K_p^2)\begin{bmatrix} E_z^{(p)} \\ H_z^{(p)} \end{bmatrix} = 0. \tag{3.2.1}$$

where ∇_t^2 is the transverse Laplacian Operator, and K_p^2 is given by

$$K_p^2 = (\omega/c)^2(\epsilon_p/\epsilon_o) - \beta^2 \tag{3.2.2}$$

with ϵ_p as the dielectric constant of the subregion. Continuity of the tangential electric and magnetic fields along the common interface between two contiguous regions (say the

p^{th} and q^{th}) requires that

$$
\begin{aligned}
E_z^{(p)} &= E_z^{(q)} \\
H_z^{(p)} &= H_z^{(q)} \\
\tau_p\left[\gamma\left(\frac{\epsilon_o}{\mu_o}\right)^{\frac{1}{2}} \frac{\partial E_z^{(p)}}{\partial s} - \frac{\partial H_z^{(p)}}{\partial n}\right] &= \tau_q\left[\gamma\left(\frac{\epsilon_o}{\mu_o}\right)^{\frac{1}{2}} \frac{\partial E_z^{(q)}}{\partial s} - \frac{\partial H_z^{(q)}}{\partial n}\right] \\
\tau_p\left[\frac{\epsilon_p}{\epsilon_o\gamma}\left(\frac{\epsilon_o}{\mu_o}\right)^{\frac{1}{2}} \frac{\partial E_z^{(p)}}{\partial n} + \frac{\partial H_z^{(p)}}{\partial s}\right] &= \tau_q\left[\frac{\epsilon_q}{\epsilon_o\gamma}\left(\frac{\epsilon_o}{\mu_o}\right)^{\frac{1}{2}} \frac{\partial E_z^{(q)}}{\partial n} + \frac{\partial H_z^{(q)}}{\partial s}\right]
\end{aligned}
\tag{3.2.3}
$$

where s and n refer to the tangential and normal directions, respectively, with $n \times s = e_z$ defining the unit normal along the z-direction. τ_i and γ are given by

$$
\begin{aligned}
\tau_i &= (\gamma^2 - 1)/(\gamma^2 - \epsilon_i/\epsilon_o) \\
\gamma &= (\beta c)/\omega
\end{aligned}
\tag{3.2.4}
$$

The variational principle [45]

$$\delta I = 0, \tag{3.2.5}$$

where

$$
\begin{aligned}
I &= \sum_{p=1} I_p \\
&= \sum_{p=1} \iint \Bigg(\tau_p |\nabla H_z^{(p)}|^2 + \gamma^2 \tau_p \frac{\epsilon_p}{\epsilon_o} \left|\frac{1}{\gamma}\left(\frac{\epsilon_o}{\mu_o}\right)^{\frac{1}{2}} \nabla E_z^{(p)}\right|^2 + 2\tau_p \hat{e}_z \gamma^2 . \left[\frac{1}{\gamma}\left(\frac{\epsilon_o}{\mu_o}\right)^{\frac{1}{2}} \nabla E_z^{(p)} \times \nabla H_z^{(p)}\right] \\
&\qquad - \left(\frac{\omega}{c}\right)^2 (1-\gamma^2) . \left\{[H_z^{(p)}]^2 + \gamma^2 \frac{\epsilon_p}{\epsilon_o}\left[\frac{1}{\gamma}\left(\frac{\epsilon_o}{\mu_o}\right)^{\frac{1}{2}} E_z^{(p)}\right]^2\right\}\Bigg) dx\, dy
\end{aligned}
\tag{3.2.6}
$$

yields as its Euler equations and natural boundary conditions the governing equations (3.2.1) and continuity conditions (3.2.3) for all regions comprising the waveguide cross-section.

3.2.2 INTERPOLATION FUNCTIONS, DISCRETIZATION AND GLOBAL MATRIX FORMULATION

The bases for the Finite Element algorithm are equation (3.2.5) with the functional (3.2.6). The initial step is the discretization of the waveguide cross-section into a large number of subregions or elements in an arbitrary manner, provided that all the dielectric interfaces coincide with the element sides. Although a variety of different elements can be chosen, the triangular [20], [42] second order elements are adopted in this study. The nodal values of E_z and H_z will be considered as the primary dependent variables of the problem. As mentioned in the chapter II, the E_z and H_z fields are approximated in each triangle by a linear combination of a complete set of interpolation polynomials $\{\alpha_i, i = 1, 2, 3, \cdots, n\}$ of degree N

$$\begin{aligned} E_z &= \sum_{i=1}^{n} E_{zi}\ \alpha_i(\zeta_1, \zeta_2, \zeta_3) \\ H_z &= \sum_{i=1}^{n} H_{zi}\ \alpha_i(\zeta_1, \zeta_2, \zeta_3) \end{aligned} \tag{3.2.7}$$

where

$$n = \frac{(N+1)(N+2)}{2}$$

The coefficients E_{zi} and H_{zi} represent the values of E_z and H_z respectively at the interpolation nodes. After substituting the above expressions for E_z and H_z into (3.2.6), I_p can be written in matrix form as

$$I_p = [\theta_p]^T[A_p][\theta_p] - \Gamma[\theta_p]^T[B_p][\theta_p] \tag{3.2.8}$$

where Γ is the eigenvalue parameter defined by

$$\Gamma = \left(\frac{\omega}{c}\right)^2(1-\gamma^2) \tag{3.2.9}$$

and $[\theta_p]$ is the assembled array of nodal E_z and H_z values, given by

$$[\theta_p]^T = [E_{z1}, E_{z2}, \cdots, E_{zn}, H_{z1}, H_{z2}, \cdots, H_{zn}] \tag{3.2.10}$$

The matrices $[A_P]$ and $[B_P]$ are given by

$$[A_p] = \tau_p \begin{pmatrix} \frac{\epsilon_z}{\epsilon_o}\gamma^2 S & 2\gamma^2 U \\ -2\gamma^2 U & S \end{pmatrix} \tag{3.2.11}$$

$$[B_p] = \begin{pmatrix} \frac{\epsilon_z}{\epsilon_o}\gamma^2 T & O \\ O & T \end{pmatrix} \tag{3.2.12}$$

The S, T and U matrices are square matrices of order n, the first two have already been given in Section 2.2 and the last has been derived in [42]. All three matrices are independent of the properties of the medium. These base (local) matrices are successively applied to the total number of triangles of a given structure to obtain the final (global) matrices. Thus summing the contributions I_p of all the triangles yields the following equation for I.

$$I = [\theta]^T[A][\theta] - \Gamma[\theta]^T[B][\theta] \tag{3.2.13}$$

where $[\theta]$ is an ordered array of the longitudinal electromagnetic nodal variables, $[A]$ is a large-sparse-indefinite-symmetric matrix and $[B]$ is a large-sparse-positive-definite-symmetric matrix. Taking the variation of equation (3.2.13) with respect to the nodal variables leads to the following algebraic eigenvalue problem:

$$[A][\theta] = \Gamma[B][\theta] \tag{3.2.14}$$

3.2.3 COMPUTATION OF THE PROPAGATION CONSTANT AND THE FIELD DISTRIBUTION

The normalized propagation constant γ is present in the matrices $[A]$ and $[B]$ of equation (3.2.14). For a given value of γ, the generalized eigenvalue equation (3.2.14) is solved for the frequency and the longitudinal electromagnetic nodal variables. All transverse field components can be derived from the longitudinal field values by the equations

$$\begin{aligned}
E_x^{(p)} &= \frac{j\omega\mu_o}{K_p^2}\left[\frac{\partial H_z^{(p)}}{\partial y} + \left(\frac{\epsilon_o}{\mu_o}\right)^{\frac{1}{2}}\gamma\frac{\partial E_z^{(p)}}{\partial x}\right], \\
E_y^{(p)} &= \frac{j\omega\mu_o}{K_p^2}\left[\frac{-\partial H_z^{(p)}}{\partial x} + \left(\frac{\epsilon_o}{\mu_o}\right)^{\frac{1}{2}}\gamma\frac{\partial E_z^{(p)}}{\partial y}\right], \\
H_x^{(p)} &= \frac{j\omega\epsilon_o}{K_p^2}\left[-\frac{\epsilon_p}{\epsilon_o}\frac{\partial E_z^{(p)}}{\partial y} + \left(\frac{\mu_o}{\epsilon_o}\right)^{\frac{1}{2}}\gamma\frac{\partial H_z^{(p)}}{\partial x}\right], \\
H_y^{(p)} &= \frac{j\omega\epsilon_o}{K_p^2}\left[\frac{\epsilon_p}{\epsilon_o}\frac{\partial E_z^{(p)}}{\partial x} + \left(\frac{\mu_o}{\epsilon_o}\right)^{\frac{1}{2}}\gamma\frac{\partial H_z^{(p)}}{\partial y}\right].
\end{aligned} \tag{3.2.15}$$

It is possible to use the symmetry conditions to reduce the number of elements by imposing the following boundary conditions on the axes:

$E_z = 0$ at the nodes on electric wall.

$H_z = 0$ at the nodes on magnetic wall.

The normalized propagation constant γ, which is a variational quantity, is obtained much more accurately than the associated field solution. Therefore, good accuracy of the loss and impedance calculations demands a larger number of elements than would be required for obtaining only γ with a similar accuracy.

3.2.4 SPURIOUS MODE DETECTION

The generalized eigenvalue equation (3.2.14) has a number of spurious solutions, especially for $\gamma > 1$. These solutions do not correspond to a physical mode of propagation. It has been observed by many authors working with the Finite Element method. There are some ways to identify such a mode and are given below:

1. Plot equipotential lines of suspected modes. These are not as smooth as they are for real modes. Sharp contours are usually absent from the real modes.

2. For $\gamma = 0$, the Vectorial Functional (3.2.6) becomes scalar, which is supposed to be free from spurious modes. Hence, by plotting the field distribution at cut off ($\gamma = 0$), one can have an idea of the actual field distribution.
3. The secondary parameters associated with spurious solutions, such as transmitted power and attenuation constants differ by orders of magnitude from those obtained for regular solutions.
4. Recompute with a different discretization and check.
5. Compare with other numerically stable procedure such as the TLM method.

3.2.5 COMPUTATION OF CONDUCTOR AND DIELECTRIC LOSSES

The perturbational approach is employed to solve for the attenuation constants due to dielectric and conductor losses

$$\alpha_d = \frac{P_d}{2P_{av}}, \quad \alpha_c = \frac{P_c}{2P_{av}} \tag{3.2.16}$$

where P_{av} is the time-average power flow along the line, and P_d and P_c are the time-average powers dissipated in the dielectric and conductors, respectively .

Dielectric losses are calculated using the formula

$$P_d = \omega \epsilon \ tan\delta \iint_{S_{diel}} |E_o|^2 \, dS \tag{3.2.17}$$

where the loss tangent tanδ is assumed to be very small so that the perturbed fields can be approximated by the fields for the lossless condition E_o, H_o ; S_{diel} is the area of the cross-section covered by the dielectric; and $\omega = 2\pi f$ is the angular frequency. Expanding (3.2.17), P_d can be written as

$$P_d = \omega \epsilon \ tan\delta \iint_{S_{diel}} (E_x^2 + E_y^2 + E_z^2) \, dx \ dy \tag{3.2.18}$$

For any generalized structure, the above integrals can be written in terms of standard matrices as follows:

$$P_d = \omega \sum_{i=1}^{NOTRD} \epsilon_i \tan\delta_i \Big([\theta^i_{1E}]^T [T] [\theta^i_{1E}] + [\theta^i_{2E}]^T [T] [\theta^i_{2E}] + [\theta^i_{3E}]^T [T] [\theta^i_{3E}] \Big) \tag{3.2.19}$$

where $NOTRD$ is the number of elements in the dielectric region, the matrix T is given in the Section 2.2.2, and $[\theta^i_{1E}]$, $[\theta^i_{2E}]$ and $[\theta^i_{3E}]$ are the electric field values at the nodes of ith triangle.

$$\begin{aligned} [\theta^i_{1E}]^T &= [E^i_{x1}, E^i_{x2}, \cdots, E^i_{xn}] \\ [\theta^i_{2E}]^T &= [E^i_{y1}, E^i_{y2}, \cdots, E^i_{yn}] \\ [\theta^i_{3E}]^T &= [E^i_{z1}, E^i_{z2}, \cdots, E^i_{zn}] \end{aligned} \tag{3.2.20}$$

Thus by knowing the electric nodal variables, the dielectric loss P_d can be computed.

The time-average power flow along the z-direction can be written as

$$P_{av} = \iint_S Re(\vec{E}_o \times \vec{H}^*_o).\hat{a}_z \, ds \tag{3.2.21}$$

where S is the cross section of the guide. In terms of the transverse field components, this latter equation is written as

$$P_{av} = \iint_S Re(E_x H^*_y - E_y H^*_x) \, dx \, dy \tag{3.2.22}$$

After substituting the expressions (3.2.15) for E_x, E_y, H_x and H_y into the above equation, one obtains:

$$\begin{aligned} P_{av} = \frac{\omega^2 \mu_o}{2} \sum_{p=1}^{NOTR} \frac{\epsilon_o}{K_p^4} \iint_S \Bigg[\Bigg\{ & \epsilon_p \frac{\partial H^p_z}{\partial y} \frac{\partial E^p_z}{\partial x} + \sqrt{\frac{\mu_o}{\epsilon_o}} \, \gamma \frac{\partial H^p_z}{\partial y} \frac{\partial H^p_z}{\partial y} + \epsilon_p \sqrt{\frac{\epsilon_o}{\mu_o}} \, \gamma \frac{\partial E^p_z}{\partial x} \frac{\partial E^p_z}{\partial x} \\ & + \gamma^2 \frac{\partial E^p_z}{\partial x} \frac{\partial H^p_z}{\partial y} \Bigg\} - \Bigg\{ \epsilon_p \frac{\partial H^p_z}{\partial x} \frac{\partial E^p_z}{\partial y} - \sqrt{\frac{\mu_o}{\epsilon_o}} \, \gamma \frac{\partial H^p_z}{\partial x} \frac{\partial H^p_z}{\partial x} - \epsilon_p \sqrt{\frac{\epsilon_o}{\mu_o}} \, \gamma \frac{\partial E^p_z}{\partial y} \frac{\partial E^p_z}{\partial y} \\ & + \gamma^2 \frac{\partial H^p_z}{\partial x} \frac{\partial E^p_z}{\partial y} \Bigg\} \Bigg] \, dx dy \end{aligned} \tag{3.2.23}$$

By substituting the expressions for E_z and H_z from equation (3.2.7) and using the matrix equivalents of the various integrals [44], the above equation can be written in matrix form as follows:

$$\begin{aligned} P_{av} = \omega^2\mu_o \sum_{i=1}^{NOTR} \frac{\epsilon_i}{K_i^4} \Bigg[\Bigg\{ & (\epsilon_i + \gamma^2)[\theta_{3H}^i]^T[Z][\theta_{3E}^i] + \sqrt{\frac{\mu_o}{\epsilon_o}}\gamma\,[\theta_{3H}^i]^T[D][\theta_{3H}^i] \\ & + \epsilon_i\gamma\sqrt{\frac{\epsilon_o}{\mu_o}}[\theta_{3E}^i]^T[E][\theta_{3E}^i] \Bigg\} - \Bigg\{ (\epsilon_i + \gamma^2)[\theta_{3E}^i]^T[Z][\theta_{3H}^i] \\ & - \sqrt{\frac{\mu_o}{\epsilon_o}}\gamma\,[\theta_{3H}^i]^T[E][\theta_{3H}^i] - \epsilon_i\sqrt{\frac{\epsilon_o}{\mu_o}}\gamma\,[\theta_{3E}^i]^T[D][\theta_{3E}^i] \Bigg\} \Bigg] \end{aligned} \quad (3.2.24)$$

where

$$\begin{aligned} [\theta_{3E}^i]^T &= [E_{z1}^i, E_{z2}^i, \cdots, E_{zn}^i] \\ [\theta_{3H}^i]^T &= [H_{z1}^i, H_{z2}^i, \cdots, H_{zn}^i] \end{aligned} \quad (3.2.25)$$

The matrices $[Z]$, $[D]$ and $[E]$ are those given in [44] and can be computed by knowing the coordinates and areas of the triangles. $NOTR$ is the total number of elements. Thus by knowing the longitudinal field values, the time averaged power flow can be computed.

The perturbational formula for calculating the conductor loss of a transmission line with high conductivity conductor is given by

$$P_c = R_s \int_C |\vec{H}_o|^2{}_{tang}\,dl \quad (3.2.26)$$

where R_s is the surface resistance and $|\vec{H}_o|_{tang}$ is the magnitude of the tangential magnetic field at the conducting surfaces for the lossless case. For a conducting surface lying on the x-axis,

$$\int_C |\vec{H}_o|^2{}_{tang}\,dl = \sum \int_C (H_x^2 + H_z^2)\,dx \quad (3.2.27)$$

Expresssing (3.2.27) in terms of the longitudinal components yields,

$$P_c = R_s \int_C \left\{ \left(\frac{\omega\epsilon_o}{K_p^2}\right)^2 \left[\epsilon_r^2 \left(\frac{\partial E_z}{\partial y}\right)^2 + \frac{\mu_o}{\epsilon_o}\gamma^2 \left(\frac{\partial H_z}{\partial x}\right)^2 - 2\,\epsilon_r\gamma\sqrt{\frac{\mu_o}{\epsilon_o}}\frac{\partial E_z}{\partial y}\frac{\partial H_z}{\partial x} \right] + H_z^2 \right\} dx \quad (3.2.28)$$

Similarly, for a conducting surface lying on the y-axis,

$$\int_C |\vec{H}_o|^2{}_{tang}\, dl = \sum \int_C (H_y^2 + H_z^2)\, dx \tag{3.2.29}$$

In terms of the longitudinal components,

$$P_c = R_s \int_C \left\{ \left(\frac{\omega\epsilon_o}{K_p^2}\right)^2 \left[\epsilon_r^2 \left(\frac{\partial E_z}{\partial x}\right)^2 + \frac{\mu_o}{\epsilon_o}\gamma^2 \left(\frac{\partial H_z}{\partial y}\right)^2 - 2\epsilon_r \gamma \sqrt{\frac{\mu_o}{\epsilon_o}} \frac{\partial E_z}{\partial x}\frac{\partial H_z}{\partial y}\right] + H_z^2 \right\} dy \tag{3.2.30}$$

Since E_z and H_z are polynomials in x and y, the above expressions can be calculated analytically. Note that no numerical differentiation or integration is involved in the computation of losses.

3.2.6 COMPUTATION OF CHARACTERISTIC IMPEDANCE

Due to the hybrid wave propogation in the considered transmission lines (Finlines, Ridge waveguides, etc.) a unique definition of characteristic impedance does not exist. However, the most appropriate definition of characteristic impedance for most slot-type transmission structures has generally been found to be

$$Z_o = \frac{V^2}{2P_{av}} \tag{3.2.31}$$

where P_{av} is computed from equation (3.2.24). The voltage V can be expressed as follows:

$$V = \int_C |E_y|_{x=x_p}\, dy \tag{3.2.32}$$

where x_p is the x-coordinate of the position of the fin. The voltage can be further expressed in terms of the longitudinal components as follows:

$$V = \frac{j\omega\mu_o}{K_p^2} \int_C \left(-\frac{\partial H_z}{\partial x} + \sqrt{\frac{\epsilon_o}{\mu_o}}\, \gamma\, \frac{\partial E_z}{\partial y} \right)\Bigg|_{x=x_p} dy \tag{3.2.33}$$

Again, since E_z and H_x are polynomials in x and y, the above integral can be calculated analytically. Alternatively, by integrating the tangential magnetic fields, the current around the fins can be computed, leading to current-power definition of characteristic impedance.

3.3 APPLICATIONS OF THE FINITE ELEMENT METHOD

On the basis of this Finite Element procedure, a computer program has been developed. This program has unprecedented flexibility since it can evaluate structures with arbitrary cross-sectional geometry. Two additional algorithms have also been developed to simplify the initialization, or geometry definition and they do the following:

i. Convert the parameters (node numbers, x and y coordinates) of first order triangles to those of second order triangles. This greatly simplifies the inputting procedure.

ii. Search for the triangle, among a set of triangles, on which a given point lies. This helps in plotting the equipotential lines.

A very large number of elements are taken around the fin edges to account for the singularities. A CRAY X-MP/22 Supercomputer has been used for computation.

In order to test the program, the characteristics of some standard structures have been recalculated, knowing well that for these cases, other methods are more efficient. After program validation, some novel structures have been analyzed.

3.3.1 DIELECTRICALLY LOADED RIDGED WAVEGUIDES

The computed values of the normalized propagation constant, characteristic impedance and losses of a dielectric-loaded ridged waveguide are plotted in Figs. 3.1(a) and 3.1(b). It is seen that with the dielectric present, the cutoff frequencies are reduced, and the propagation constants are increased. The results for propagation constant and characteristic

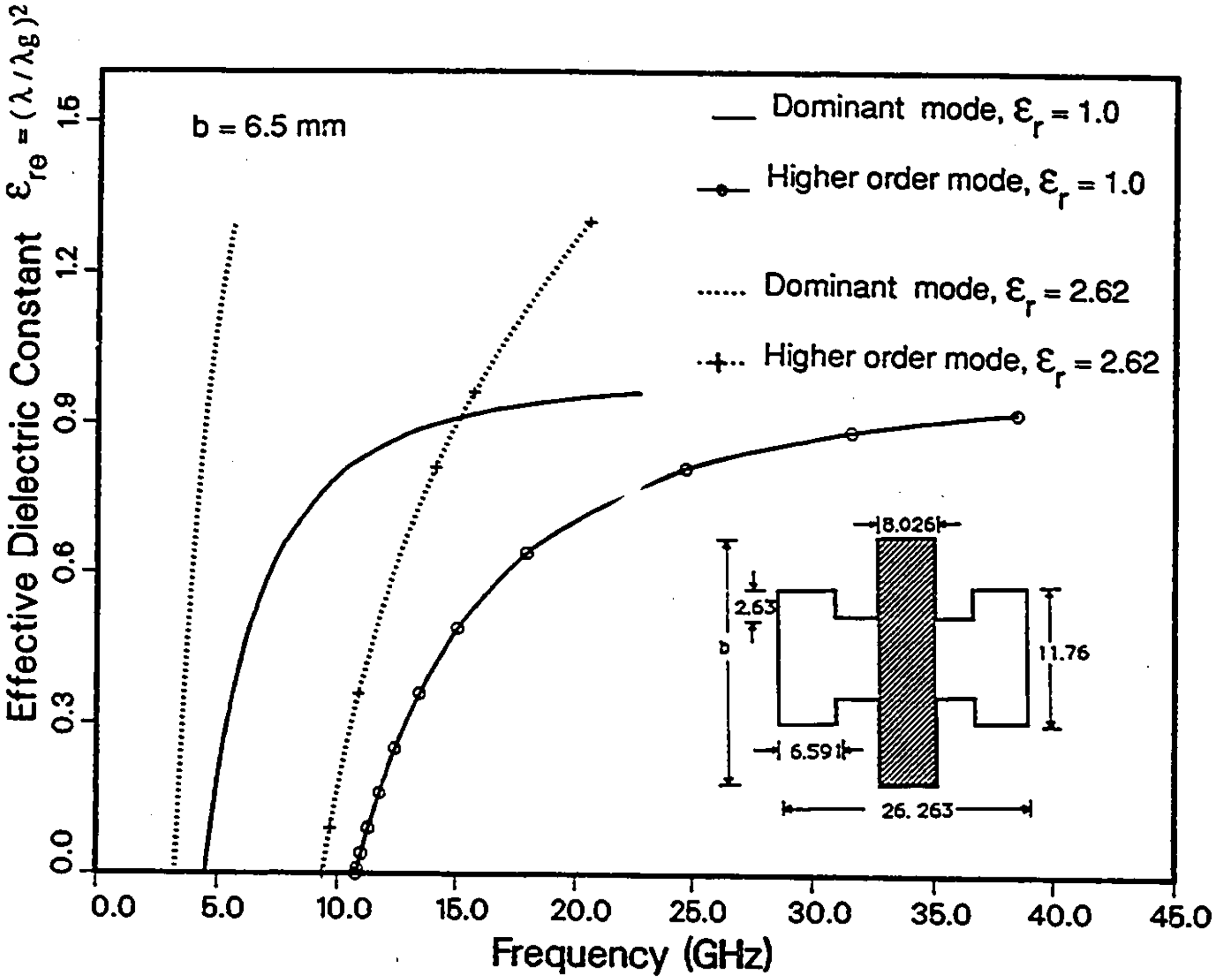

Fig. 3.1(a) : Dispersion Characteristics of a Dielectrically Loaded Ridge Waveguide (Dimensions are in millimeters).

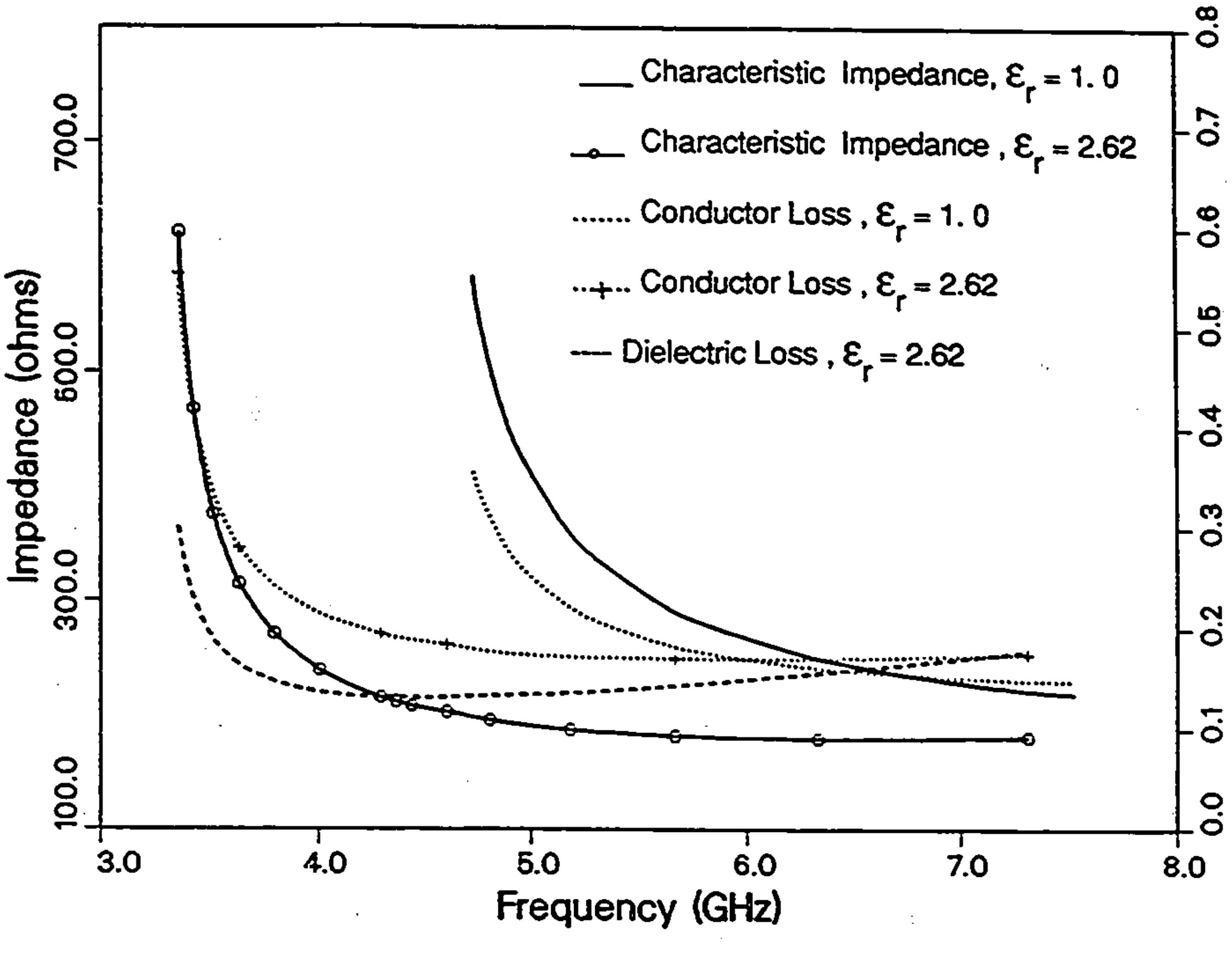

Fig. 3.1(b) : Characteristic Impedance and Losses of a Dielectrically Loaded Ridge Waveguide. $\tan\delta = 2*10^{-4}$, $\rho = 3*10^{-8}$ Ohm m.

impedance are compared with the available data [73] in Table 3.1 for different slot heights. In all cases close agreement is observed.

SLOT HEIGHT b(mm)	$\varepsilon_r = 1.0$						$\varepsilon_r = 2.62$					
	ε_{re}	Frequency (GHz)		Char. Impedance (Ohms)			ε_{re}	Frequency (GHz)		Char. Impedance (Ohms)	
		Present Method	Results of [73]	Present Method	Results of [73]			Present Method	Results of [73]	Present Method	Results of [73]
6.502	0.4277	5.969	5.950	267.56	265.16		1.366	5.955	5.950	179.91	177.83
7.620	0.3869	5.976	5.950	303.60	300.77		1.2668	5.977	5.950	202.17	202.83
8.890	0.3558	5.977	5.950	333.70	330.40		1.1063	6.074	5.950	231.19	224.47

Table 3.1 : Effect of Slot Height on the Guide Parameters of Dielectrically Loaded Ridge Waveguide (Dimensions defined in Fig. 3.1(a))

3.3.2 BILATERAL FINLINES IN RECTANGULAR WAVEGUIDE ENCLOSURES

The computed dispersion characteristics of the dominant and higher-order modes in a bilateral finline are shown in Fig. 3.2. The results for zero metallization thickness are in good agreement with data published by Schmidt [14] computed with the Spectral Domain Technique. For a metallization thickness t =35 μm, the cutoff frequency of the dominant mode is slightly reduced because of increased capacitive loading of the guide. However, as the frequency increases, the crossover of the dispersion curves takes place. This may be attributed to the parallel plate phenomenon because of the confinement of energy into the slot region. The dispersion characteristics of the higher mode remain unchanged. These results for finite metallization thickness conform with those given in [17]. The influence of the groove depth g on the propagation constant was also studied. It was found that the effect is negligible for the fundamental mode and the higher order mode $HE7$ (which are

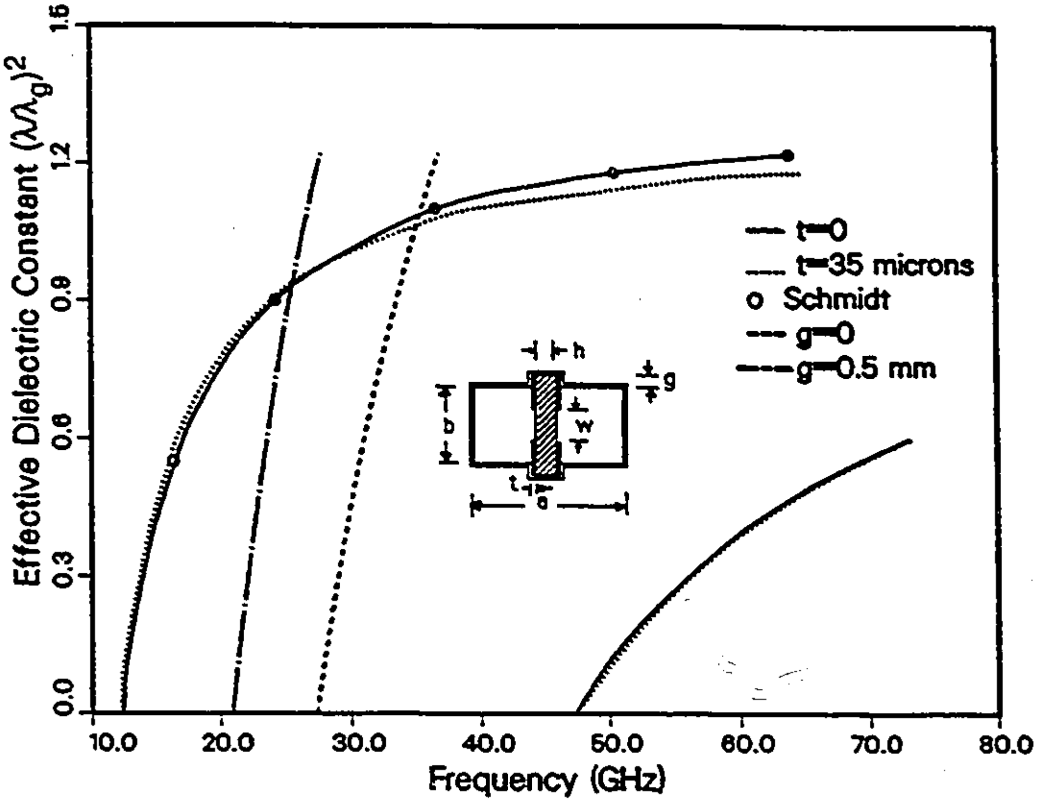

Fig. 3.2 : Dispersion Characteristics of a Bilateral Finline in Rectangular Waveguide (WR28) Housing. ε_r= 3.0, h=0.125 mm, w=0.5 mm. — HE1 and HE7 modes for t=0 and g=0; ..... HE1 and HE7 modes for t=35 μm and g=0; --- HE2 mode for t=0 and g=0; _ . _ HE2 mode for t=0 and g=.5 mm.

excited by a TE_{10} mode of the empty waveguide) as reported in [16] and [18]. However, the propagation characteristics of the second higher order mode $HE2$ is strongly affected. This behaviour is illustrated in Fig 3.2. The sensitivity of the second mode may be due to the fact that the fields for this mode are not concentrated around the fin edges and are rather confined between the two metal fins as in a parallel-plate capacitor. Hence, the cutoff frequency for this mode is reduced with increasing groove depth.

In order to test the program for loss calculations, the conductor and dielectric losses of a homogeneously filled rectangular waveguide ($WR28$) have been computed at various frequencies. The dielectric had an ϵ_r of unity and a loss tangent of 2×10^{-8}. The resistivity of the walls was 3×10^{-8} Ω m. Results are summarised in Table 3.2. The results agree very well with the analytical values, thus supporting the accuracy of the presented numerical algorithm.

The conductor and dielectric losses of a bilateral finline in rectangular waveguide enclosure ($WR28$) are given in Fig. 3.3(a). It is seen that as the gapwidth is reduced, the conductor loss increases exponentially. This can be explained by the fact that, with small gapwidths there is heavy concentration of fields near the gap. The dielectric losses are very small compared to the conductor losses. The conductor loss per wavelength for various gapwidths is plotted in Fig. 3.3(b) as function of frequency. It appears that the losses obtained are between those of Mirshekar and Davies [74] and Olley and Rozzi [75] (assuming that the losses for bilateral and unilateral finlines are almost equal [74]). Independent measurement results are difficult to obtain. R.N. Bates and M.D. Coleman [76] have reported measured losses for bilateral finlines with slot widths of 400 μm. These are given in Table 3.3. These measured losses are higher than our computed results. When the number of elements around the fin edges is increased (to account for the singularities),

Finite Element Method Results			Analytical Results	
Frequency (GHz)	Conductor Loss (dB/m)	Dielectric Loss (dB/m)	Conductor Loss (dB/m)	Dielectric Loss (dB/m)
20.000	0.528	0.549	0.530	0.550
25.000	0.425	0.567	0.427	0.568
28.474	0.402	0.608	0.403	0.609
38.273	0.389	0.755	0.389	0.756

Table 3.2 : Losses in Homogeneously Filled Waveguide
a=10 mm, b=5 mm, $\tan\delta=2*10^{-4}$, $\rho=3*10^{-8}$ Ohm m, $\varepsilon_r=1.0$

Substrate	Thickness (microns)	Cu Metal-lization (microns)	Loss (dB/cm)		
			27 GHz	33.5 GHz	40GHz
Duroid 5880	127	17	0.06	0.06	0.06
Duroid 5880	254	17	0.07	0.07	0.13
Mylar	100	5	0.08	0.10	0.13
Kapton	75	34	0.13	0.14	0.20
Kapton	150	34	0.24	0.34	0.36

Table 3.3 : Measured Losses for Bilateral Finlines in WR28 Waveguide Enclosures. w=0.4 mm

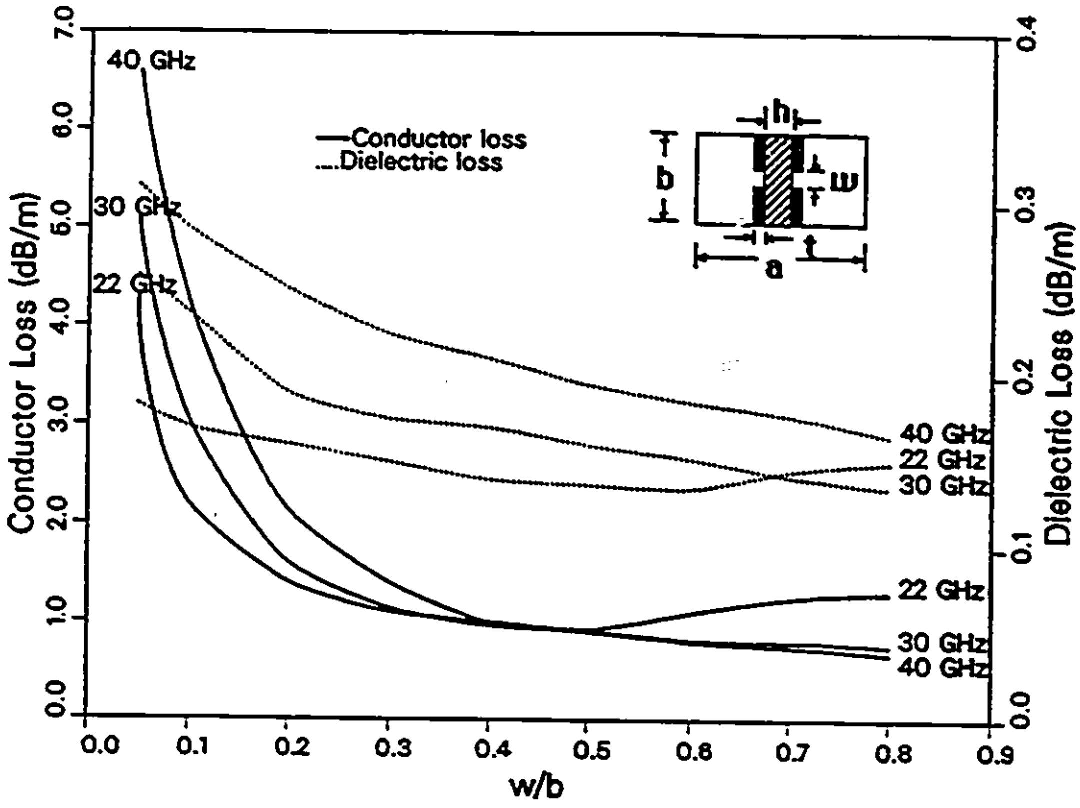

Fig. 3.3(a) : Conductor and Dielectric Losses as Function of Gapwidth (w) of a Bilateral Finline in Rectangular Waveguide Housing (WR28). h=0.254 mm, ε_r=2.22, tanδ=2*10^{-4}, ρ=3*10^{-8} Ohm m.

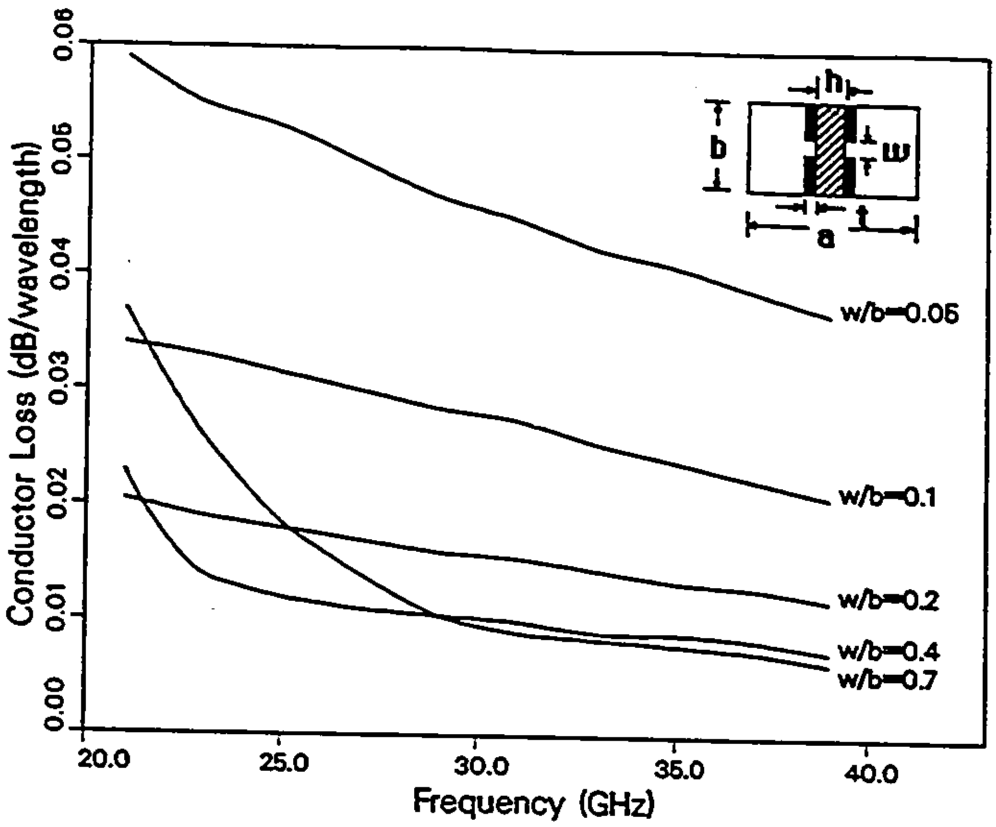

Fig. 3.3(b) : Conductor Loss per Wavelength as Function of Frequency of a Bilateral Finline in Rectangular Waveguide Housing (WR28). h=0.254 mm, ε_r=2.22, tanδ=2*10^{-4}, ρ=3*10^{-8} Ohm m.

the results changed by about two percent. Since in practice the measured losses are always higher than predicted by theory because of the surface roughness, irregularities in the structure, and anomalous skin effect, etc., the computed losses with the Finite Element algorithm are believed to be more accurate.

Having validated the Finite Element program by analysing some well known structures, it has been applied to analyse some new structures, and to study the effect of substrate bending which were not addressed before.

3.3.3 EFFECT OF SUBSTRATE BENDING

Bending of the substrate can occur when soft materials are used (mounting grooves too narrow result in displacement of dielectric material, producing bending). The propagation characteristics computed with bent substrate for deflections d equal to 0.125 mm and 0.25 mm are compared with those of the straight substrate in Fig 3.4. It is found that the change in the propagation constant is negligible near cutoff, and is slightly higher in the operating frequency band of the waveguide enclosure. This is attributed to the increased volume of dielectric material (due to bending) in the structure and the progressive confinement of energy in the dielectric as frequency increases.

3.3.4 BILATERAL FINLINES IN CIRCULAR WAVEGUIDE ENCLOSURES

It is interesting to note that an Ultra-Bandwidth Finline Coupler in circular waveguide housing was reported as early as in 1955 [77]. However, no theoretical analysis of such a structure has ever been published, probably due to the complexity of the problem. The advantages of such structures are easy fabrication and compatibility of the dominant mode with TE_{11} mode of the circular waveguide.

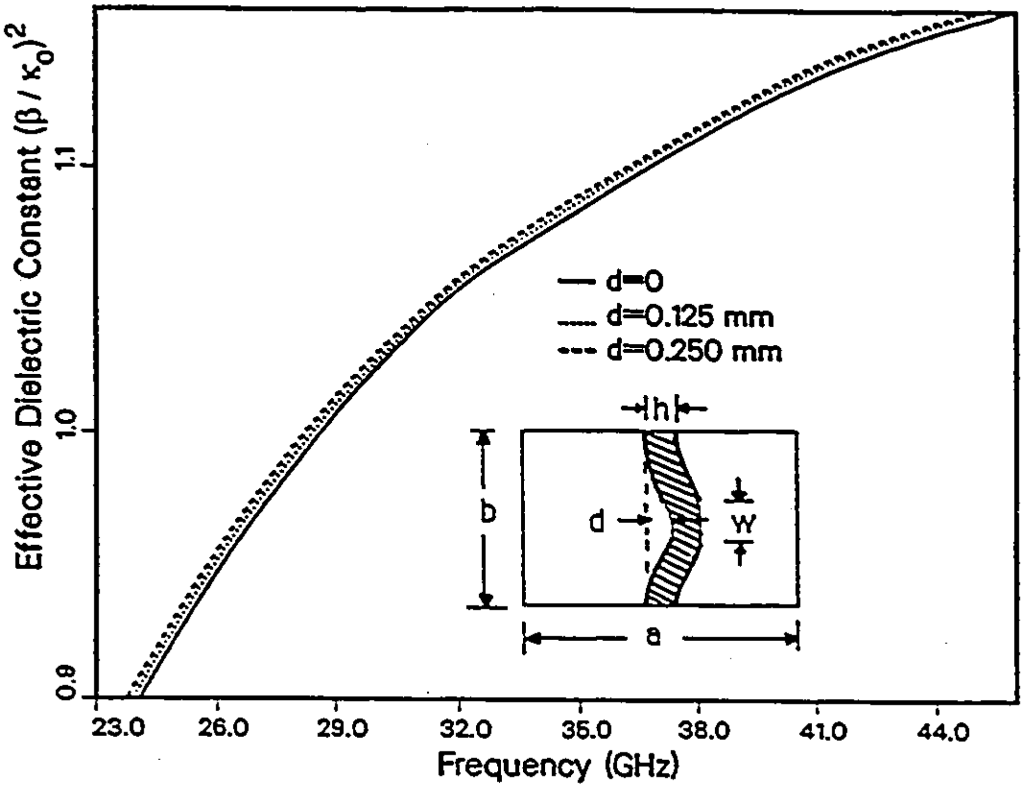

Fig. 3.4 : Dispersion Characteristics of a Bilateral Finline in Rectangular Waveguide Housing (WR28) with Bent Substrate for Different Values of Deflection d. ε_r= 3.0, h=0.125 mm, w=0.5 mm.

The dispersion characteristics for the fundamental mode and six higher order modes are given in Fig 3.5. All the results are obtained by analysing only one quarter of the structure with four combinations of electric and magnetic walls. The HE_1 and HE_7 modes (solid lines), which are excited by a TE_{11} wave incident on the empty circular waveguide, will define the actually relevant monomode range. The electric field plots for the various modes are shown in Fig. 3.6.

3.3.5 RIDGED BILATERAL FINLINES IN RECTANGULAR WAVEGUIDE ENCLOSURES

The computed dispersion characteristics of the dominant and higher-order modes in a bilateral finline with and without the ridge are shown in Fig. 3.7. The results for zero ridge thickness are in good agreement with the results obtained using the Spectral Domain Method [14]. With the ridge present, the cutoff frequency of the dominant mode is not affected, as expected. This is because the capacitive loading of the fins dominates that of the ridge. However, the effective dielectric constant decreases as the frequency increases. The cutoff frequency of the higher-order mode is increased considerably, thus increasing the monomode bandwidth. Note that in this operating range the dispersion is very small. The conductor loss is not expected to be highly influenced by the ridge. The electric field plots for the dominant mode are shown in Fig. 3.8. The average power distribution (power density across the structure) for the dominant mode is shown in Fig. 3.9. It is seen that the power density is very large near the fins. A PIN-diode attenuator in this technique has been realized successfully by AEG [78] with a bandwidth of two octaves.

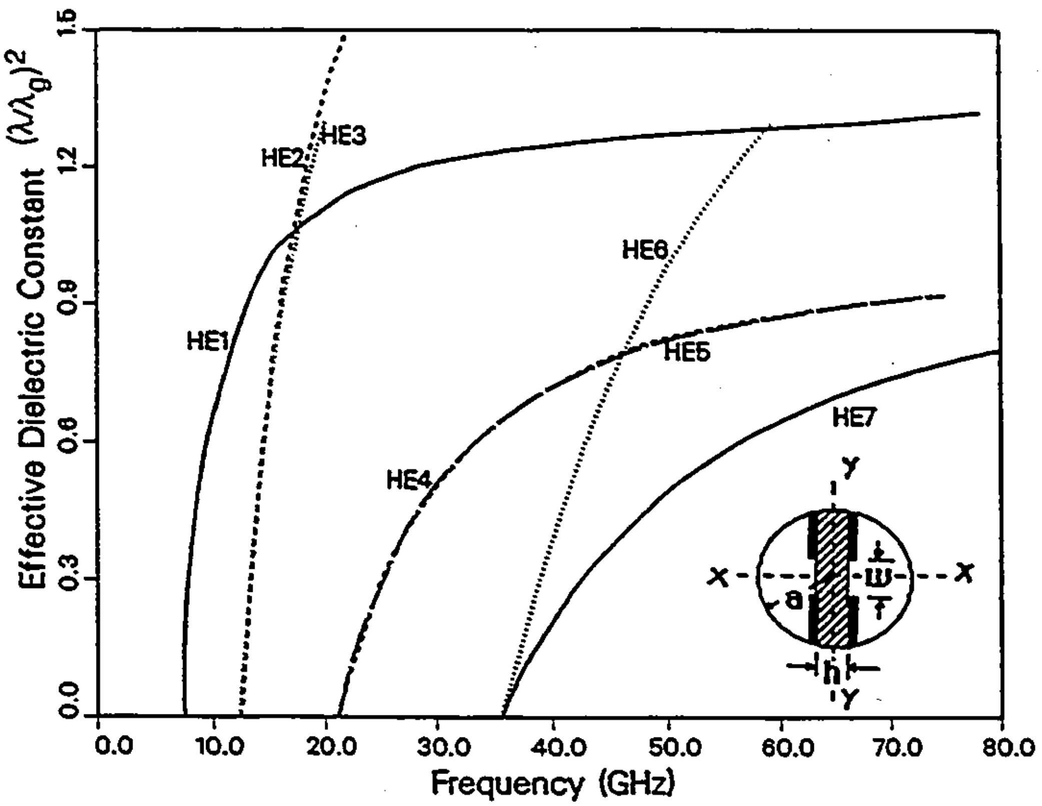

Fig. 3.5 : Dispersion Characteristics of a Bilateral Finline in Circular Waveguide Housing (WC33). a=4.165 mm, h=0.254 mm, w=0.3 mm, ε_r=2.2.

__ Magnetic Wall along YY, Electric Wall along XX;
— Electric Wall along YY, Magnetic Wall along XX;
..... Electric Wall along YY, Electric Wall along XX;
_._ Magnetic Wall along YY, Magnetic Wall along XX.

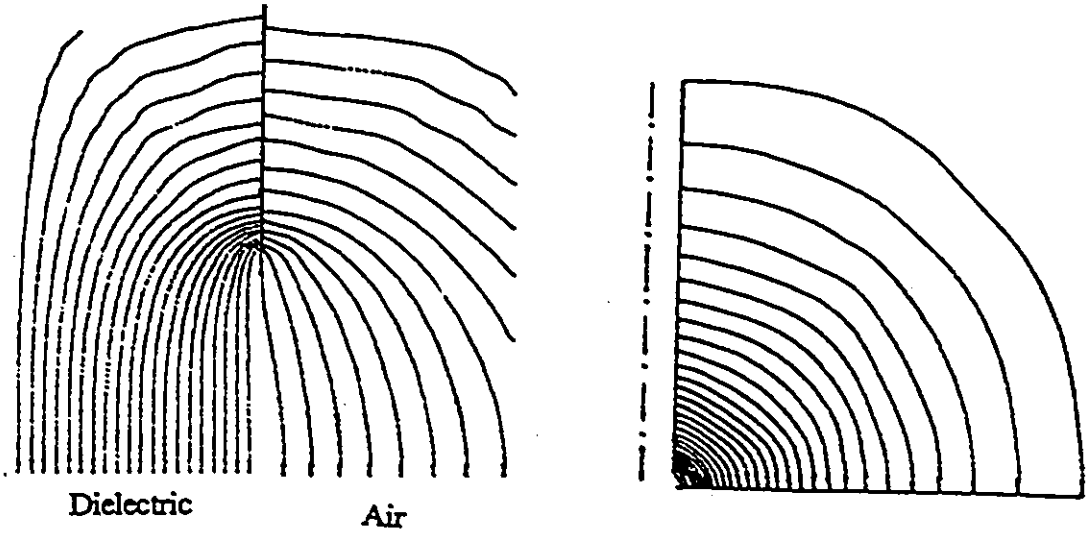

(a) (b)

Dominant Mode (HE1 Mode)

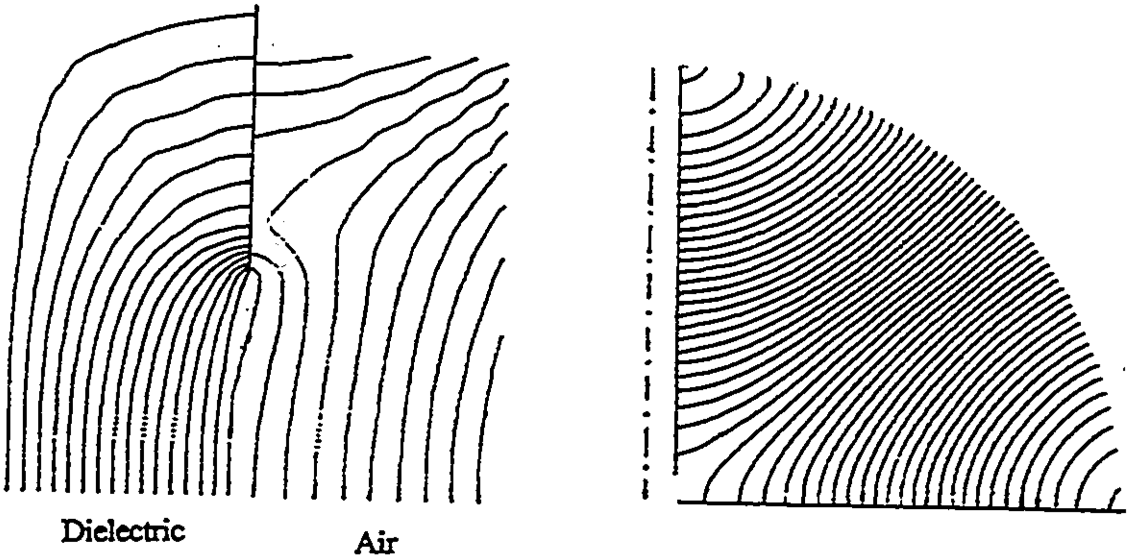

(a) (b)

HE7 Mode

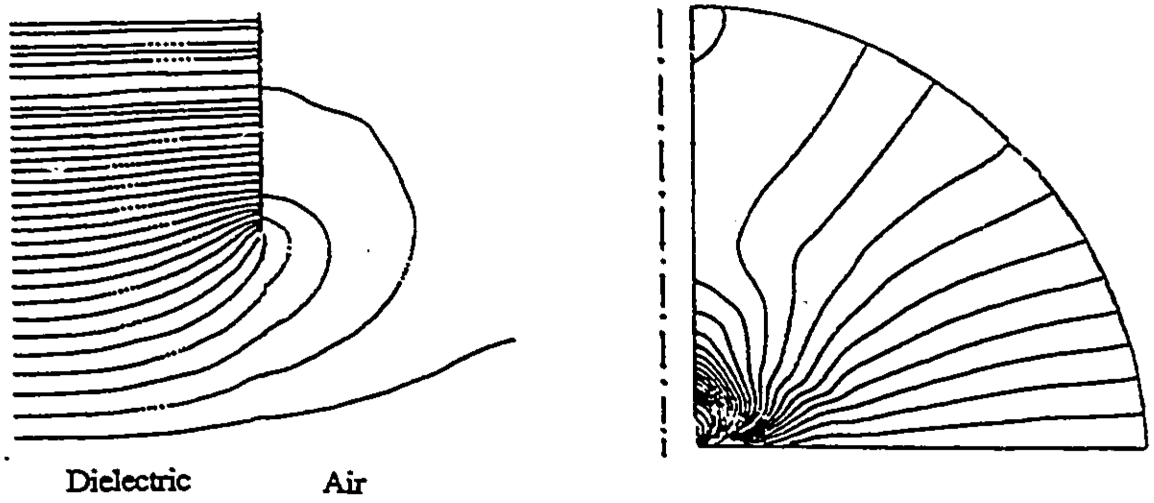

(a) (b)

HE2 Mode

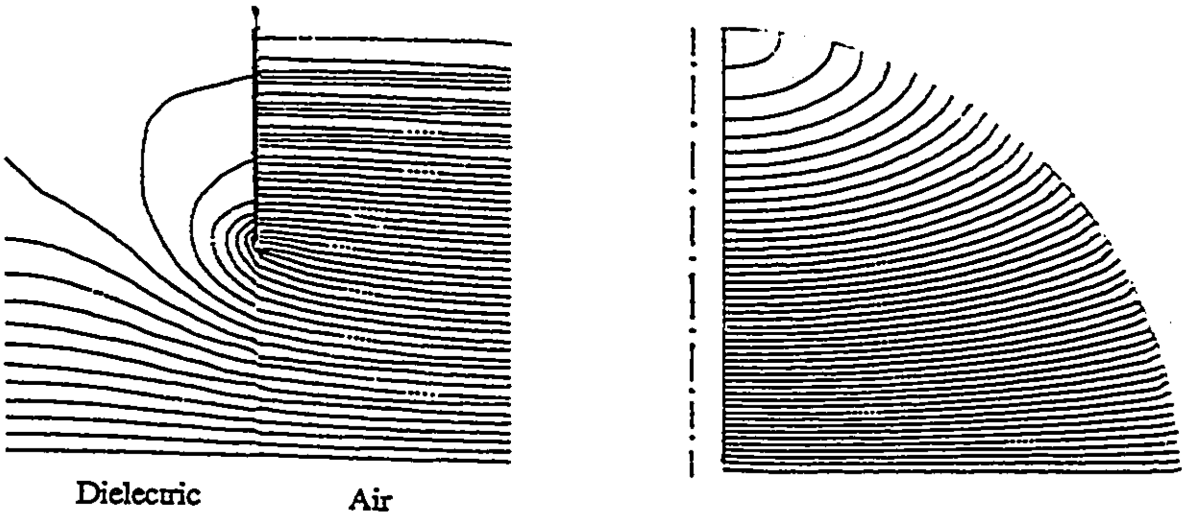

(a) (b)

HE4 Mode

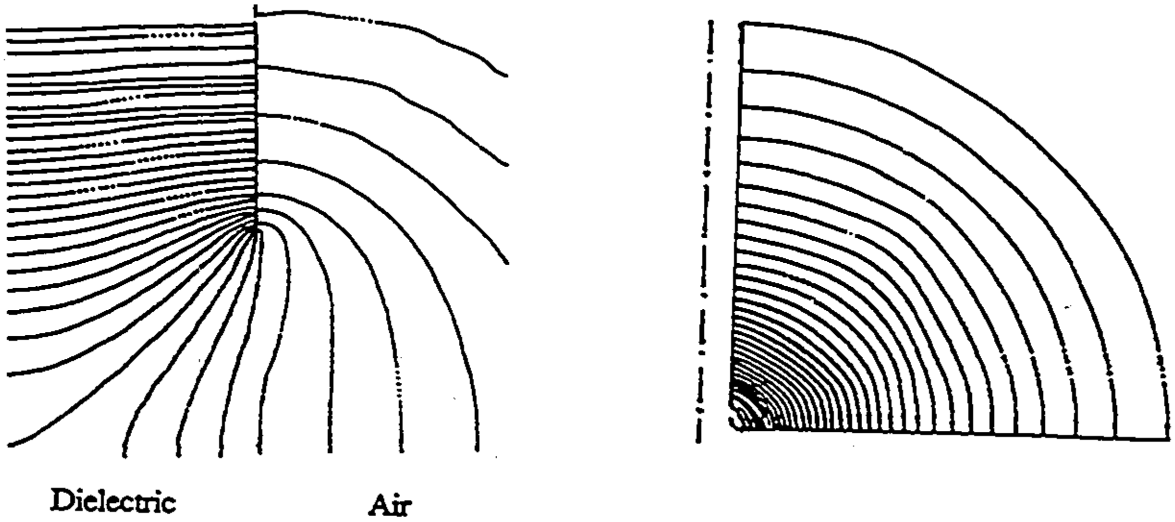

(a) (b)

HE3 Mode

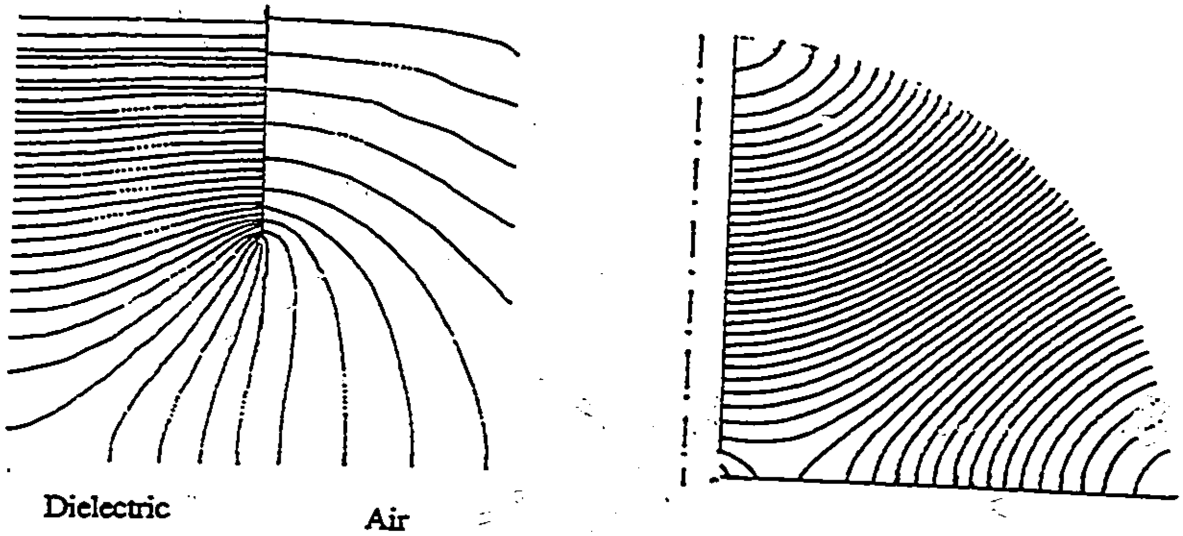

(a) (b)

HE6 Mode

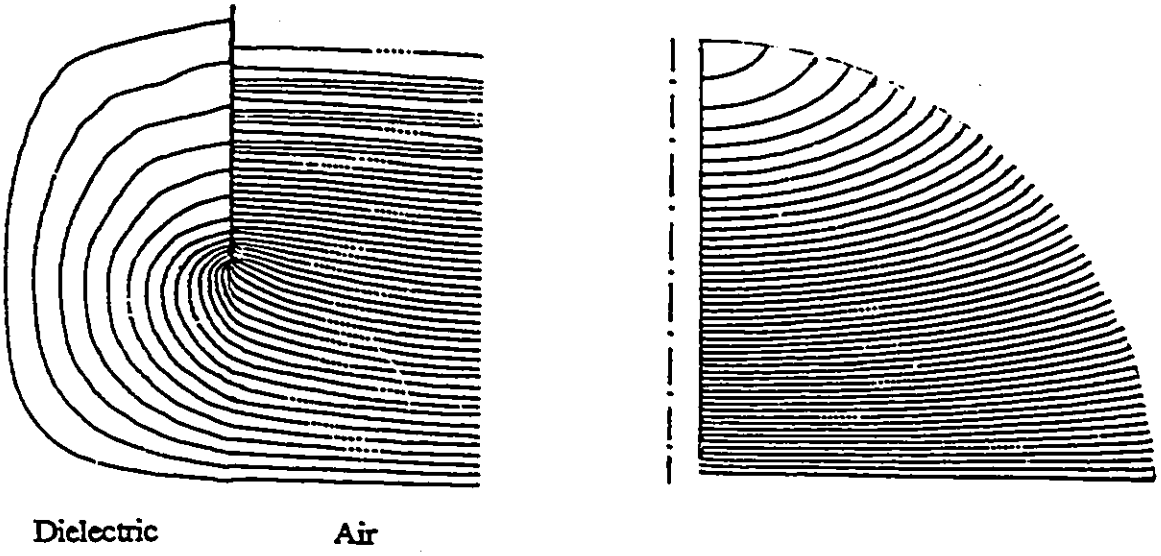

(a)

(b)

HE5 Mode

Fig. 3.6 : Electric Field Lines of the Dominant Mode and Higher Order Modes at Cutoff in a Bilateral Finline in Circular Waveguide Housing (WC33). a=4.165 mm, h=0.254 mm, w=0.3 mm, ε_r= 2.2.

(a) : Field in the Slot Region

(b) : Field in the Air Region (Only One Quarter of Cross-Section Shown).

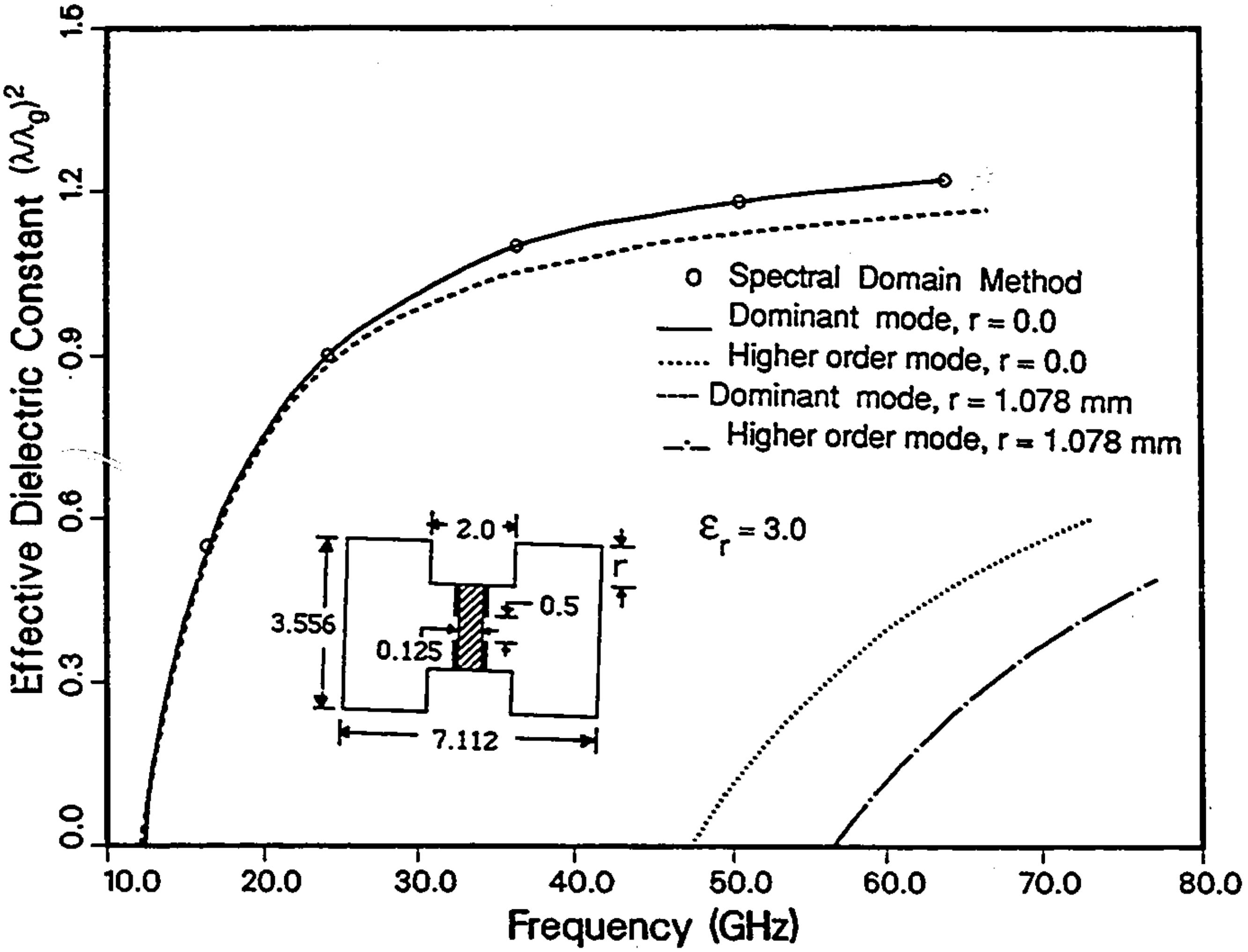

Fig. 3.7 : Dispersion Characteristics of a Ridged Bilateral Finline
(Dimensions are in millimeters)

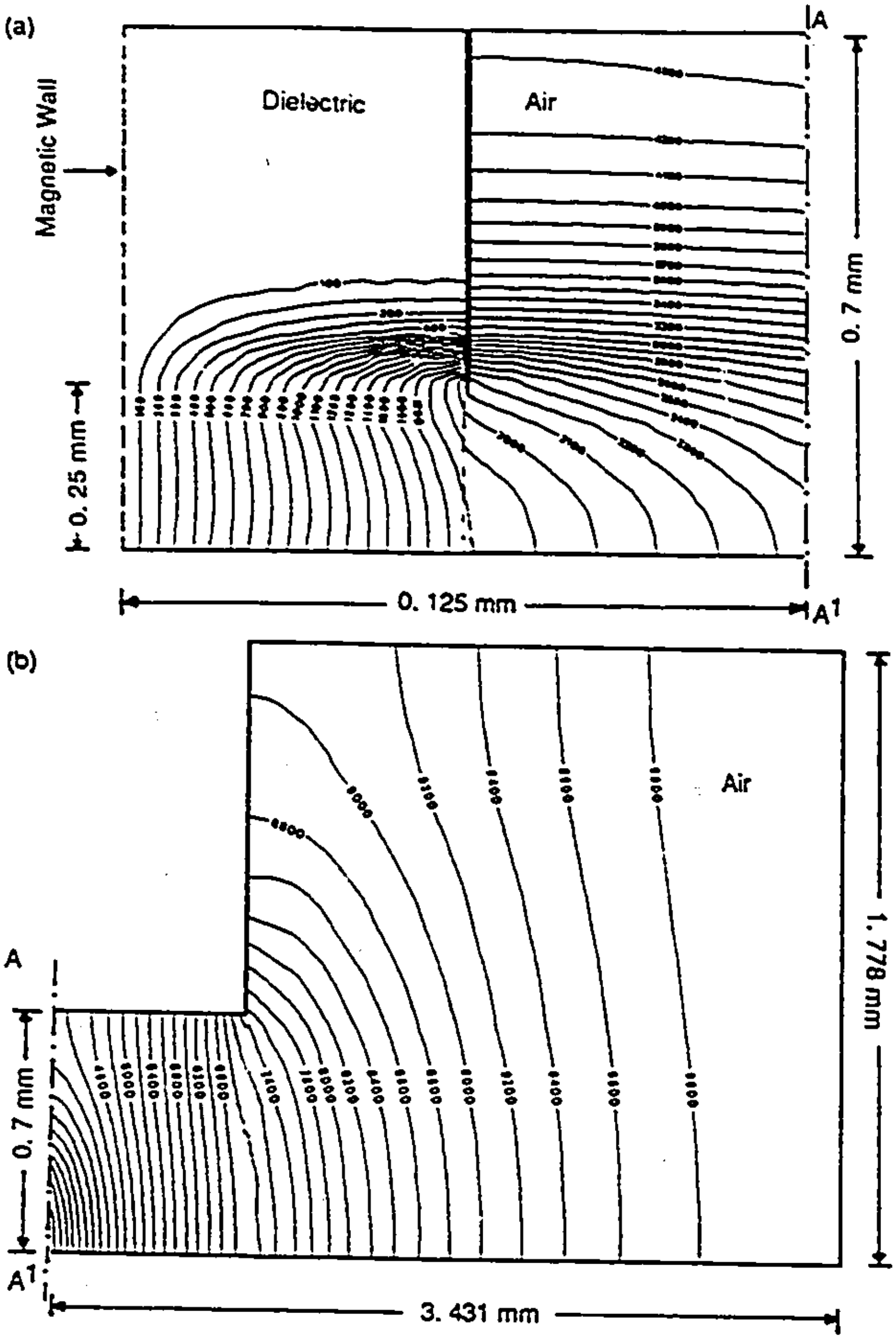

Fig. 3.8 : Electric Field Lines of the Dominant Mode at Cutoff in a Bilateral Ridged Finline (Only the upper right quadrant of the cross-section is shown).

(a) Enlarged region around the fin edge,

(b) Remaining air-filled region.

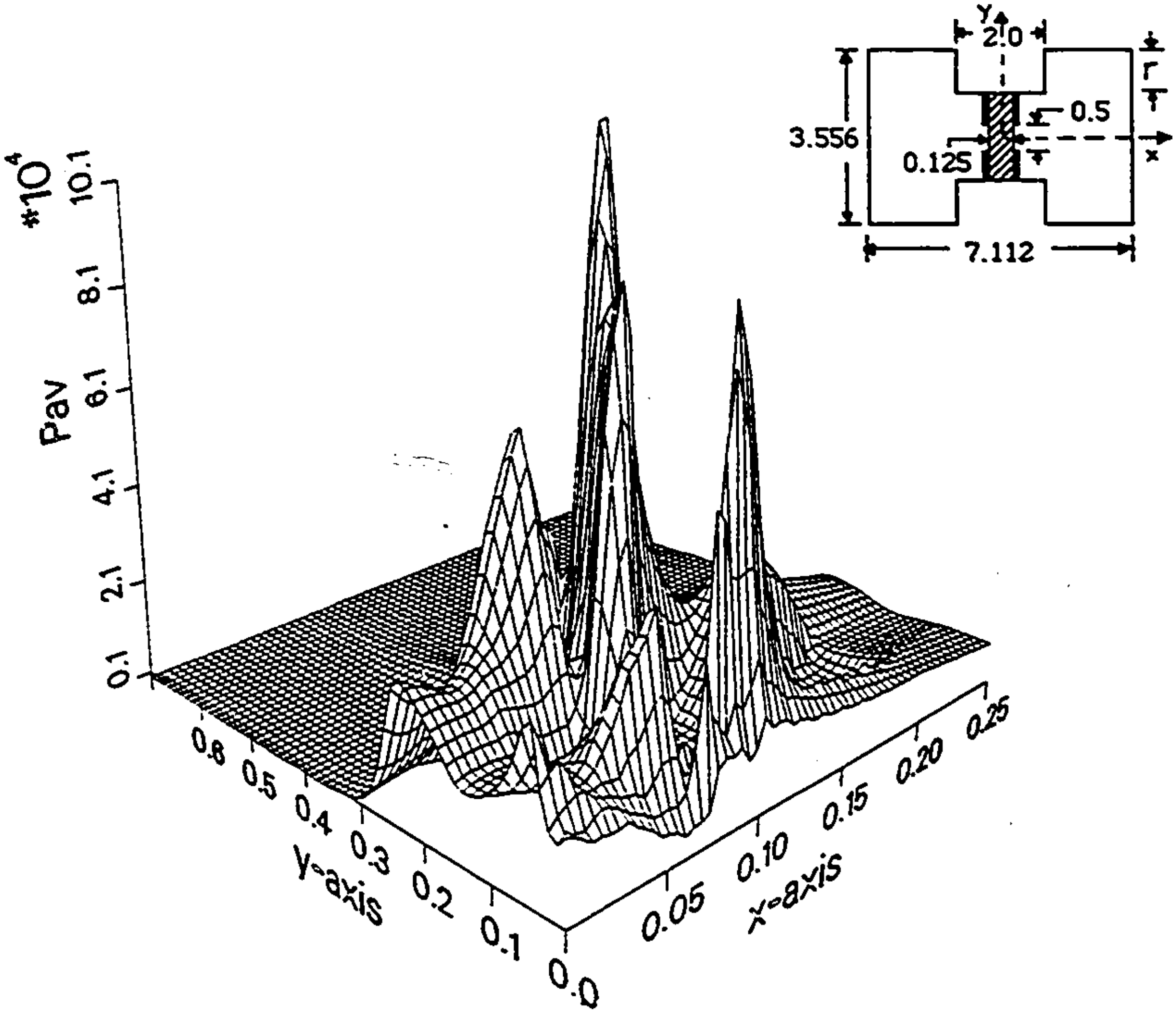

Fig. 3.9 : Average Power (Watts/mt^2) Distribution Around the Fin for the Fundamental Mode of Ridged Bilateral Finline

3.4 STUDY OF BILATERAL FINLINES IN RECTANGULAR AND CIRCULAR WAVEGUIDE ENCLOSURES WITH 2D-GRADED MESH TLM METHOD

Bilateral finlines in circular and rectangular waveguides have also been analysed using the graded mesh TLM technique discussed in Section (2.3.2).

The bilateral finlines in rectangular and circular waveguide enclosures are shown in Fig. 3.10. The cutoff frequencies computed for a bilateral finline in rectangular waveguide enclosure with different grading ratios are shown in Table 3.4. Only one quarter of the structure is analysed because of the symmetry of the structure. It is seen that as the number of iterations increases, the peaks of E_y, H_x and H_z come closer. The results compare well with the results obtained using the Spectral Domain Method. The comparison of the CPU time for various grading ratios is shown in the Table 3.5. The CPU time is four times less for a grading ratio of 5:1.

The computed cutoff frequencies for bilateral finlines in circular waveguide enclosure are given in Table 3.6. The results agree with the results computed using Finite Element Method. As expected, for finite metallization thickness, the cutoff frequency is decreased because of increased capacitive loading. Higher-order mode cutoff frequencies computed with various combinations of electric and magnetic walls along the symmetry lines XX and YY are compared with the results obtained using the Finite Element Method in Table 3.7. The discrepancies in cutoff frequencies may be attributed to the coarse discretization.

3.5 CONCLUSION

In this chapter, a Finite Element procedure is described to handle shielded microwave and millimeter wave transmission lines with arbitrary cross-sectional geometries. This

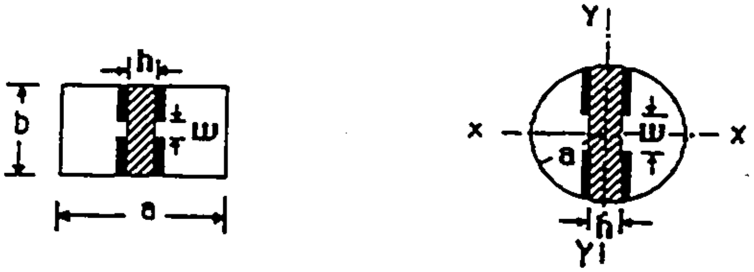

Fig. 3.10 : Bilateral Finlines in Rectangular and Circular Waveguide Enclosures.

GRAD.RATIO	(a) 1:1			(b) 3 : 1			(c) 5 : 1		
B (mm)	3.556			3.4544			3.6707		
NO. OF ITERATIONS	FREQUENCY (GHz)			FREQUENCY (GHz)			FREQUENCY (GHz)		
	Ey	Hx	Hz	Ey	Hx	Hz	Ey	Hx	Hz
1000	12.20	13.30	13.30	13.00	15.10	13.90	12.30	13.85	13.60
1500	11.80	12.30	12.30	12.40	13.30	13.15	11.80	12.45	12.45
2000	11.60	11.90	11.90	12.10	12.50	12.55	11.60	12.00	11.90
2500	11.60	11.80	11.80	11.95	12.25	12.25	11.60	11.95	12.10
3000	11.60	11.70	11.70	11.95	12.10	12.10	11.40	11.60	11.60
Spectral Domain Result	11.734			11.903			11.487		

Table 3.4 : Cutoff Frequencies of a Bilateral Finline in Rectangular Waveguide Housing (WR 28), computed with the TLM Method.

$a = 7.112$ mm, $\varepsilon_r = 2.2$

(a), (b) : $w = h = 0.7112$ mm, (c) : $w = h = 0.688$ mm

GRADING RATIO N	CPU TIME (minutes)	GRID SIZE
1:1	12	52x27
3:1	6	33x21
5:1	3	22x16

Table 3.5 : Comparison of Computer Run Time for different Grading Ratios (TLM)

METALLIZATION THICKNESS (mm)	NO. OF ITERATIONS	FREQUENCY (GHz)		
		Ey	Hx	Hz
0.0	1000	9.53	10.60	10.40
	1500	9.265	9.81	9.655
	2000	9.18	9.50	9.39
	2500	9.16	9.30	9.32
0.085	2500	9.11	9.265	9.265

Table 3 6 : Cutoff Frequencies of a Bilateral Finline in Circular Waveguide Housing (WC33) (TLM) $\varepsilon_r = 2.2$, w = h = 1.53 mm

SYMMETRY CONDITIONS		TLM METHOD		FINITE ELEMENT METHOD	
XX	YY	First mode (GHz)	Second mode (GHz)	First mode (GHz)	Second mode (GHz)
electric	magnetic	9.26	37.116	9.266	37.795
magnetic	electric	12.46	21.816	13.346	22.576
electric	electric	12.55	33.875	13.789	34.683
magnetic	magnetic	21.916	–	22.639	–

Table 3.7 : Higher order mode cutoff frequencies of a Bilateral Finline in Circular Waveguide Housing (WC 33). Comparison between TLM and Finite Element Methods.

method can also include the effect of finite metallization thickness, substrate mounting grooves, bending of the substrate, and even the cross-sectional profile of the metallization edges.

Results obtained for the dispersion characteristics for dielectrically loaded ridge waveguides, and bilateral finlines in rectangular waveguide enclosure agree, within better than one percent, with the available data in the literature. Bending of the substrate causes a slight increase in the propagation constant of the dominant finline mode.

For the first time, the dispersion characteristics of the bilateral finlines in circular waveguide enclosures are presented. A structure called ridged finline has been described as well.

Graded mesh TLM procedure has also been applied to study the mode spectrum of finlines in rectangular and circular waveguide enclosures. The spurious solutions inherent in the Finite Element Method can be checked with the numerically stable TLM procedure.

It may be noted that the Finite Element and TLM algorithms require one to two orders of magnitude more CPU time and memory than other numerical methods. However, these approaches utilise their full potential when second-order effects and irregular geometries must be evaluated, a task at which most other numerical techniques fail.

Chapter IV

DIAKOPTICS FOR MICROWAVE STRUCTURES

4.1 INTRODUCTION

The TLM method is a numerical technique in which both space and time are discretized. Hence for large structures, the computer memory and time required to discretize the field space are enormous, sometimes beyond the scope of normal computers. This is also true with other numerical techniques such as FD-TD. Hence a Diakoptics procedure, where a network is broken up into substructures which are solved independently and then later reassembled, must be applied for the analysis of large structures.

Also, in applications such as monolithic microwave integrated circuits of high density or EMI/EMC simulations, the field interaction between all parts of the structure must be considered. Hence the traditional way of cascading the scattering parameters (of the dominant mode) of the individual circuits to get the overall response does not give accurate results. Fullwave, wideband analysis must be carried out for such structures. This is intrinsic in the TLM-Diakoptics procedure if the mesh is excited with an impulse.

In steady-state network theory, the Diakoptics technique was first applied by Kron [54]. In 2-D analysis of planar components, a similar approach known as the " Segmentation Method " has been applied by Okoshi and others [55]-[57]. In this approach, the irregular planar components are segmented into regular shapes for which the analytical Green's functions are known. The technique has been extended to the time domain for 2-D TLM modeling by Johns and Akhtarzad in 1981 [58]-[59]. These three approaches, namely, the network Diakoptics, the Segmentation approach for planar components and Diakoptics for 2-D TLM method are described in this chapter.

4.2 STEADY-STATE SOLUTION USING DIAKOPTICS

Kron [62]-[63] has produced lumped networks to represent Maxwell's eletromagnetic field equations in two- and three-dimensions. Recently, some improved lumped network models have been proposed by P. B. Johns [79]. The lumped networks with branches consisting of components like capacitors, inductors and resistors, form a space discrete model of a field because the solution of the field is described only along the branches or at the nodes. A simple lumped network model to represent Maxwell's equations in two-dimensions has been discussed in Section 2.3.1. From the steady-state solution of the network models, the discrete steady-state solution for the electromagnetic field can be obtained. The procedure for applying Diakoptics technique for steady-state solution of such networks is described in [58] and summarized below for convenience.

The large network to be analysed is divided into substructures by lines parallel to the co-ordinate axes, and midway between the nodes, as shown in Fig. 4.1. The branches which cross the substructure are called " removed branches " and are not considered to belong within any structure. The solution for substructure A may be written as

$$Y_A \, V_A = I_{RA} + I_{SA} \tag{4.2.1}$$

where Y_A is the nodal admittance matrix of substructure A, V_A is the vector of nodal voltages, I_{RA} are currents flowing in the removed branches, and I_{SA} are source currents

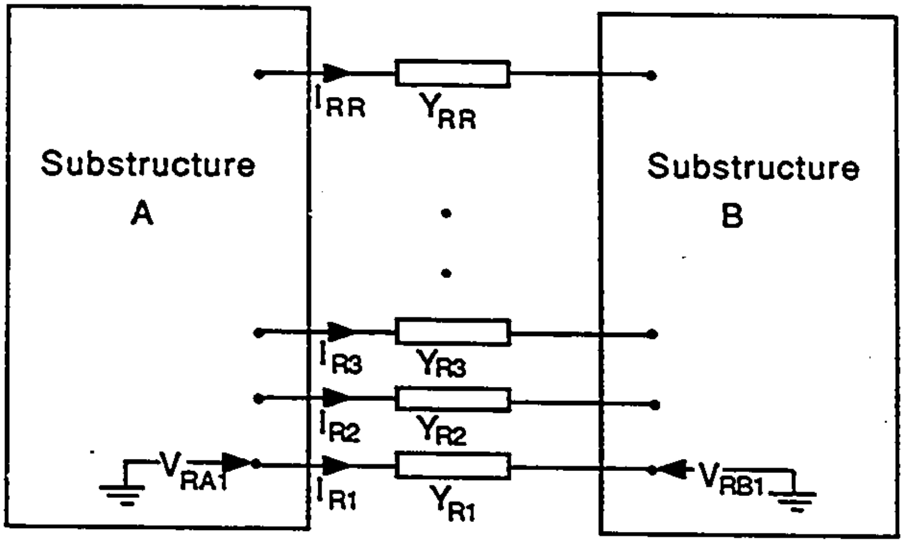

Fig. 4.1 : Network Substructures Connected by Removed Branches

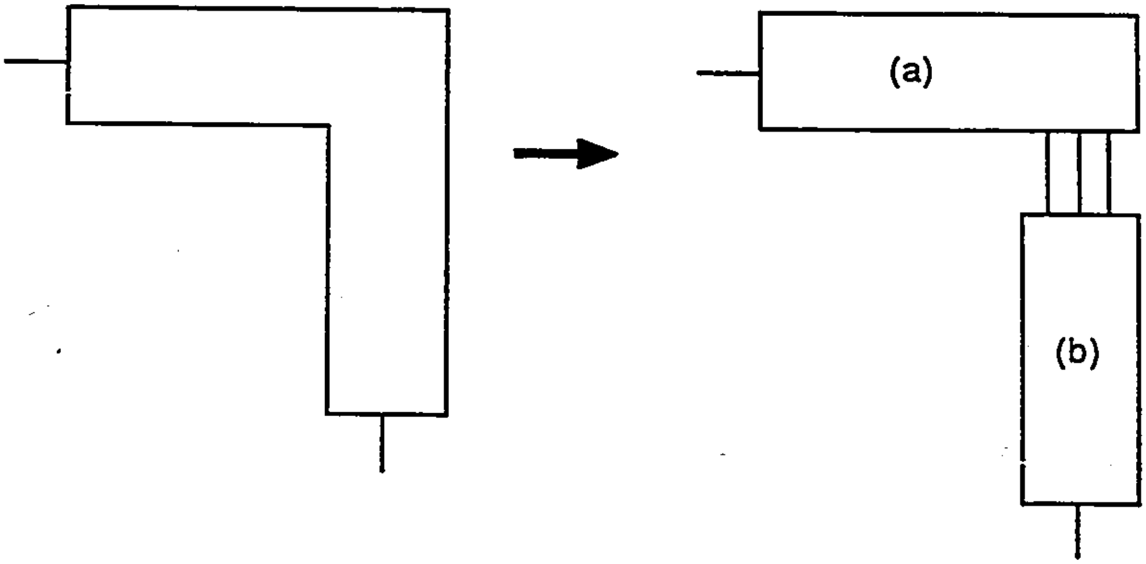

Fig. 4.2 : Segmentation of Planar Elements [57]

in A. The voltages V_{RA} on the nodes at the end of removed branches are related to the currents I_{RA} flowing in these branches through the equation

$$V_{RA} = V_{RSA} + Z_{RA}\, I_{RA} \tag{4.2.2}$$

where V_{RSA} are the removed branch nodal voltages due to the source currents I_{SA} alone i.e.

$$V_{RSA} = Y_A^{-1} I_{SA} \tag{4.2.3}$$

and Z_{RA} is the response of the substructure A to a unit current excitation on the removed branches. Each column of Z_{RA} is obtained from $Y_A^{-1} I_{RA}$, with each element of I_{RA} successively set to unity.

Connection is made by solving for the removed branch currents

$$I_R = Y_R\, (V_{RA} - V_{RB}) \tag{4.2.4}$$

where

$$I_R = I_{RA} = -I_{RB} \tag{4.2.5}$$

and Y_R contains the removed branch admittances on the diagonal.

Substituting from equation (4.2.2), one obtains

$$I_R = Y_R\big((V_{RSA} + Z_{RA} I_R) - (V_{RSB} - Z_{RB} I_R)\big) \tag{4.2.6}$$

When the removed branch currents I_R have been found from equation (4.2.6), multiplication with Y^{-1} of any substructure yields the nodal voltages for that substructure.

From the foregoing analysis, the procedure for obtaining the steady-state response of large networks using Diakoptics can be summarized as follows:

1. For each substructure, compute V_{RSA}, the removed branch nodal voltages due to the source currents present in that substructure.

2 For each substructure, compute Z_{RA}, the response of the substructure due to unit current excitation on the removed branches.

3 Solve the system of equations given by (4.2.6) for I_R, the removed branch currents using any standard procedure such as Crout's factorization method.

4 Obtain the nodal voltages in any substructure by multiplying I_R with Y^{-1} of that substructure.

Brewitt-Taylor and Johns have applied this technique to solve for fields in a rectangular waveguide supporting TE_{10} mode and containing a dielectric obstacle and absorbing material [80]. The whole structure was divided into three substructures. They reported that for the repeated solution involving a change in properties of one substructure (consisting of dielectric obstacle) requires 20 seconds of computer time, compared with 149 seconds for the problem as a whole (assuming that the solutions for the remaining substructures are available).

The matrix Y_R in (4.2.6) is quite full. The size of this system of equations limits the number of removed branches allowed. The size of the matrix Z_{RA} is $R \times R$, where R is the number of removed branches. To reduce the computational expenditure, linear, second or higher - order space approximations can be applied. For example, in the case of linear space approximation, the matrix Z_{RA} relates the removed branch voltages to the removed branch currents for any two of the removed branches and a linear relationship is assumed for the remaining (R-2) branches. If the current distribution is highly non uniform in the removed branches, higher-order space approximations are required to get accurate results. Space approximations have been applied for a network consisting of a large resistive mesh by Johns and Aktharzad [58].

4.3 SEGMENTATION FOR PLANAR CIRCUITS

In many practical microwave planar circuits, the thickness of the substrate is so small that the field variation in that direction can be neglected, hence, the structure can be treated as a two-dimensional problem. One method for analyzing such planar components involves determination of Z-matrix of the component using a Green's function from the equation

$$Z_{ij} = \frac{1}{W_i W_j} \int_{W_i} \int_{W_j} G(s/s_o)\, ds_o\, ds \tag{4.3.1}$$

where the periphery of the planar circuit is divided into several sections of small widths (W) so that the field variation over the width of each of these sections is negligibly small. Each one of these sections is considered as a port of the multiport network model; s_o is the excitation point.

The Green's functions are available for only a few regular shapes. Analysis of irregular shapes is done by segmenting these into regular shapes such as squares, rectangles, circles, etc., for which the Green's functions are known. The " Segmentation Method " combines the characteristics of the segmented elements to get the characteristics of the complicated circuit [56]. This results in reduced computational effort. A brief description of the method is given below:

In a general planar network of segments (see Fig. 4.2 for a simple example), the Z-matrices can be written together as

$$\begin{pmatrix} V_p \\ V_c \end{pmatrix} = \begin{pmatrix} Z_{pp} & Z_{pc} \\ Z_{cp} & Z_{cc} \end{pmatrix} \begin{pmatrix} I_p \\ I_c \end{pmatrix} \tag{4.3.2}$$

where V_p, I_p and V_c, I_c are voltages and currents at the p externally and c internally connected ports. The c internally connected ports are divided into groups q and r, each containing $c/2$ ports. This is done in such a way that q_1 and r_1 ports are connected together, q_2 and r_2 ports are connected together and so on. This involves reordering of the rows and/or columns of Z_{cp}, Z_{pc}, and Z_{cc} as given in equation (4.3.2). The Z-matrices can now be written together as

$$\begin{pmatrix} V_p \\ V_q \\ V_r \end{pmatrix} = \begin{pmatrix} Z_{pp} & Z_{pq} & Z_{pr} \\ Z_{qp} & Z_{qq} & Z_{qr} \\ Z_{rp} & Z_{rq} & Z_{rr} \end{pmatrix} \begin{pmatrix} I_p \\ I_q \\ I_r \end{pmatrix} \tag{4.3.3}$$

The interconnections can be expressed as

$$V_q = V_r \tag{4.3.4}$$

$$I_q + I_r = 0 \tag{4.3.5}$$

Substituting (4.3.4) and (4.3.5) in (4.3.3) and eliminating V_q, V_r, I_q and I_r, the Z-matrix of the overall network is given by

$$Z_p = Z_{pp} + (Z_{pq} - Z_{pr})(Z_{qq} - Z_{qr} - Z_{rq} + Z_{rr})^{-1}(Z_{rp} - Z_{qp}) \tag{4.3.6}$$

The unknowns in the above equation can be obtained from the Green's functions of the segmented regular shapes. This technique has been applied extensively to model microstrip circuits and antennas [56], [81].

4.4 TIME DOMAIN DIAKOPTICS FOR 2-D TLM METHOD

The TLM method discretizes a field in space and time, while the lumped network model discussed in Section 4.2 discretizes the field in space only. Hence the procedure for application of Diakoptics to TLM method should be similar to that of steady-state networks, except for the extra dimension of time associated with TLM method.

Fig. 4.3 shows the TLM representation of a large network divided into two substructures named S_{super} and S_{sub}. The structure S_{sub} contains a small portion of the network geometry which needs to be modified many times, and the structure S_{super} is the major portion of the large network which remains unchanged. The time domain response of S_{super} can be interpreted as a numerical Green's function with respect to the 'N' interconnection ports. This Green's function needs only be computed once and stored (this can be identified with Z_{RA}, the response of the substructure due to unit current excitation on the removed branches, of the steady-state Diakoptics). Unlike the analytical Green's function, this numerical Green's function is a discrete function of space and time, defined only at discrete space points which are integer multiples of the mesh parameter Δl (i.e. x = i Δl, y = j Δl), and at integer multiples of the time parameter Δt (i.e. k Δt). An element $g(i,j,k;i',j',k')$ of the numerical Green's function is the output voltage impulse arriving at the output node $(x = i\Delta l, y = j\Delta l)$ at the time $t = k\Delta t$ due to an unit impulse excitation at the input node $(x = i'\Delta l, y = j'\Delta l)$ at the time $t' = k'\Delta t$.

4.4.1 COMPUTATION OF THE NUMERICAL GREEN'S FUNCTION OF S_{super}

The branches penetrating through the interface (also called " removed branches ") are numbered 1 through $M = N$ (See Fig. 4.3). A single impulse injected at any of these branches will cause impulses, separated by the iteration time interval, to flow in streams out of the branches of this structure. These impulse functions result from the scattering at the nodes and boundaries of the structure, and can be interpreted as a Green's function in numerical form. All removed branches are terminated in their own characteristic impedance during this procedure so as to absorb the emerging output streams. If we simplify our notations of Green's function and denote $g(m,n,k)$ as the output impulse

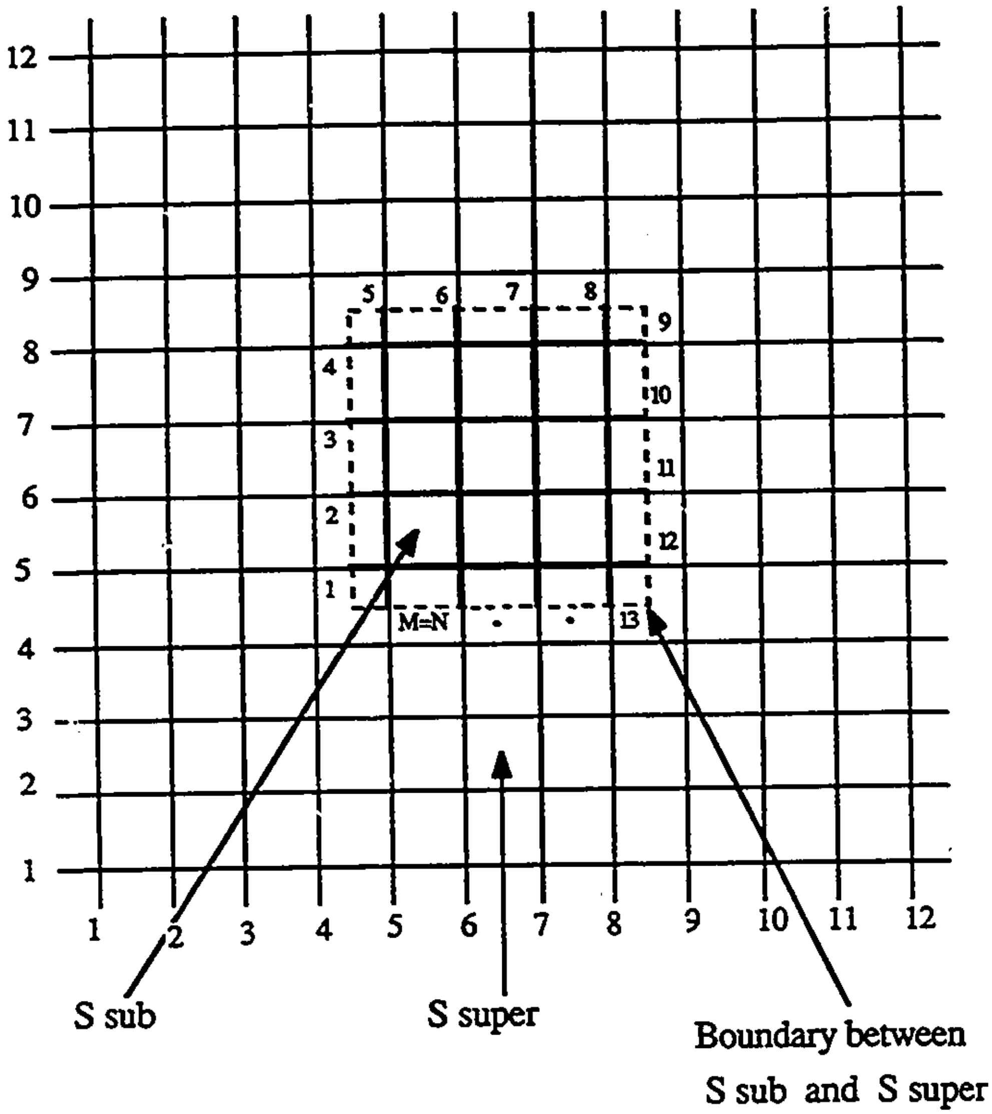

Fig. 4.3 : Segmentation of a large network for Diakoptics

function emerging at the m-th branch (emanating from the node $x = i\Delta l, y = j\Delta l$) at $t = k\Delta t$ due to a unit excitation of the n-th branch (emanating from the node $x = i'\Delta l, y = j'\Delta l$) at t=0, the complete Green's function for the structure S_{super} can be written in matrix form as follows:

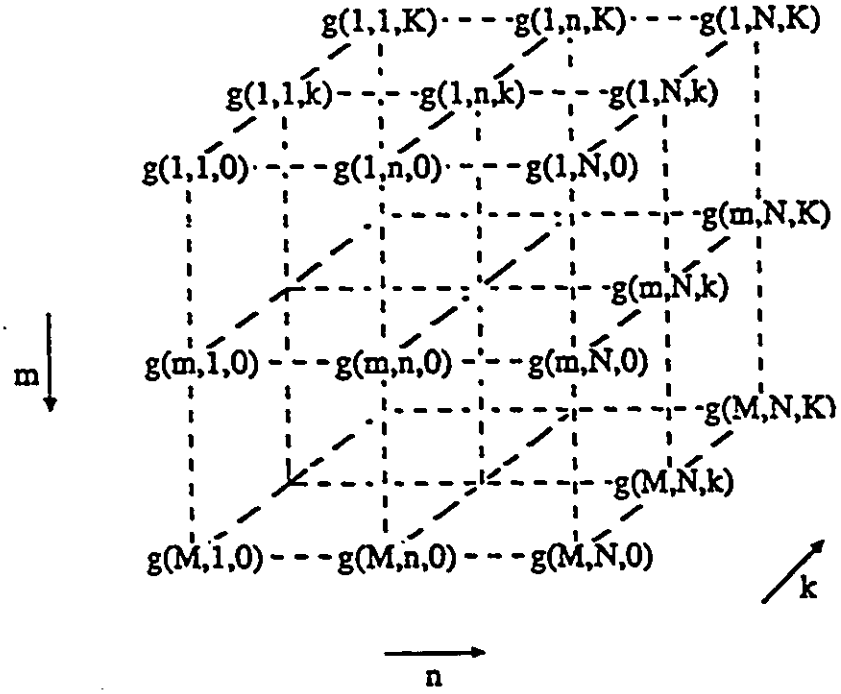

(4.4.1)

It is a three-dimensional array of dimension ($M \times N \times K$), where K is the total number of iterations, and $M = N$ is the number of branches or transmission lines along the reference plane. We call this numerical Green's function a " Johns Matrix " in honour of the late P. B. Johns, pioneer of TLM and time domain diakoptics [58]. Note that the above matrix is computed only once and is stored.

For the example shown in Fig. 4.3, N, the total number of interconnecting ports is 16. To compute the Johns matrix of S_{super} (with electric walls passing between the nodes 1 and 2, and 11 and 12), an voltage impulse of unit magnitude is applied at port number

1 (*i.e.*, $V^i(4,4,5) = 1.0$ *at* $t\prime = k\prime\,\Delta t = 0$). Then the elements of the first column of the Johns Matrix are obtained as follows:

$$\begin{array}{ll}
g(1,1,k) = {}_kV^r(4,4,5) & g(2,1,k) = {}_kV^r(4,4,6) \\
g(3,1,k) = {}_kV^r(4,4,7) & g(4,1,k) = {}_kV^r(4,4,8) \\
g(5,1,k) = {}_kV^r(1,5,9) & g(6,1,k) = {}_kV^r(1,6,9) \\
g(7,1,k) = {}_kV^r(1,7,9) & g(8,1,k) = {}_kV^r(1,8,9) \\
g(9,1,k) = {}_kV^r(2,9,8) & g(10,1,k) = {}_kV^r(2,9,7) \\
g(11,1,k) = {}_kV^r(2,9,6) & g(12,1,k) = {}_kV^r(2,9,5) \\
g(13,1,k) = {}_kV^r(3,8,4) & g(14,1,k) = {}_kV^r(3,7,4) \\
g(15,1,k) = {}_kV^r(3,6,4) & g(16,1,k) = {}_kV^r(3,5,4)
\end{array} \tag{4.4.2}$$

The Johns Matrix elements $g(1,1,k)$, $g(2,1,k)$ and $g(3,1,k)$ are shown in Figs. 4.4 (a) and (b) for 16 iterations. The remaining 15 columns of the Johns Matrix are obtained by exciting S_{super} at the other 15 interconnection ports.

The next step is to discretize the substructure S_{sub} and convolve its time domain impulse response with the Johns Matrix.

4.4.2 ANALYSIS OF THE OVERALL STRUCTURE BY DISCRETIZING ONLY THE STRUCTURE S_{sub} AND USING THE JOHNS MATRIX

When impulses are injected into the substructure S_{sub} at any node, they are scattered at nodes and boundaries and reach, after some time, the interconnection ports at the periphery. Any impulse which hits a boundary between S_{sub} and S_{super} will give rise to streams of impulses separated by the iteration time interval to flow back into the structure through all branches. For example, a series of k impulses incident on the n-th branch will

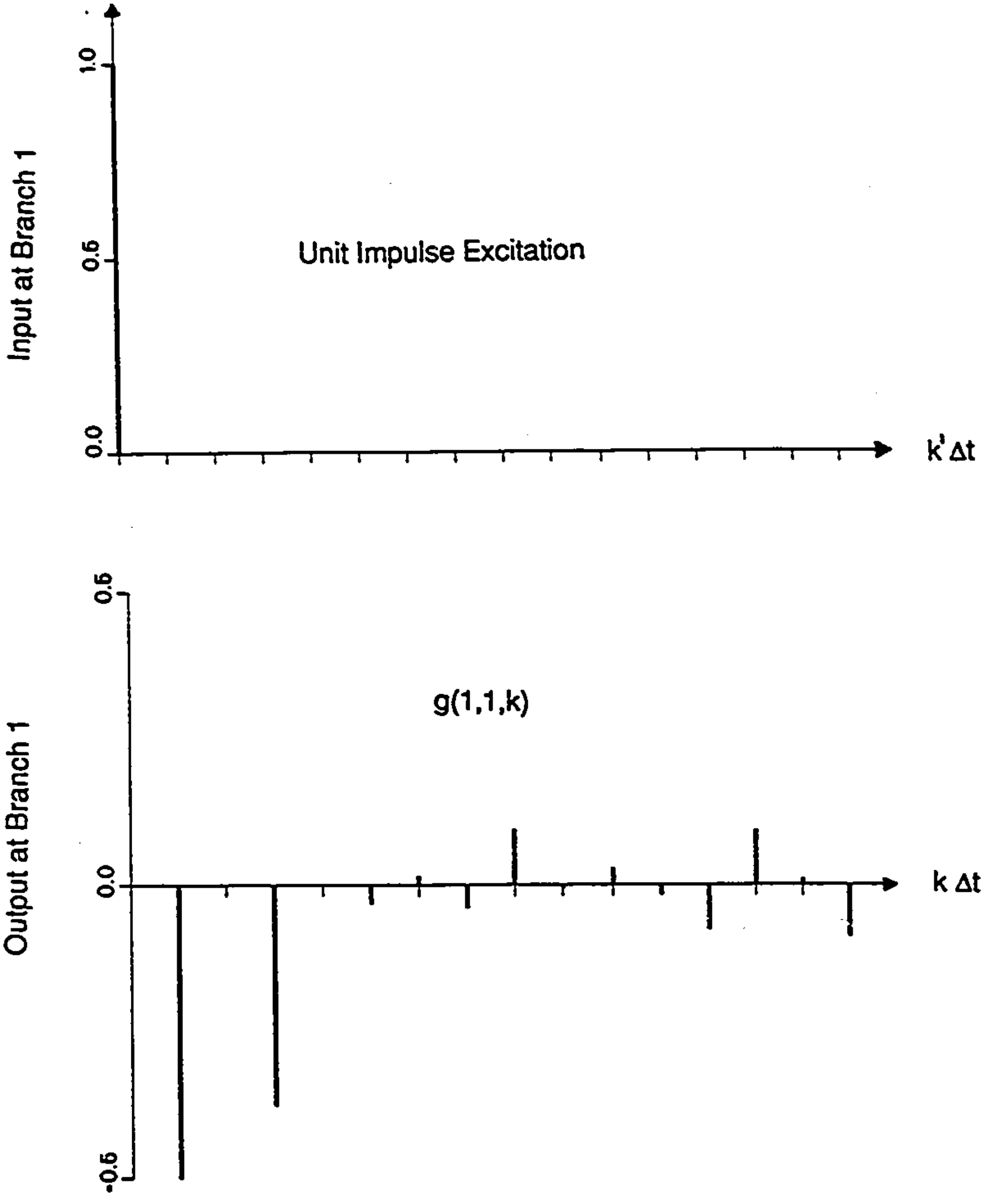

Fig. 4.4 (a) : g(1,1,k) term of Johns Matrix

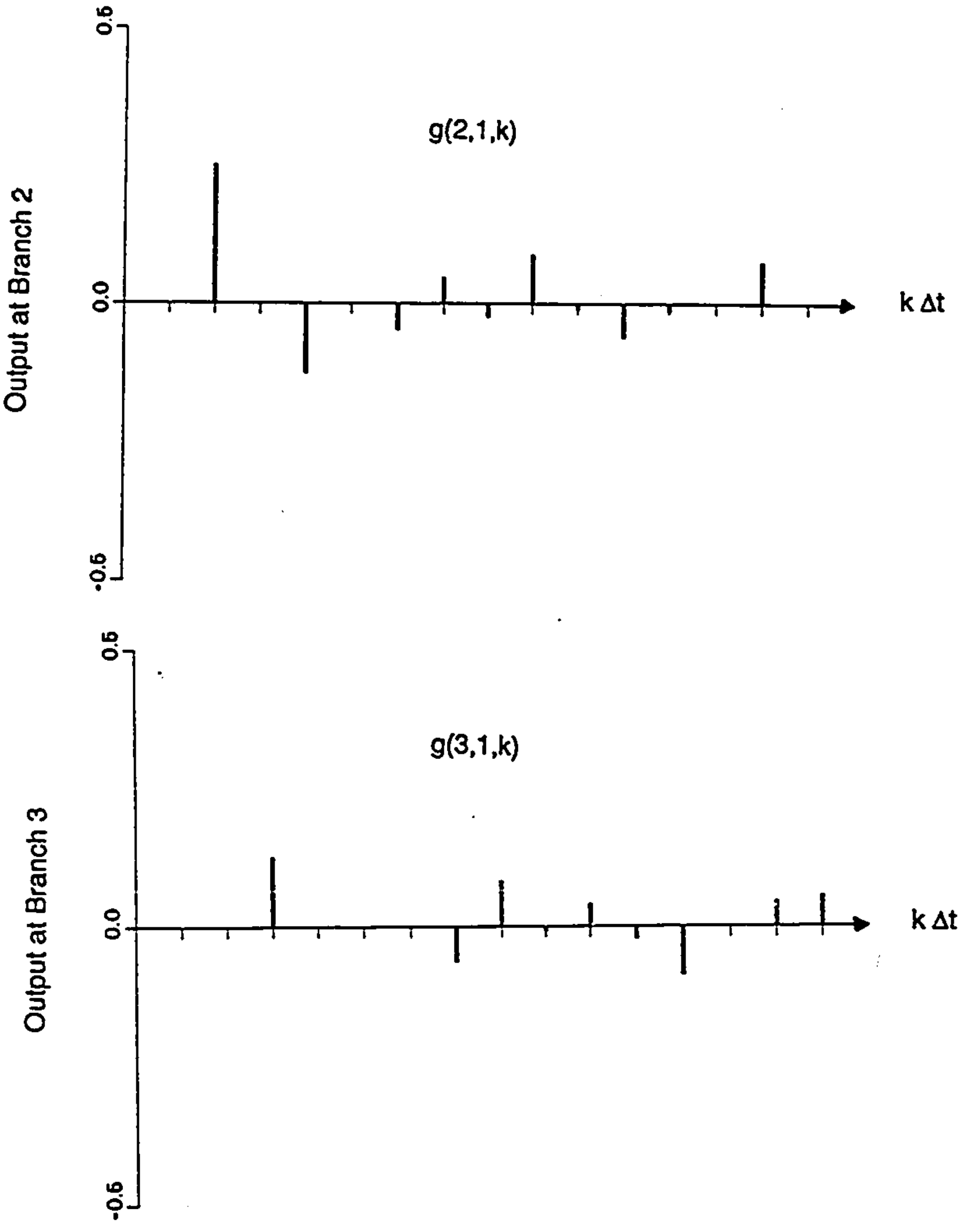

Fig. 4.4 (b) : g(2,1,k) and g(3,1,k) terms of Johns Matrix

give rise to the following reflected impulse voltage on the m-th branch:

$$V^r(m,k) = V^i(n,k) * g(m,n,0) + V^i(n,k-1) * g(m,n,1) + \cdots + V^i(n,0) * g(m,n,k) \tag{4.4.3}$$

This can be further written as follows:

$$V^r(m,k) = \sum_{k'=0}^{k} g(m,n,k') * V^i(n,k-k') \tag{4.4.4}$$

The total reflected impulse voltage on the m-th branch at time $k\Delta t$ due to the impulses incident on all N branches in previous iterations is the summation of the above term for the N branches.

$$V^r(m,k) = \sum_{n=1}^{N} \sum_{k'=0}^{k} g(m,n,k') * V^i(n,k-k') \tag{4.4.5}$$

This equation forms the basis of the Diakoptics algorithm.

The TLM algorithms with and without Diakoptics approach are shown in Fig. 4.5. Note the extra module to be implemented for convolution purposes with the Diakoptics approach. The computer run time and memory required with the conventional TLM algorithm is proportional to

$$(NX^{super} \times NY^{super} \times K) \tag{4.4.6}$$

while that with Diakoptics technique is

$$(NX^{sub} \times NY^{sub} \times K) + (K \times (K+1) \times N^2)/2 \tag{4.4.7}$$

where NX is the number of grids along the x-axis and NY is the number of grids along the y-axis and K is the total number of iterations. In equation (4.4.7), the first term corresponds to the discretization of the structure S_{sub} and the second part corresponds

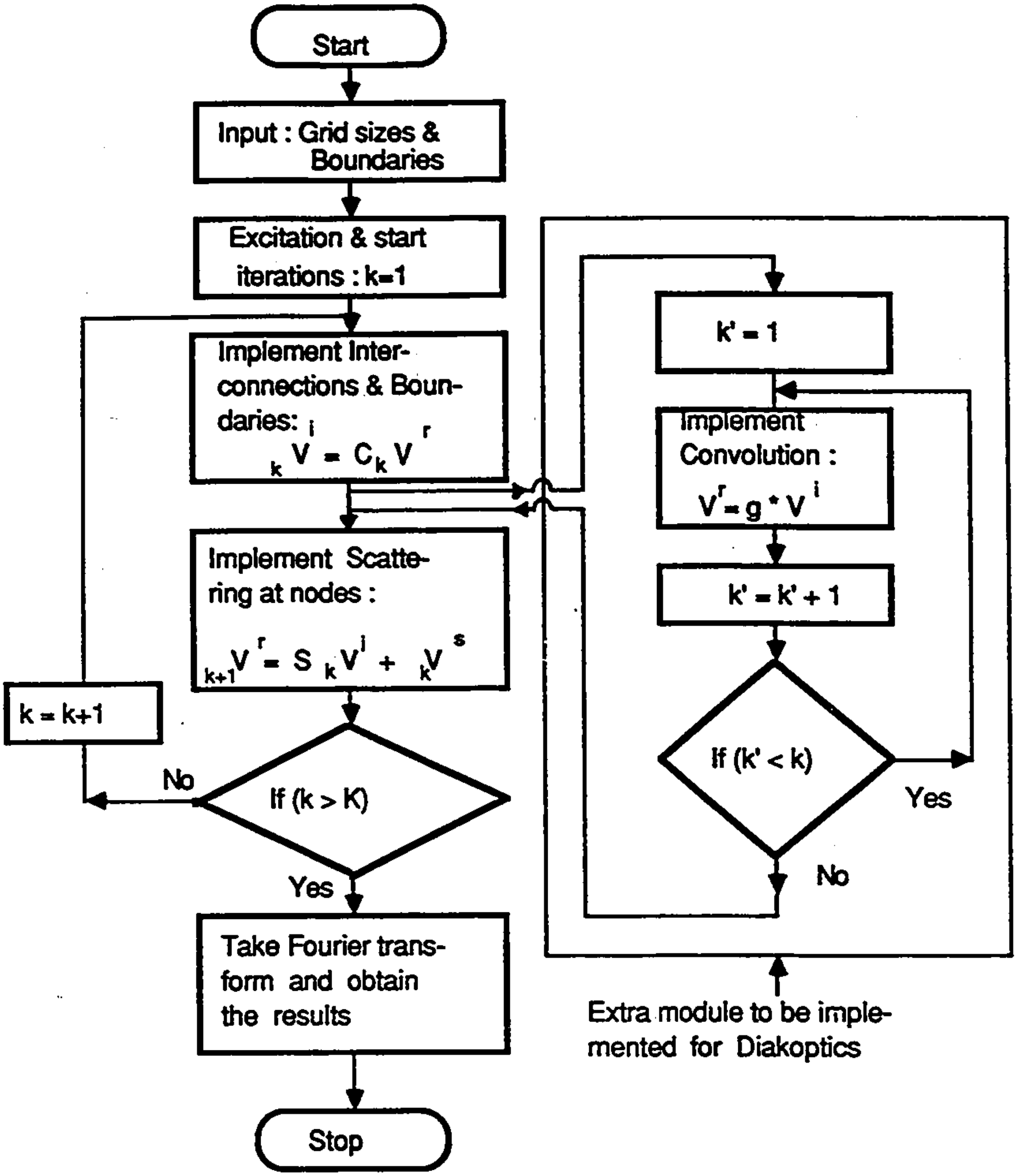

Fig 4. 5 : TLM Algorithms with and without Diakoptics

to the convolution with the Johns Matrix. For very big structures and small number of removed branches, the quantity given by (4.4.6) becomes more than that given by (4.4.7) and hence the Diakoptics procedure is economical.

To check the validity of the above approach, the algorithm was applied to compute the mode spectrum of bilateral finlines for different gap widths. One quarter of the finline is divided into structures S_{super} and S_{sub} as shown in the Fig. 4.6. S_{sub} is a small part (4×5 *grid size*) of the finline around the fin and S_{super} is the remaining large structure (42×22 *grid size*) . The numerical Green's function of S_{super} was computed once and stored. Then S_{sub} was discretized for two different gap widths and convolved with the numerical Green's function. The results are shown in Fig. 4.6 and they compare well with those computed using the Spectral Domain Method.

4.5 DISCUSSION

The network Diakoptics, the Segmentation approach for planar components and the time domain Diakoptics for 2-D TLM method are described. For the latter, it was found that there was no accumulation of errors (even with single precision computation) while convolving, and the impulse values obtained with Diakoptics agree with those of the conventional TLM method to within six decimal places.

In network Diakoptics, the responses of the substructures due to unit current excitation on the removed branches are computed and stored, while in the TLM-Diakoptics procedure, the responses of the substructures due to unit impulse excitation on the removed branches are computed and stored. Even though the memory requirements are more for the latter procedure, it can do the fullwave analysis over a wide frequency range. The segmentation approach for planar components uses analytical Green's functions, and hence the method is not very versatile.

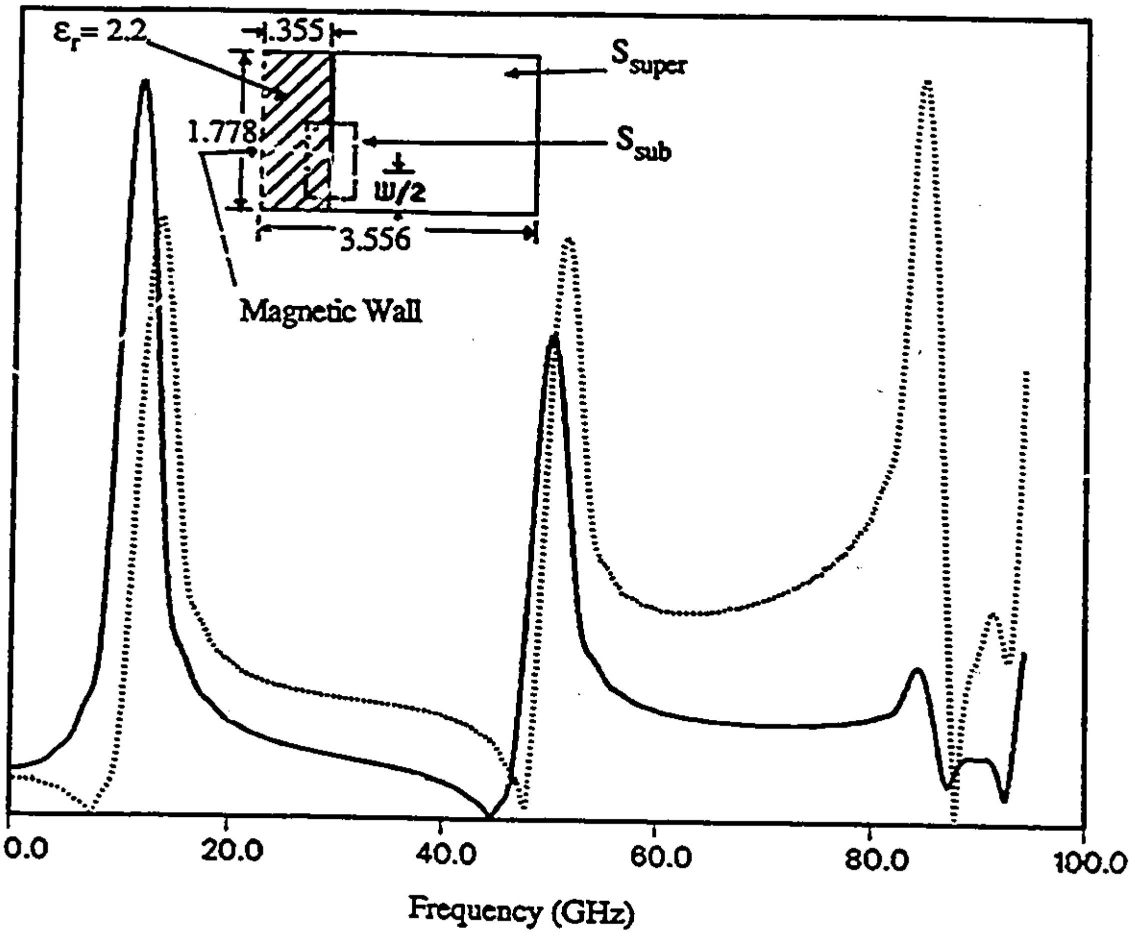

Fig. 4.6 : Frequency Response of a Bilateral Finline Computed Using Diakoptics. __ w = 0.7112 mm, ... w = 0.8534 mm

Chapter V

2-D TLM MODELING OF DISPERSIVE WIDEBAND ABSORBING BOUNDARIES WITH TIME DOMAIN DIAKOPTICS

5.1 INTRODUCTION

The importance of absorbing boundary conditions has been discussed in the Chapters I and II. An absorbing boundary should permit the electromagnetic waves to propagate through it with minimum reflections so as to limit the computational domain required for characterizing microwave structures. The quality of an absorbing boundary is judged by its reflection coefficient. This reflection coefficient depends on the incident angle of the wave striking the boundary. For wideband absorbing boundaries, the reflection coefficient should be very small for a large range of incident angles and these are required in order to extract the scattering parameters, propagation constants, and other field related parameters such as the characteristic impedance, etc., over a wide frequency range from a single TLM simulation. Normally, the reflection should be less than one percent to get accurate results, otherwise Fourier transformed data will be corrupted.

There are several publications [82]-[85] dealing with various approaches to implement absorbing boundaries for the FD-TD method. The simple approach is the open-and short-circuit boundary condition method. In this method, the problem is solved twice, once with vanishing tangential electric field and once with vanishing tangential magnetic field. These two solutions are then averaged (their sum should cancel out the reflected fields) to get the desired result. This scheme will work well for uniform guides, but for discontinuities, the multiple reflections may not be cancelled out.

To the best of the author's knowledge, not much has been reported on the implementation of wideband absorbing boundaries, except for the work of Roy and Choi [85], who claim less than one percent reflections over a bandwidth of 7.7 percent for TE_{10} mode propagation in a standard rectangular waveguide.

The time domain diakoptics technique presented in the last chapter has been successfully applied for the implementation of wideband absorbing boundary conditions. Frequency dispersive boundaries are represented in the time domain by their characteristic impulse response or Johns Matrix. Space interpolation techniques based on the dominant field spatial distribution have been proposed to make the Diakoptics technique very efficient, thus saving considerable computer run time and memory. In the following sections, these procedures are described.

5.2 TEM ABSORBING BOUNDARIES

Consider a shunt-connected 2-D TLM mesh (shown in Fig. 5.1) in which the voltage V_y simulates an electric field. To simulate a TEM mode propagating in the z-direction in a parallel-plate waveguide, the boundaries A and B should be perfect magnetic walls, and the boundary C should be an absorbing wall. To simulate the absorbing conditions at the boundary C, the mesh lines should be terminated with the intrinsic impedance of the TLM mesh, $Z_0/\sqrt{2\epsilon_r}$, where Z_0 is the characteristic impedance of the mesh lines, and ϵ_r is the relative permittivity of the simulated medium. Hence for simulation of TEM mode

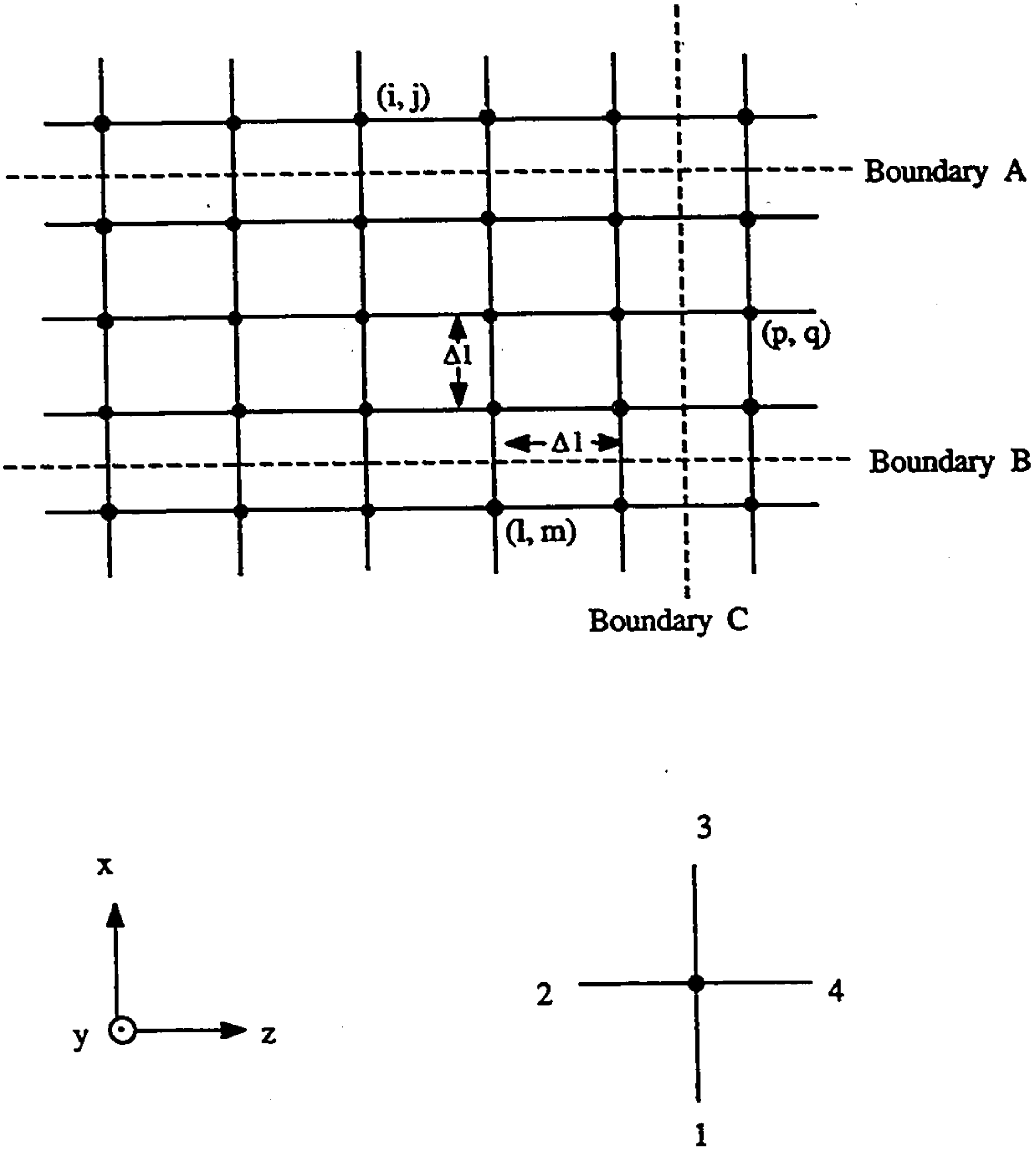

Fig. 5.1 : Modeling of General Boundaries in a 2-D Shunt Connected TLM Mesh

propagation in the z-direction, the following computations are done at the boundaries:

$$ {}_kV_3^i(i,j-1) = {}_kV_3^r(i,j-1) \tag{5.2.1}$$

for each external node at $(z=i,\ x=j)$,

$$ {}_kV_1^i(l,m+1) = {}_kV_1^r(l,m+1) \tag{5.2.2}$$

for each external node at $(z=l,\ x=m)$, and

$$ {}_kV_4^i(p-1,q) = \rho\, {}_kV_4^r(p-1,q) \tag{5.2.3}$$

for each external node at $(z=p,\ x=q)$,

where

$$\rho = \frac{Z_0/\sqrt{2\epsilon_r} - Z_0}{Z_0/\sqrt{2\epsilon_r} + Z_0} = \frac{1-\sqrt{2\epsilon_r}}{1+\sqrt{2\epsilon_r}} \tag{5.2.4}$$

Note that the condition (5.2.3) results in a non-zero reflection coefficient for the individual impulses travelling on the mesh lines towards the boundary, while the total energy moving in the form of a traveling " mass action " wave is completely absorbed by it. This is consistent with Huygens's principle which stipulates that each point of a moving wavefront emits secondary wavelets in all directions, including the backward one.

5.3 NARROW-BAND NON-TEM ABSORBING BOUNDARIES

To simulate TE_{n0} modes traveling in z-direction in a waveguide, the boundaries A and B should be electric walls, and at the boundary C, the mesh lines should be terminated with the dispersive wave impedances. This is done by doing the following computations:

$$ {}_kV_3^i(i,j-1) = -{}_kV_3^r(i,j-1) \tag{5.3.1}$$

for each external node at $(z = i,\ x = j)$,

$$ {}_kV_1^i(l, m+1) = -{}_kV_1^r(l, m+1) \tag{5.3.2} $$

for each external node at $(z = l,\ x = m)$, and

$$ {}_kV_4^i(p-1, q) = \rho\ {}_kV_4^r(p-1, q) \tag{5.3.3} $$

for each external node at $(z = p,\ x = q)$,

where

$$ \rho = \frac{\frac{Z_0\lambda_g}{\sqrt{2\epsilon_r}\lambda_0} - Z_0}{\frac{Z_0\lambda_g}{\sqrt{2\epsilon_r}\lambda_0} + Z_0} = \frac{\lambda_g - \lambda_0\sqrt{2\epsilon_r}}{\lambda_g + \lambda_0\sqrt{2\epsilon_r}}, \tag{5.3.4} $$

λ_g is the guide wavelength and λ_0 is the free space wavelength.

Since the reflection coefficient ρ is a function of frequency, the termination is totally absorbing only at one frequency. At best this approach leads to a narrowband absorbing condition, which is acceptable when the frequency range of interest is only a fraction of an octave. The frequency behaviour of such a back to back termination for $WR28$ waveguide is shown in Fig. 5.2, where the value of ρ was taken to be at the midband frequency of 33 GHz. Results are shown for two different numbers of iterations. Reflections are small only between 32 and 34 GHz and depend on the number of iterations. Since the Fourier transform of the time domain results is very sensitive to imperfect absorbing boundary conditions, the accurate computation of S-parameters is not possible over a wide band of frequencies with this termination.

5.4 WIDEBAND ABSORBING BOUNDARIES

To simulate a dispersive absorbing boundary over a wide frequency range, use has been made of the characteristic impulse response, or Johns Matrix, proposed in the previous

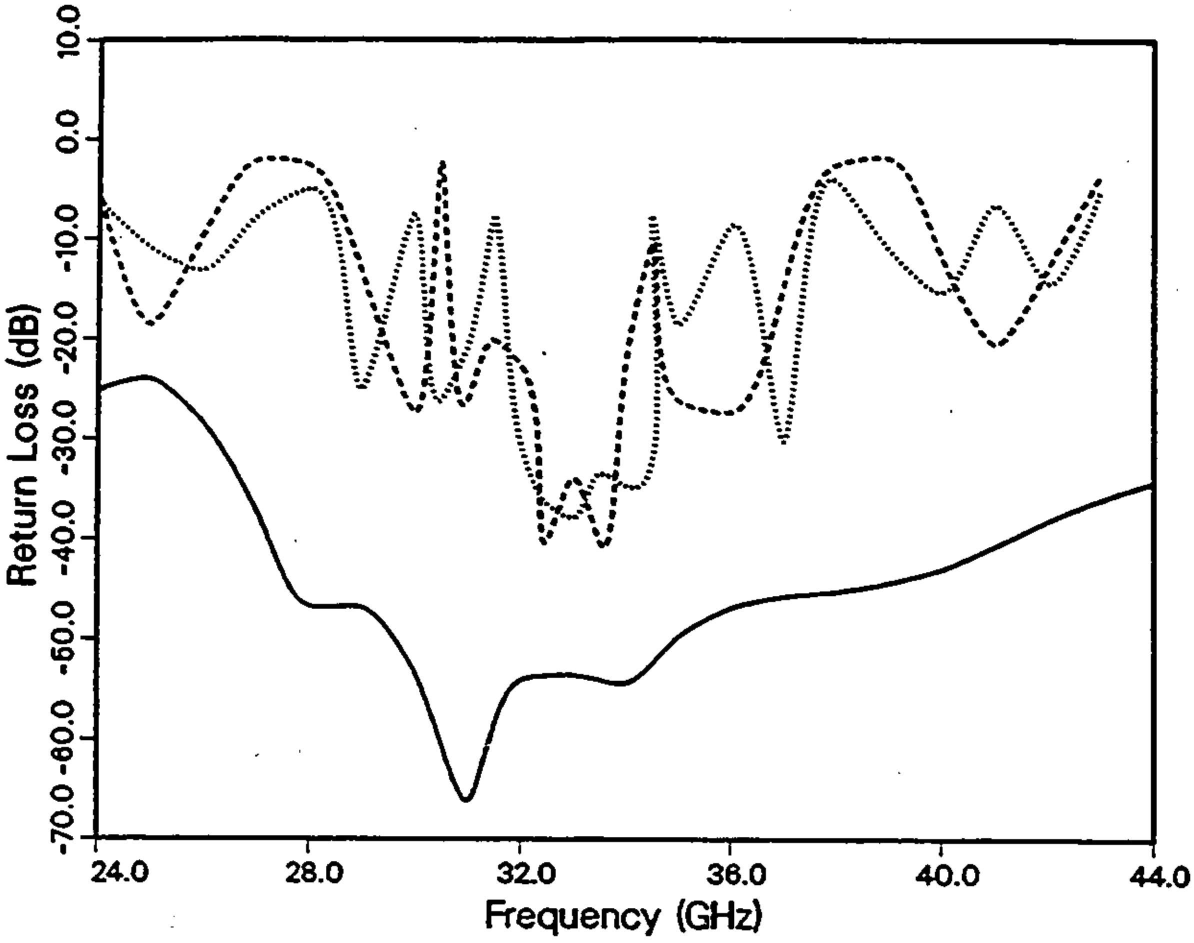

Fig. 5.2 : A comparison of the return loss characteristics of absorbing boundaries obtained by two different methods.

...... Termination with wave impedance and 1500 iterations.

---- Termination with wave impedance and 2500 iterations.

—Termination with Johns Matrix.

chapter. Since the Johns Matrix contains the time history of the absorbing boundary due to impulse excitation, it can adequately represent dispersive impedances. Two different approaches have been employed to achieve this:

i) Modeling of a waveguide termination with gradually increasing losses,

ii) Modeling of a very long uniform waveguide section.

5.4.1 MODELING OF A WAVEGUIDE TERMINATION WITH GRADUALLY INCREASING LOSSES

Practical waveguide terminations are made by arranging for the gradual absorption of the incident wave. A tapered resistive sheet or pyramid gradually increases the effective attenuation constant in the termination. Providing the taper is made several wavelengths long, the reflection is very small. An alternative approach, more appropriate for theoretical modeling purposes, is to simulate the wideband termination by cascading a number of uniform lossy sections of waveguide as shown in Fig. 5.3(a). The loss tangent of the sections is progressively increased in such a way that reflection is minimized over a wide frequency range. We have used the optimization feature of *Touchstone*^{TM}*CAD* software to obtain the theoretical loss profile providing minimum return loss over the operating band of the waveguide. About nine sections of different lengths and loss tangents (the dielectric loss tangent is taken as the variable quantity) are needed to get a return loss of less than -40 dB over the operating band of a standard rectangular waveguide. The optimized lengths and dielectric loss tangents are given in Fig. 5.3(b). For a WR28 waveguide, the total length of the termination which consists of nine sections is 42.5819 mm (= 3.785 λg at the center frequency of the operating band). The return loss optimized with *Touchstone* is shown in Fig. 5.4. It is less than -40 dB throughout the operating band of the WR28

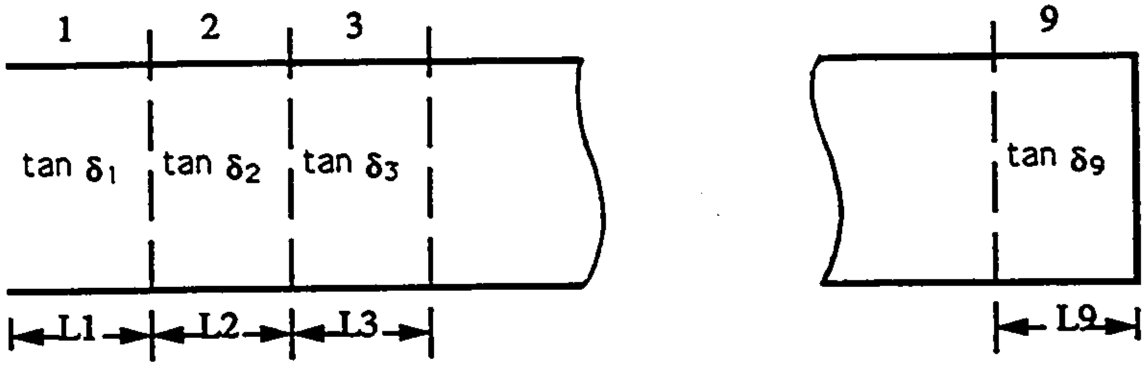

(a)

Section	Length (mm)	Dielectric Loss tangent ($\tan\delta$)
1	1.275	0.0095
2	1.739	0.0112
3	3.095	0.0499
4	3.031	0.1162
5	3.166	0.1990
6	7.980	0.2708
7	7.990	0.3686
8	7.536	0.8907
9	6.769	0.5960

(b)

Fig. 5.3 : (a) Modeling of a wideband absorbing waveguide termination by a cascade of nine increasingly lossy line sections
(b) Optimized lengths and dielectric loss tangents for a matched WR28 load (TE_{10} - mode)

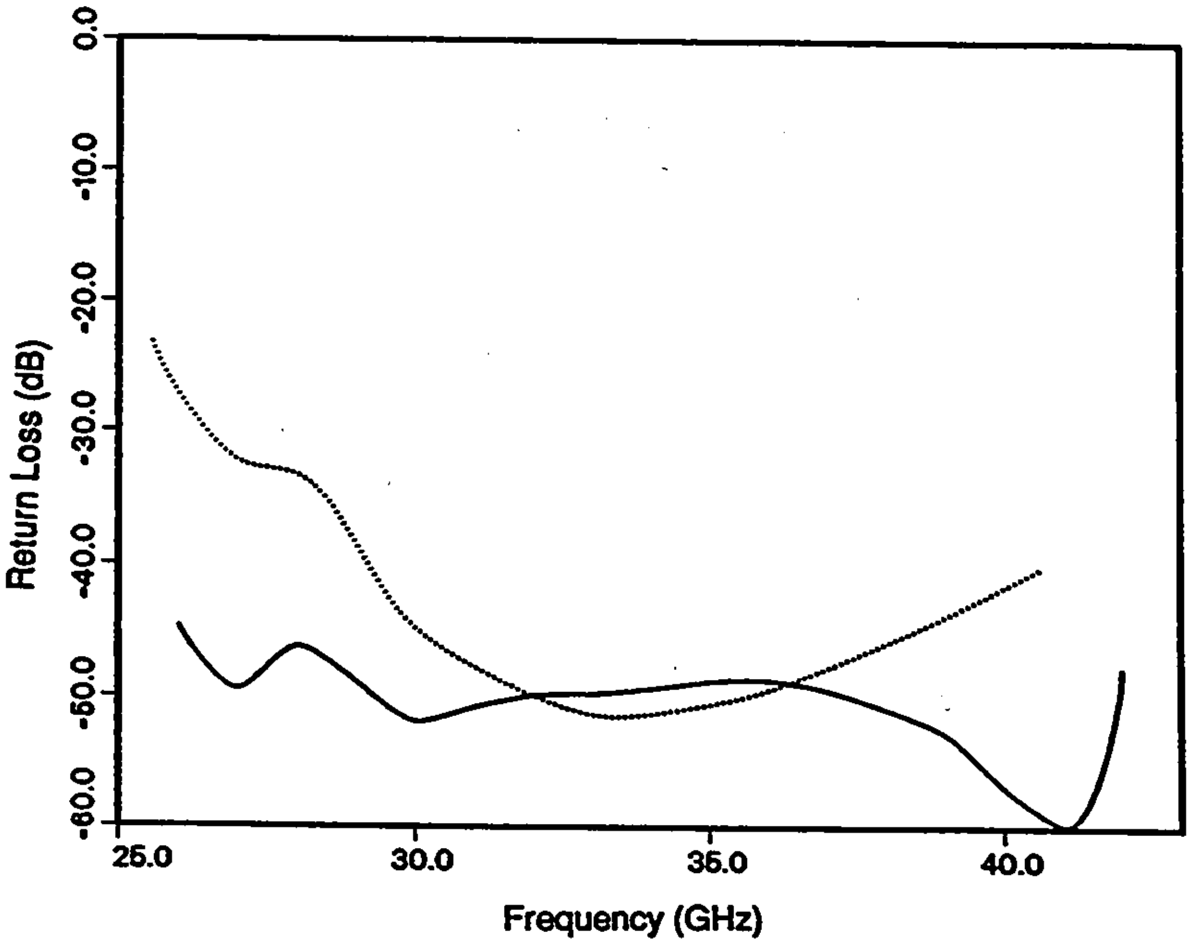

Fig. 5.4: Return loss of the lossy waveguide termination
__ Theoretical result optimized using Touchstone
..... Simulation using TLM method

waveguide. The theoretically generated lossy termination was then emulated by a TLM network containing loss stubs [29]: each node is resistively loaded with a matched transmission line of appropriate characteristic admittance g_0, extracting energy from each node at every iteration. The values of g_0 are directly proportional to the local loss tangent and can be derived as follows:

A lossy medium represented by,

$$\epsilon = \epsilon_0 \epsilon_r + \frac{\sigma}{j\omega} = \epsilon_0 \epsilon_r (1 - j \ tan\delta) \tag{5.4.1}$$

is modeled in a shunt-connected mesh by adding an open-ended shunt stub of length $\Delta l/2$ and normalized characteristic admittance y_0, and a lumped normalized shunt conductance g_0. The lumped element equivalent circuit of such a lossy node can be derived as follows [29]:

The voltage and current changes in the x and z directions can be expressed for very small mesh parameter Δl as

$$\frac{\partial V_y}{\partial x} = -L \frac{\partial I_x}{\partial t} \tag{5.4.2}$$

$$\frac{\partial V_y}{\partial z} = -L \frac{\partial I_z}{\partial t} \tag{5.4.3}$$

$$\frac{\partial I_z}{\partial z} + \frac{\partial I_x}{\partial x} = -2C(1 + y_0/4) \frac{\partial V_y}{\partial t} - g_0 \ C \ c \ V_y/\Delta l \tag{5.4.4}$$

The Maxwell's equations for $\frac{\partial}{\partial y} = 0$, and $E_x = E_z = H_y = 0$ (which describe the TE_{n0} modes in a rectangular waveguide) can be written as

$$\frac{\partial E_y}{\partial x} = -\mu \frac{\partial H_z}{\partial t} \tag{5.4.5}$$

$$\frac{\partial E_y}{\partial z} = \mu \frac{\partial H_x}{\partial t} \tag{5.4.6}$$

$$\frac{\partial H_x}{\partial z} - \frac{\partial H_z}{\partial x} = \epsilon_0 \epsilon_r \frac{\partial E_y}{\partial t} + \sigma E_y \tag{5.4.7}$$

From equations (5.4.2)-(5.4.4) and (5.4.5)-(5.4.7), the following equivalences between field and TLM parameters can be established :

$$E_y \equiv V_y \quad H_z \equiv I_x \quad H_x \equiv -I_z \tag{5.4.8}$$

$$\mu_0 \equiv L \;\; \epsilon_0 \equiv 2C \;\; \epsilon_r \equiv 1 + y_0/4 \;\; \sigma \equiv g_0 Cc/\Delta l \tag{5.4.9}$$

From the above equations, the equivalent attenuation constant α of the mesh lines can be expressed as

$$\alpha = \frac{g_0}{4\sqrt{1 + y_0/4}\,\Delta l} \; nepers/m \tag{5.4.10}$$

The attenuation constant α_n of the network in terms of the mesh parameters is

$$\alpha_n = \frac{g_0}{2\sqrt{2}\sqrt{1 + y_0/4}\,\Delta l} \; nepers/m \tag{5.4.11}$$

The attenuation constant for dielectric losses in the medium can be expressed in terms of the material constants as

$$\alpha_n = \frac{\omega \epsilon_0 \epsilon_r \; tan\delta}{2} \sqrt{\frac{\mu_0}{\epsilon_0 \epsilon_r}} \tag{5.4.12}$$

By equating equations (5.4.11) and (5.4.12) , g_0 follows:

$$g_0 = \frac{2\sqrt{2}\;\pi\;\Delta l\;\epsilon_r\;tan\delta}{\lambda_0} \tag{5.4.13}$$

If $tan\delta$ and Δl are known, g_0 can be computed. The frequency can be taken as the midband frequency since g_0 does not change very much across the operating band of the waveguide. The only condition for equations (5.4.11) to (5.4.13) to be valid is that

$$\alpha_n \Delta l \ll 1 \tag{5.4.14}$$

The TLM discretization of a matched termination (of Fig. 5.3) is shown in Fig. 5.5. Note that all boundaries are placed halfway between nodes to ensure time synchronism of impulses throughout the TLM mesh. g_1 and g_9 are the characteristic admittances of the loss stubs of sections 1 and 9, respectively. To satisfy the condition given by (5.4.14), and to keep the velocity dispersion error to a tolerable level, the width of the waveguide is discretized into $30\Delta l$ (i.e. N=30 in Fig. 5.5), and about $180\Delta l$ are needed along the length to realize a $WR28$ waveguide matched termination (shown in Fig. 5.3(a)). The return loss obtained with a TLM simulation is given in Fig. 5.4. A minimum return loss of 32 dB is obtained over the operating band of $WR28$ waveguide. This means that the reflections of the absorbing boundary (input plane of the matched termination) are less than 2.5 percent. This proves the ability of the TLM method to properly account for the losses. The results can be further improved with finer discretization and more iterations.

5.4.2 MODELING OF A VERY LONG UNIFORM WAVEGUIDE SECTION

In this approach, the wideband termination is represented by a very long waveguide section, and computations are stopped before the reflections from the far end return to the reference plane. For example, for a computation covering 2000 iterations, we need to discretize a waveguide section which is 1000 Δl long.

To compute the scattering parameters of a microwave two-port over a wide frequency band in a single TLM run, two absorbing boundaries are needed, one at each port. If the absorbing boundary conditions of Section 5.4.1 is used, the total additional length to discretize two absorbing boundaries would be about $400\Delta l$, while for the approach discussed in this Section, it would be about $2000\Delta l$ (for a computation requiring 4000 iterations). This indicates that enormous computer run time and memory are required to

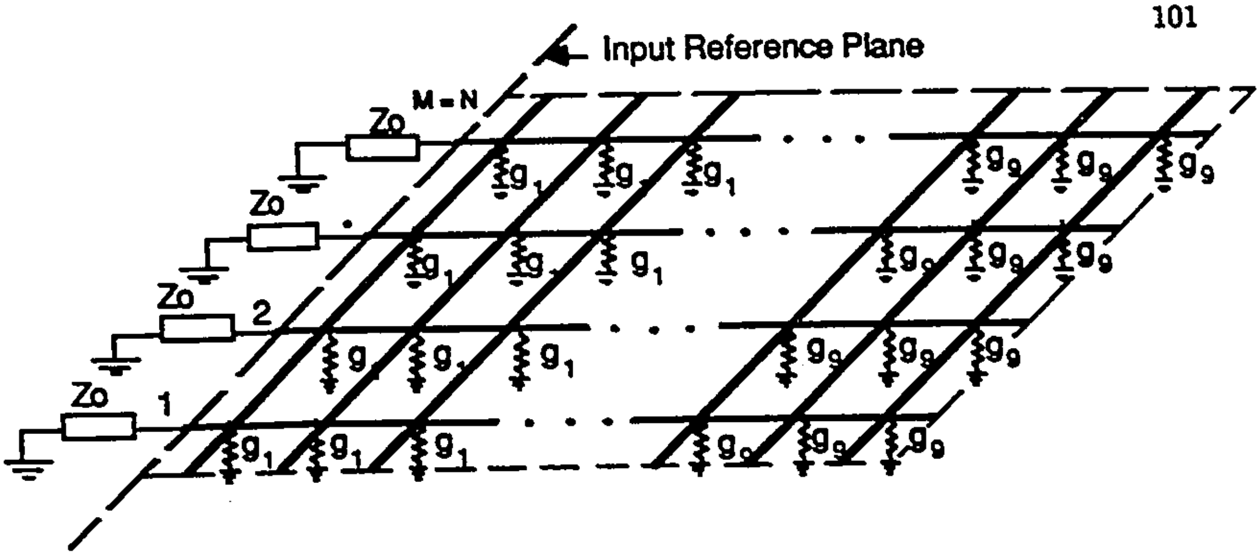

Fig. 5.5 : Configuration for Computing the Discrete Numerical Green's Function or Johns Matrix of a Lossy Waveguide Matched Termination

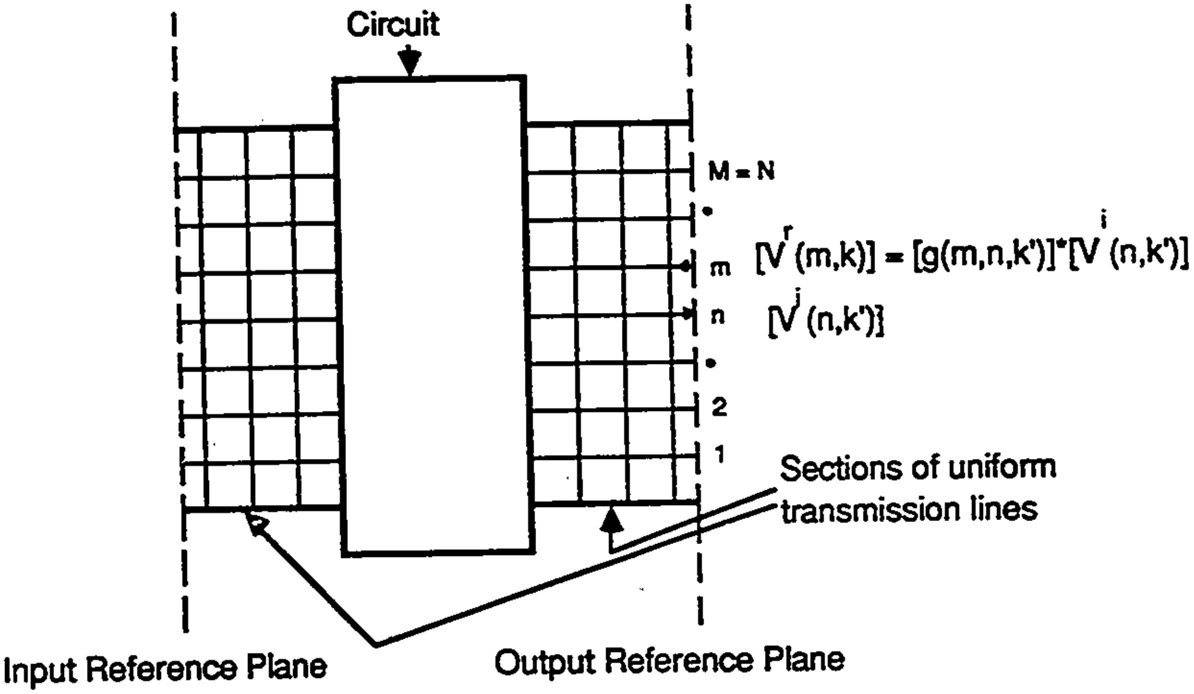

Fig. 5.6 : Convolution of the Johns Matrices of Wideband Matched Terminations with the Impulse Response of the Circuit

achieve the absorbing boundaries with the conventional TLM algorithm. However, these problems can be solved effectively, with less computational effort, by using Diakoptics and space interpolation techniques as described in the following section.

5.4.3 IMPLEMENTATION OF WIDEBAND ABSORBING BOUNDARY CONDITIONS WITH TIME DOMAIN DIAKOPTICS APPROACH

The Diakoptics technique has been used to represent wideband matched terminations (shown in Fig. 5.5) at the input reference plane by their time domain characteristic impulse response or Johns Matrix. Then only the circuit to be characterized is discretized and its time domain response is convolved with the Johns Matrices at the input and output reference planes of the circuit (see Fig. 5.6).

The computer run time and memory required with the conventional TLM algorithm (i. e. to discretize the circuit and two matched terminations together) is proportional to

$$(NX^c + 2 \times NX^m) \times N \times K \tag{5.4.15}$$

while that with Diakoptics technique is

$$(NX^c \times N \times K) \; + \; (K \times (K+1) \times N^2) \tag{5.4.16}$$

where NX^c is the number of grids along the length of the circuit, NX^m is the number of grids along the length of a matched load and N is the total number of branches along the reference plane. In equation (5.4.16), the first term corresponds to the discretization of the circuit and the second part to the convolution with the Johns Matrices of the matched loads. Note that this representation of absorbing boundaries is mode independent and is accurate for any incident field configuration, including hybrid modes, where the transverse field distribution is frequency dependent.

However, to compute the scattering parameters for dominant mode excitation, the computer resources required for convolution can be reduced if the input and output reference planes are placed far away from the circuit or discontinuity under consideration. This ensures that only the dominant mode propagates along the uniform guide (higher order mode effects on the transverse field distribution can be neglected). In such cases, if the circuit is excited at all the nodes along the input reference plane with impulses whose magnitudes are spatially distributed according to the dominant field distribution, the reflected impulses from these nodes at any iteration will have the same spatial distribution. Hence the impulse response of a matched load can be represented by just storing the reflected impulse values at any one node for the required number of iterations. Knowing the transverse field distribution of the propagating mode (e.g., $sin(\pi x/a)$ variation for TE_{10} mode propagation in waveguides), the reflected impulses at the other nodes can be calculated. Hence the Johns Matrix $G(M, N, K)$ becomes one - dimensional and of size K, the total number of iterations. Thus the memory required to store the Johns Matrix is reduced by a factor of N^2, and the time required to compute the Johns Matrix is reduced by a factor of N, where N is the total number of branches along the reference plane.

Note that in the convolution algorithm (described by the eqn(4.4.5), the reflected impulses on all N branches along the reference planes are computed at each iteration. The number of required computational steps are given by the second term of equation (5.4.16). However, under the above assumption, one can perform the convolution at only one node and calculate the reflected impulses at all other branches according to the spatial distribution of the dominant mode. Hence, the time and memory taken to convolve is reduced by a factor of (N^2) and the equation (5.4.16) becomes

$$(NX^c \times N \times K) \ + \ (K \times (K+1)) \tag{5.4.17}$$

Using the above technique, the return loss of the opposing absorbing boundaries (modeled as described in the Sections 5.4.1 and 5.4.3) separated by a length of WR28 waveguide (about 50 Δl long) has been computed. The return loss (obtained as $20\log\frac{VSWR-1}{VSWR+1}$) is shown in Fig. 5.7. It is less than -35 dB throughout the operating band of the $WR28$ waveguide for the approach discussed in Section 5.4.1, while for the approach discussed in Section 5.4.2, it is less than -30 dB, and the response is flat as expected. The propagation constant β can be obtained by solving

$$e^{-j\beta(\omega)(L_2-L_1)} = \frac{E_y(\omega, z = L_1)}{E_y(\omega, z = L_2)} \tag{5.4.18}$$

where L_1 and L_2 are the distances from the origin to any two points along the waveguide, and E_y are the Fourier transforms of $E_y(t)$ at $z = L_1$ and $z = L_2$. For the uniform $WR28$ waveguide, these β values agree exactly with the analytical values over the whole operating frequency band. Also, the phase difference of fields between any two consecutive nodes along the length of the waveguide is the same. This demonstrates the excellent quality of the wideband absorbing boundaries.

5.5 EXTRACTION OF SCATTERING PARAMETERS

In the past, the reflection coefficient (say S_{11}) has been computed by finding the amplitudes and positions of voltage maxima and minima in the corresponding port as in a slotted line measurement. Hence additional port lengths of several wavelengths long had to be discretized and a fine mesh was needed to compute the magnitude and phase of reflection coefficient accurately.

The scattering parameter extraction procedure has been made more simple and accurate by the application of the above absorbing boundary conditions. Extraction of the

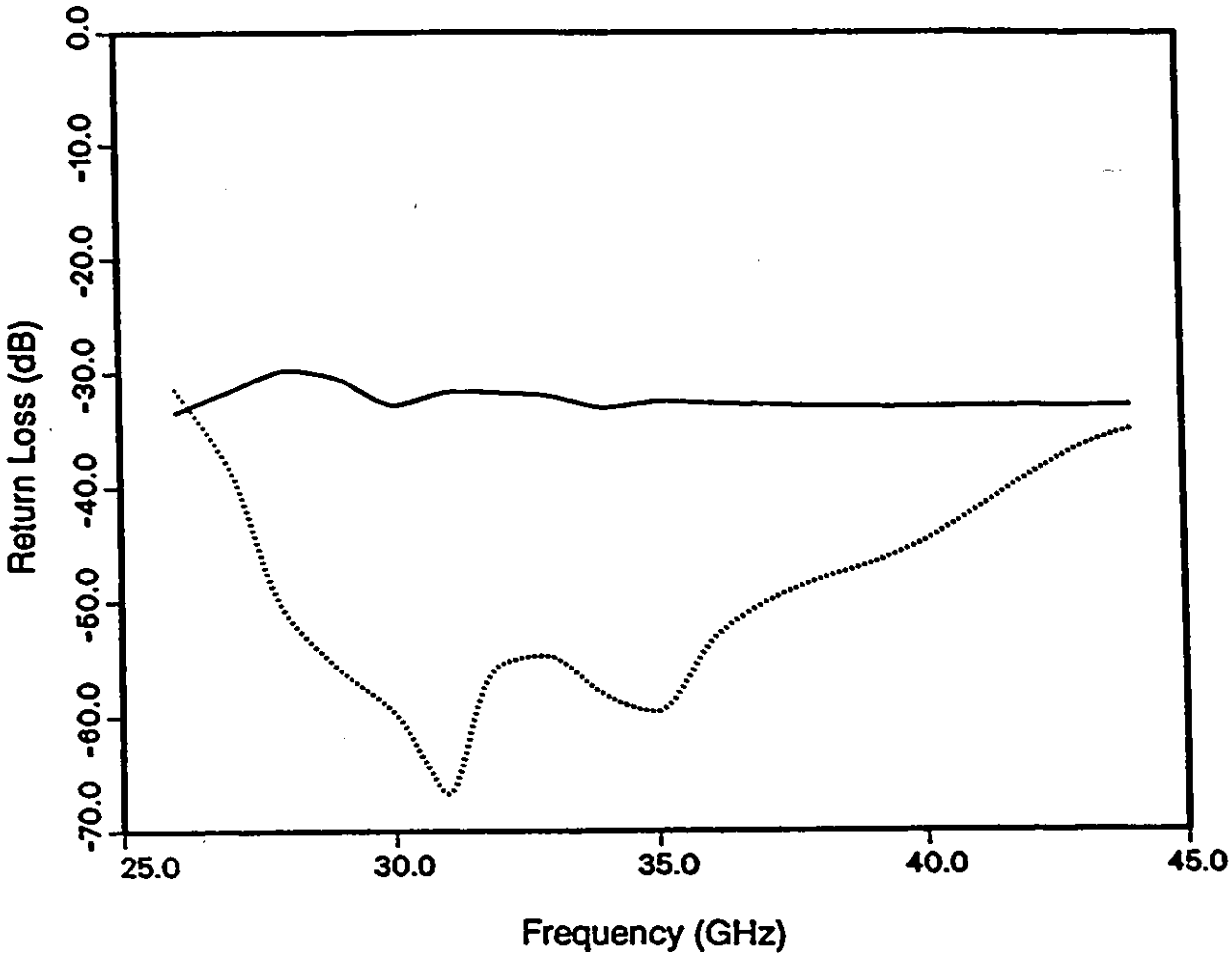

Fig. 5.7 : Return loss of back-to-back waveguide absorbing boundaries computed with Diakoptics.

...... Lossy waveguide termination

—— Long uniform guide termination

reflection coefficient demands separation of reflected field from the total field. The incident field ($\overline{V}_{inc}$) is obtained from analysis of a small section of the empty guide terminated at both ends with simulated wideband matched terminations. The total field ($\overline{V}_{tot}$) and the transmitted field ($\overline{V}_{trans}$) are obtained from analysis of the circuit with discontinuity present. The complex reflection and transmission coefficients can then be obtained as follows:

$$S_{11} = \frac{\overline{V}_{tot} - \overline{V}_{inc}}{\overline{V}_{inc}} \tag{5.5.1}$$

$$S_{12} = \frac{\overline{V}_{trans}}{\overline{V}_{inc}} \tag{5.5.2}$$

5.6 APPLICATIONS

To further check the quality of the wideband absorbing boundary conditions and to verify the validity of the proposed space interpolation techniques, the S-parameters of an inductive waveguide iris discontinuity, a Chebyshev iris-coupled waveguide bandpass filter and an E-plane bandpass filter have been computed.

5.6.1 INDUCTIVE WAVEGUIDE IRIS DISCONTINUITY

Fig. 5.8 shows the computed magnitude and phase of the S-parameters of a symmetrical inductive iris (of gap width equal to 3.556 mm) in a $WR28$ waveguide. Results compare well with those computed using empirical formulas given in [86]. The electric field variation along the center line of the waveguide around the inductive iris is shown in Fig. 5.9 for five different frequencies. Note a steep dip in the magnitude of the electric field at the discontinuity. The fields become almost constant for all frequencies on the the right-hand side of the discontinuity, indicating the excellent quality of the matched loads. Fields vary sinusoidally towards the left side of the discontinuity as expected. Also, it can

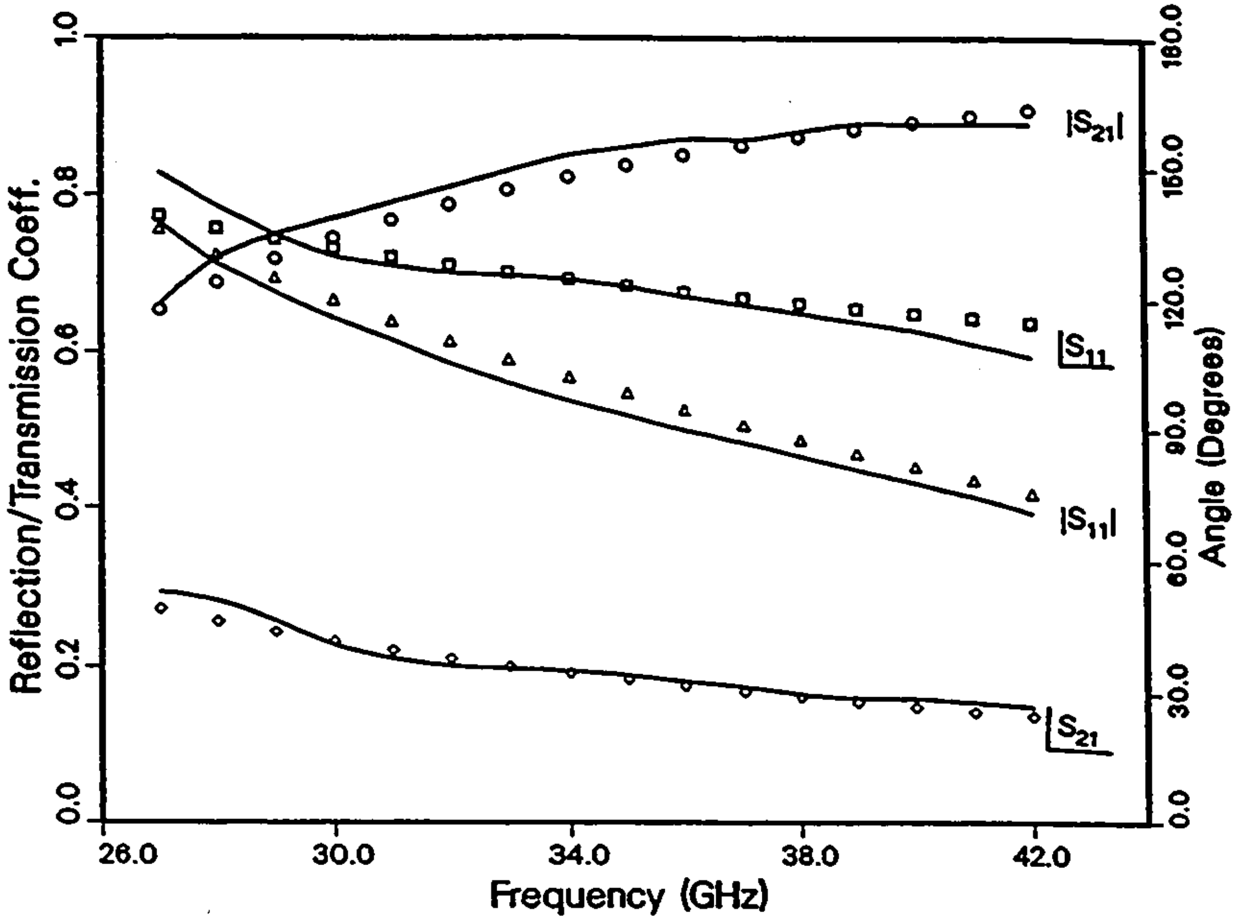

Fig. 5.8 : S-parameters of an inductive iris.
— Computed with Diakoptics
◇ □ △ ○ Marcuvitz [86]

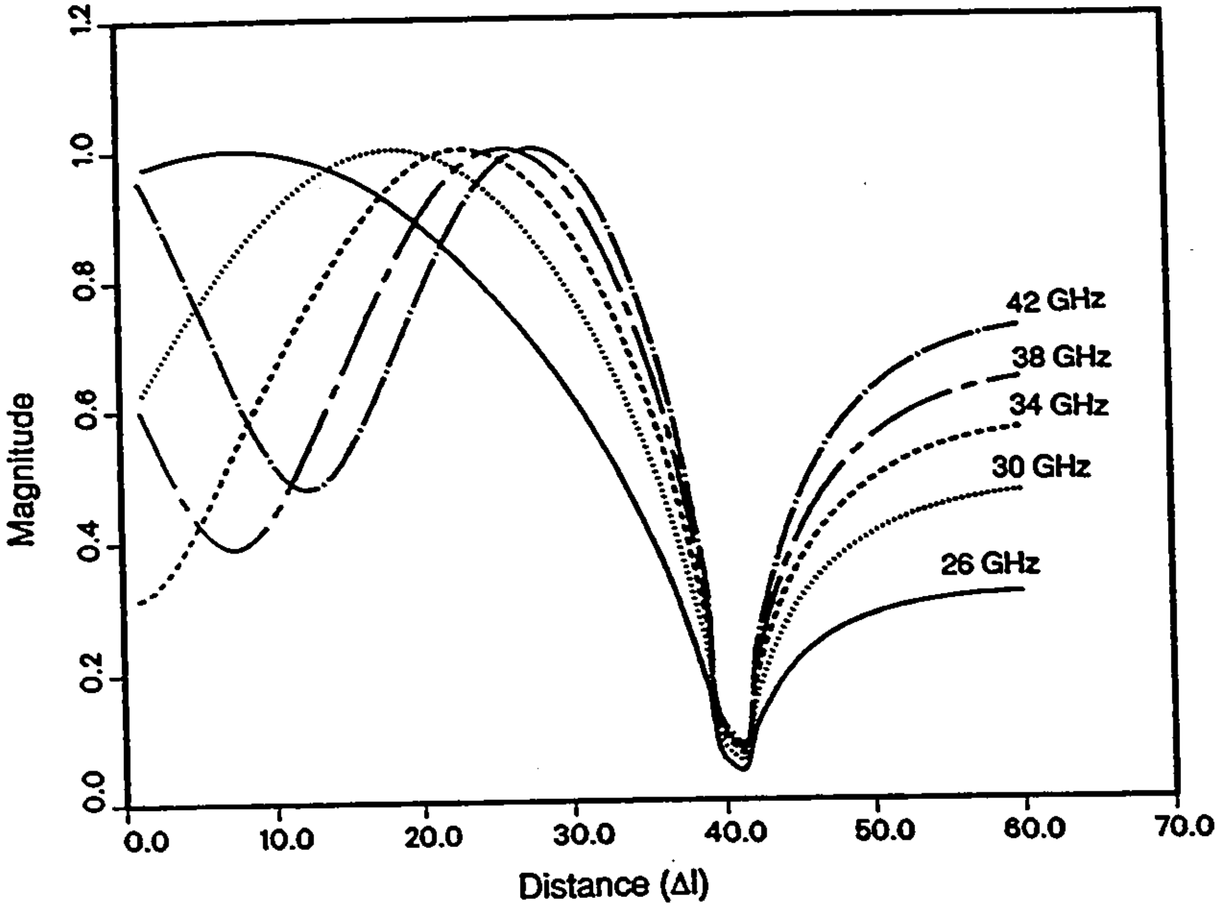

Fig. 5.9 : Electric field variation along the length of a waveguide containing the inductive iris discontinuity at 40 Δl

be seen that the higher order mode effect is almost negligible beyond a distance of about $20\Delta l$ on either side of the discontinuity.

5.6.2 E-PLANE FILTER

Fig. 5.10 (a) shows the geometry of a two-section maximum flat bandpass filter [87] with the following specifications:

Center Frequency : 10.95 GHz

Bandwidth : 218 MHz

Guide Width : 18.8 mm

Strip Thickness : 0.3 mm

The computed transmission characteristics are given in Fig. 5.10 (b). The results compare well with those computed with the Mode Matching Technique.

5.6.3 IRIS COUPLED WAVEGUIDE BANDPASS FILTER

Fig. 5.11 (a) shows the geometry of a four-section Chebyshev iris-coupled waveguide bandpass filter with the following characteristics :

Center Frequency : 32 GHz

Bandwidth : 2 GHz

Guide Width : 7.112 mm

Strip Thickness : 0.3 mm

Pass band ripple : 0.01 dB (equivalent of 26 dB return loss)

The dimensions of the filter were calculated following the design method given in [88]. They are

D_0 : 3.580 mm

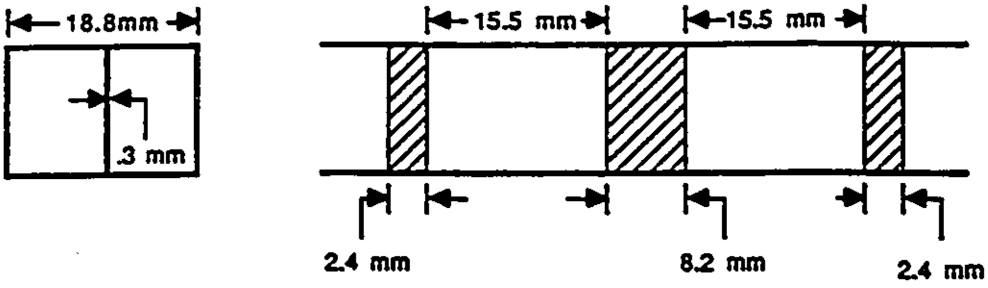

Fig. 5.10 (a) : The Geometry of a Two-Section Maximum Flat E-Plane Filter

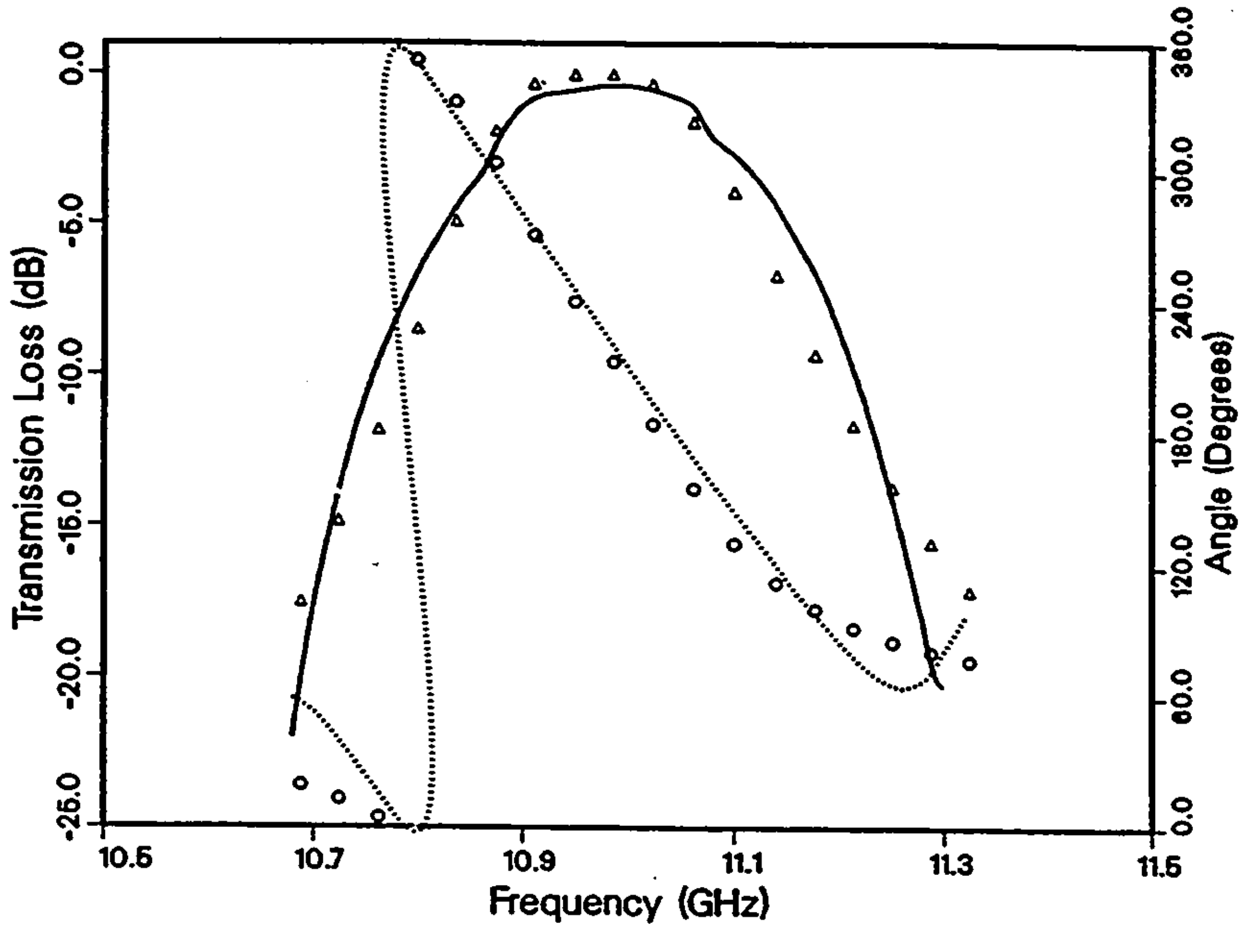

Fig. 5.10 (b) : Transmission characteristics of a E-plane filter

— |S21| computed with Diakoptics

..... $\underline{S21}$ computed with Diakoptics

△ |S21| computed with Mode Matching Technique

o $\underline{S21}$ computed with Mode Matching Technique

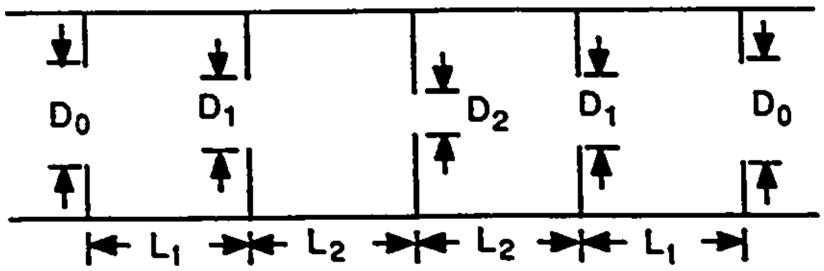

Fig. 11(a) : The geometry of a four-section Chebyshev iris-coupled bandpass filter

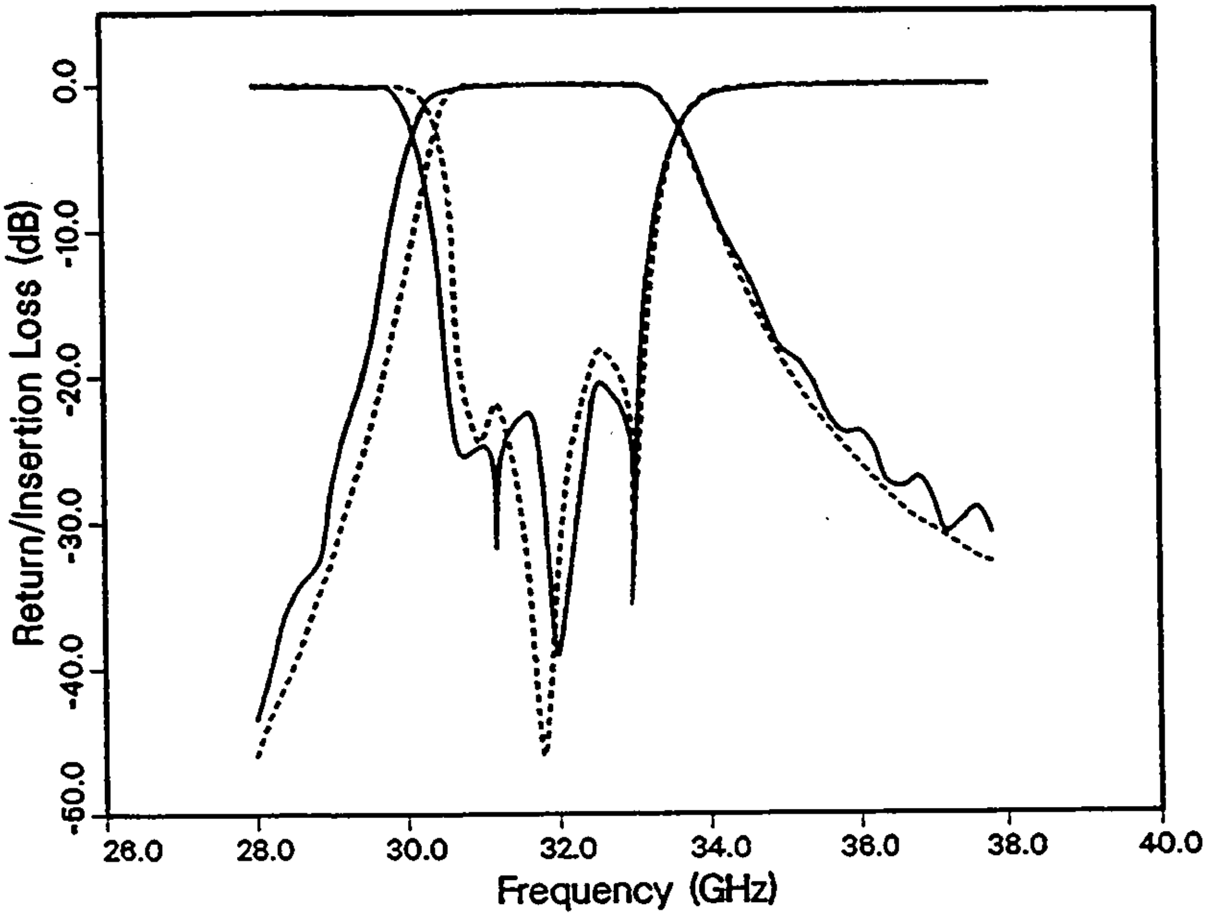

Fig. 5.11(b) : A comparison of the return loss and insertion loss characteristics, obtained by lumped element model and Diakoptics, of a waveguide iris-coupled bandpass filter.
— Diakoptics, --- Super-Compact

D_1 : 2.340 mm

D_2 : 2.050 mm

L_1 : 4.954 mm

L_2 : 5.591 mm

The computed return loss and transmission loss are given in Fig. 5.11 (b). For comparison, this bandpass filter was analyzed with $Super - Compact^{TM}$ accounting for the frequency dependent susceptance of the irises [86]. The results obtained with both methods are compared in Fig. 5.11 (b) and agree well.

5.7 CONCLUSIONS

Excellent wideband waveguide absorbing boundary conditions have been implemented using the Johns Time Domain Diakoptics approach. A space interpolation technique based on the dominant field distribution has been proposed for efficient S-parameter extraction. The good accuracy of this technique and the quality of wideband absorbing boundary conditions are illustrated by the close agreement of the computed S-parameters of waveguide components with data obtained with the other methods.

Chapter VI

DIAKOPTICS AND WIDEBAND DISPERSIVE ABSORBING BOUNDARIES IN THE 3-D TLM METHOD WITH SYMMETRICAL CONDENSED NODES

6.1 INTRODUCTION

The Diakoptics procedure and wideband absorbing boundary conditions for 2-D TLM modelling of microwave structures have been described in Chapters IV and V, respectively. For the analysis of three-dimensional microwave circuits, 3-D TLM nodes discussed in the Section 2.3.3 should be used. Among the three existing nodes, the symmetrical condensed node is the most appropriate for the description of boundaries and dielectric interfaces, and the application of Diakoptics. The characteristics of this node were described in Section 2.3.3. Furthermore, this node exhibits less dispersion. However, there have been no reports on the computation of microwave scattering parameters with these nodes. To extract the scattering parameters over a wide range of frequencies from a single TLM simulation, wideband absorbing boundaries must be modeled in the time domain.

In this chapter, the Diakoptics technique is applied in the 3-D TLM algorithm with symmetrical condensed nodes. A 3-D " Johns Matrix " is proposed for representing the impulse response of any substructure in the time domain and wideband non-TEM absorbing boundaries are implemented using this Johns Matrix concept. In Chapter V, wideband absorbing boundary conditions in the 2D-TLM model have been implemented using two approaches - one employing the Johns Matrix of a very long waveguide, and the second using the Johns Matrix of a lossy waveguide termination. It was found that the second approach gives absorbing boundaries of better performance than the first approach. However, the lossy waveguide termination cannot be modeled with the present 3-D condensed nodes. In this chapter, a novel approach to simulate a lossy waveguide termination without physically modeling the losses has been presented. This approach yields absorbing boundaries having less than one percent reflections over the entire operating frequency band of a waveguide. The performance of the algorithms based on these concepts will be examined by applying the methods to some 3-D waveguide discontinuities.

6.2 TIME DOMAIN DIAKOPTICS

The application of Diakoptics to 2-D TLM method was described in the Section 4.4. The method is similar for the 3-D case using condensed nodes except for the additional complexity associated with the 3-D algorithm.

Fig. 6.1 shows the TLM representation of a large 3-D network divided into two substructures designated S_{super} and S_{sub}. A cross-section in the $x-y$ plane is shown. There are a total of six such cross-sections which form the interface between S_{super} and S_{sub}. Let us assume that the substructure S_{sub} represents a small portion of the network which needs to be modified repeatedly (for example during an optimization process), and the structure S_{super} is the major portion of the network which remains unchanged. First, the time domain response (impulse response) of S_{super} with respect to the N interconnection

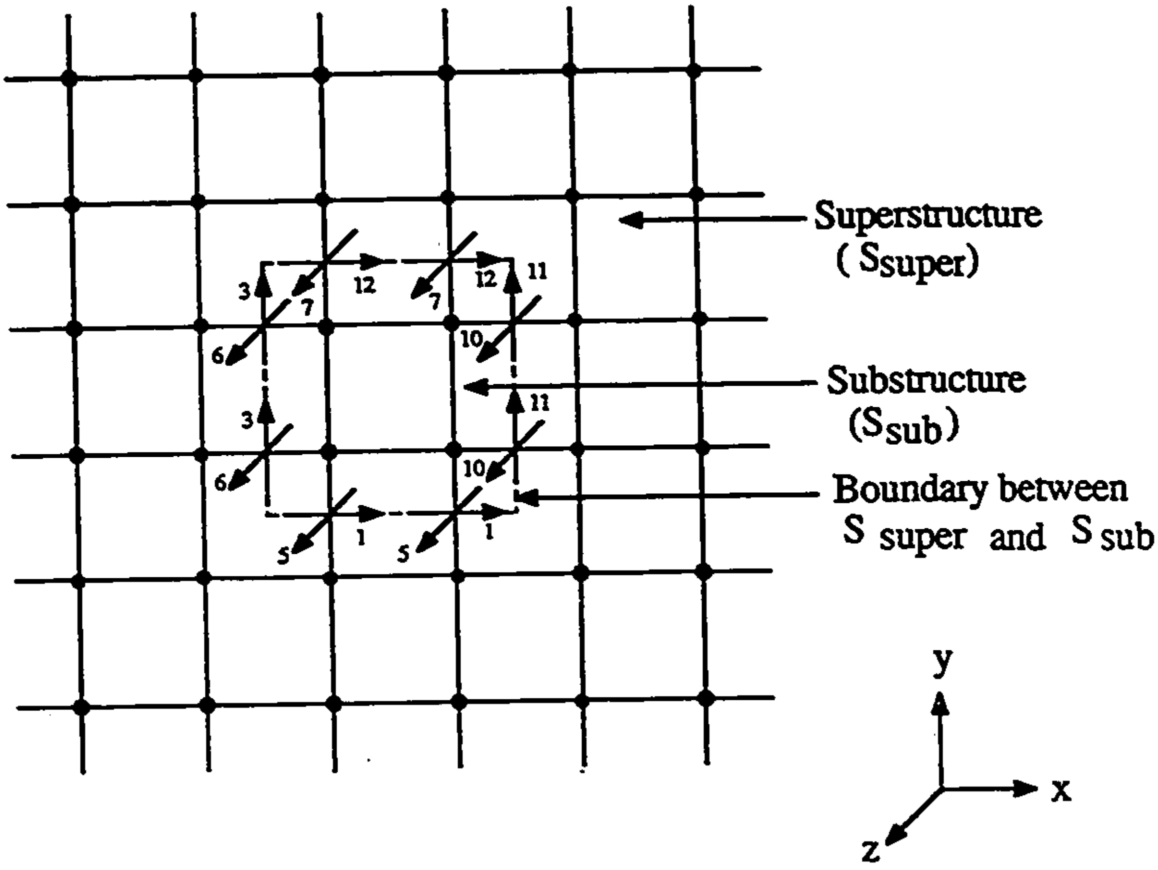

Fig. 6.1 : Partitioning of a Large Network Using Diakoptics

ports is computed and stored (where N is the total number of interconnection ports across the interface; for the example shown in Fig. 6.1, there are 16 interconnection ports in the $x-y$ plane). Then, only the substructure S_{sub} (whenever a change is made in the geometry) is discretized and excited. The impulses emerging from the " removed branches " across the interface are convolved with the impulse response of S_{super}.

To compute the impulse response of S_{super}, the transmission lines across the interface are terminated with matched loads (zero local reflection coefficient). Note that each connection (shown in Fig. 6.1) represents two transmission lines carrying two orthogonal polarizations as indicated by the arrows. A single impulse injected at any of these branches across the interface will cause impulses separated by two times the iteration time interval to flow in streams out of this structure. The impulse response, designated as $g(m,n,k)$, represents the output impulse function emerging at the m-th port (originating from the node $(x=i\Delta l, y=j\Delta l, z=l\Delta l)$) at $t=k\ \Delta t$ due to a unit excitation of the n-th port (originating from the node $(x=i'\Delta l, y=j'\Delta l, z=l'\Delta l)$) at $t=0$. It is a three-dimensional array of dimension $(M\times N\times K)$, where K is the total number of iterations, and $M=N$ is the total number of ports across the interface. Note that each port corresponds to one polarization of a branch. This numerical Green's function has been named as the " 3-D Johns Matrix " in honour of the late P. B. Johns.

When impulses are injected into the structure S_{sub} to excite it, they are scattered at nodes and reach the branches at the interface after some time. Any impulse which hits the interface will give rise to streams of impulses, separated by $2\Delta t$, which flow back into the structure through all the branches. These reflected impulse voltages are computed, using the equation (4.4.5), by convolving the incident impulses with the Johns Matrix of S_{super}.

This scheme will be more efficient than the conventional TLM algorithm only if the structure S_{super} is very big (in such cases, the convolution time will be smaller than the time needed to discretize S_{super}, every time a change is made). However, for wideband S-parameter extraction of microwave circuits in waveguide systems, this algorithm becomes very efficient; it will be discussed below:

6.3 MODELING OF ABSORBING BOUNDARY CONDITIONS

The objective is to compute the scattering parameters of a 3-D discontinuity, or a set of discontinuities, in a waveguiding structure. To this end, one must compute the incident, reflected and transmitted fields at the reference planes indicated in Fig. 6.2. It is assumed that only the dominant mode of the embedding structure exists at these reference planes over a given frequency band. The space between the two reference planes is modeled by a 3-D TLM condensed node mesh. The absorbing boundary conditions must be implemented at the reference planes. These must simulate the extension of the waveguide to infinity away from these planes. To achieve this, the following procedure has been adopted.

a) Compute the impulse response, or Johns Matrix, at the input of a very long waveguide section, and stop the computations before the reflections from the far end return to the reference plane. For example, for a computation covering 2000 iterations, one needs to discretize a waveguide section which is 500 Δl long (because the velocity of waves on the TLM mesh with condensed nodes is half the velocity of pulses on the individual mesh transmission lines).

b) Then the structure between the reference planes (shown in Fig. 6.3) is discretized and excited at one end, and the impulses emerging from these planes are convolved with the Johns Matrices computed above.

These two procedures are explained in detail below.

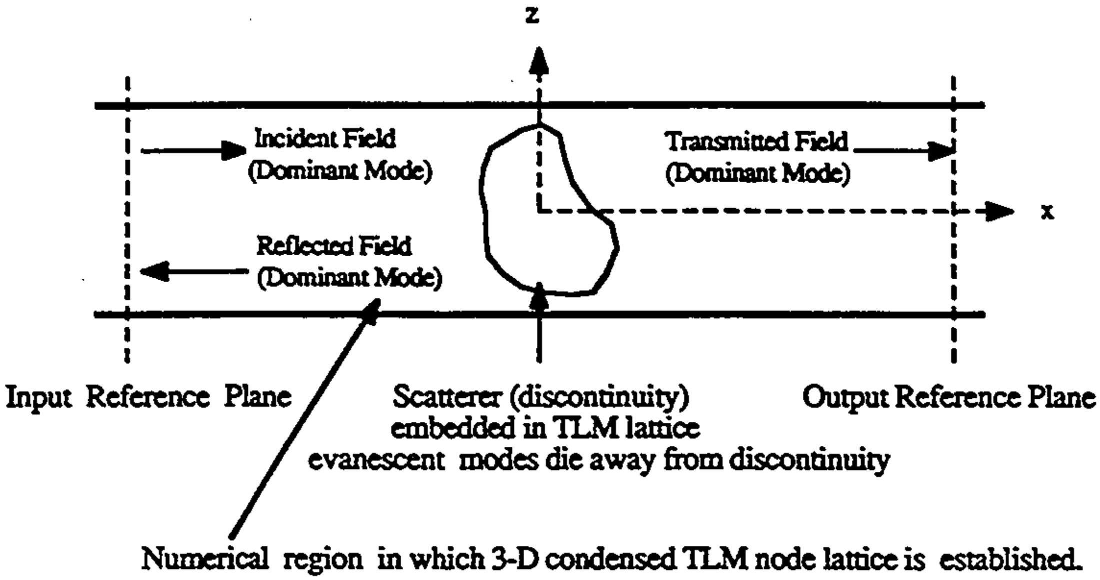

Fig. 6.2 : Discontinuity in a Waveguide Section

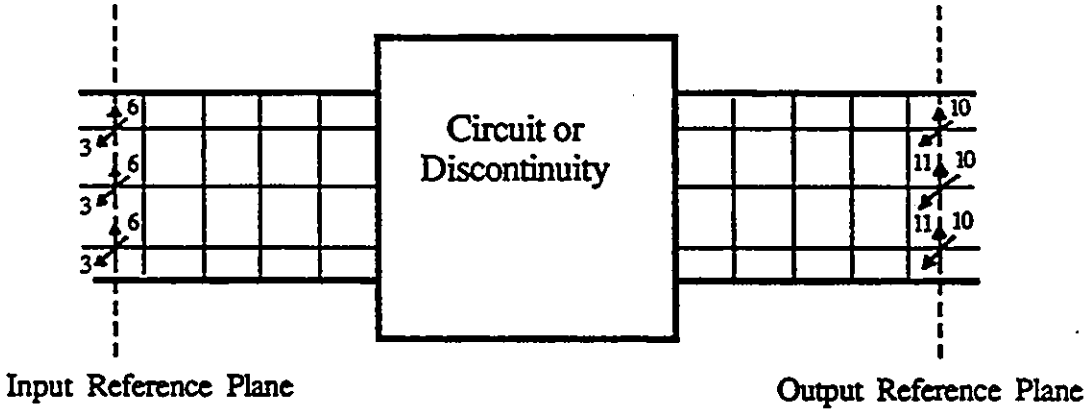

Fig. 6.3 : S-parameter Extraction Using Diakoptics

6.3.1 COMPUTATION OF IMPULSE RESPONSE OR JOHNS MATRIX OF A LONG WAVEGUIDE

A long section of waveguide is discretized with 3-D TLM condensed nodes. Note that for TE_{10} mode propagation, the pulse values on branches 6, 10, 2 and 9 of condensed nodes are always zero (because E_x and E_z are zero). Hence non-zero impulse values exist only on the remaining 8 branches. Furthermore, since there is no variation along y, a single node in the y-direction may be used. The impulses (whose magnitudes vary as $sin(\pi z/a)$ along the z-direction) are injected into branch 3 of all the nodes along the input reference plane of the structure. This will cause impulses, separated by two times the iteration time interval, to flow in streams out of branch 3 of all the nodes along the input reference plane of this structure. The impulses on branch 3 of the condensed node in the center of the waveguide cross-section are stored, and they constitute the one-dimensional "Johns Matrix".

6.3.2 CONVOLUTION WITH THE IMPULSE RESPONSE OR JOHNS MATRIX

The circuit shown in Fig. 6.3 is excited at branch 3 of all the nodes along the input reference plane with impulses whose magnitudes are spatially distributed according to the amplitude of the dominant mode (Half a sin-period for the TE_{10} mode). These impulses are scattered at nodes and boundaries and reach the input and output reference planes after some time. The impulses arriving on branch 3 of the center node on the input reference plane and branch 11 of the center node on the output reference plane are stored. Then the reflected impulse voltages on these branches are computed by convolving the incident impulses with the Johns Matrix computed previously:

$$V_{11}^{r}(k) = \sum_{k'=0}^{k} J(k') * V_{11}^{i}(k-k') \tag{6.3.1}$$

$$V_3^r(k) = \sum_{k'=0}^{k} J(k') * \ V_3^i(k - k') \qquad (6.3.2)$$

where J is the one-dimensional Johns Matrix.

Since the transverse field distribution of the propagating mode is known (e.g., $sin(\pi z/a)$ variation for the TE_{10} mode in rectangular waveguides), the reflected impulses at the other nodes in the reference planes can be calculated from those at the center.

Following the above approach, the reflections of two absorbing boundaries terminating a $WR28$ waveguide section (about 60 Δl long) have been computed. The magnitude of these reflections is shown in Fig. 6.4. They vary from 6 to 2 percent over the operating band of the waveguide and are due to the dispersive nature of the discrete TLM network. The S-parameters of a symmetrical inductive iris (of gap width equal to 3.46 mm) in a $WR28$ waveguide has been computed using these imperfect absorbing boundary conditions and compared with those computed using Marcuvitz's formulas [86] (Fig. 6.5). Note the ripple in the TLM results, especially in the phase characteristics of the S-parameters. Hence it is concluded that the quality of the absorbing boundaries described by the Johns Matrix of a long section of a uniform guide is not acceptable for S-parameter extraction. In the following, it is shown how these boundary conditions can be improved by "tapering" the Johns Matrix response in the time dimension.

6.4 TAPERED IMPULSE REPONSE OR JOHNS MATRIX

In the case of 2-D TLM absorbing boundary algorithms, it was noticed that a waveguide termination with gradually increasing losses (like in practical waveguide terminations) gives better performance than a long uniform guide. This may be due to the absorption of the stray reflections due to the finite space and time discretization steps Δl and Δt. But the present 3-D condensed node cannot account for losses. However, it is

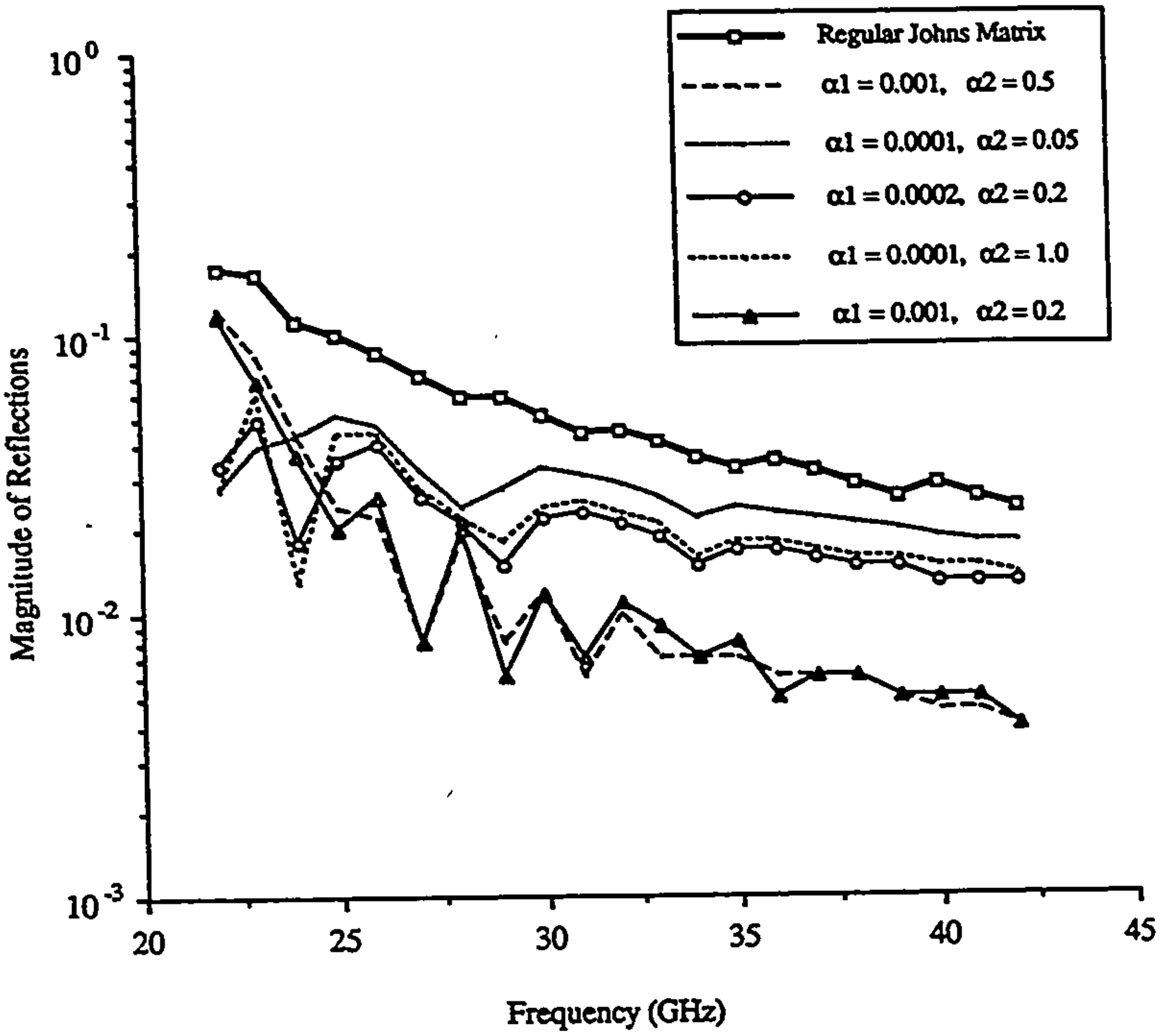

Fig. 6.4 : Reflection Characteristics of Absorbing Boundaries (WR 28) represented by Regular and Tapered Johns Matrices.

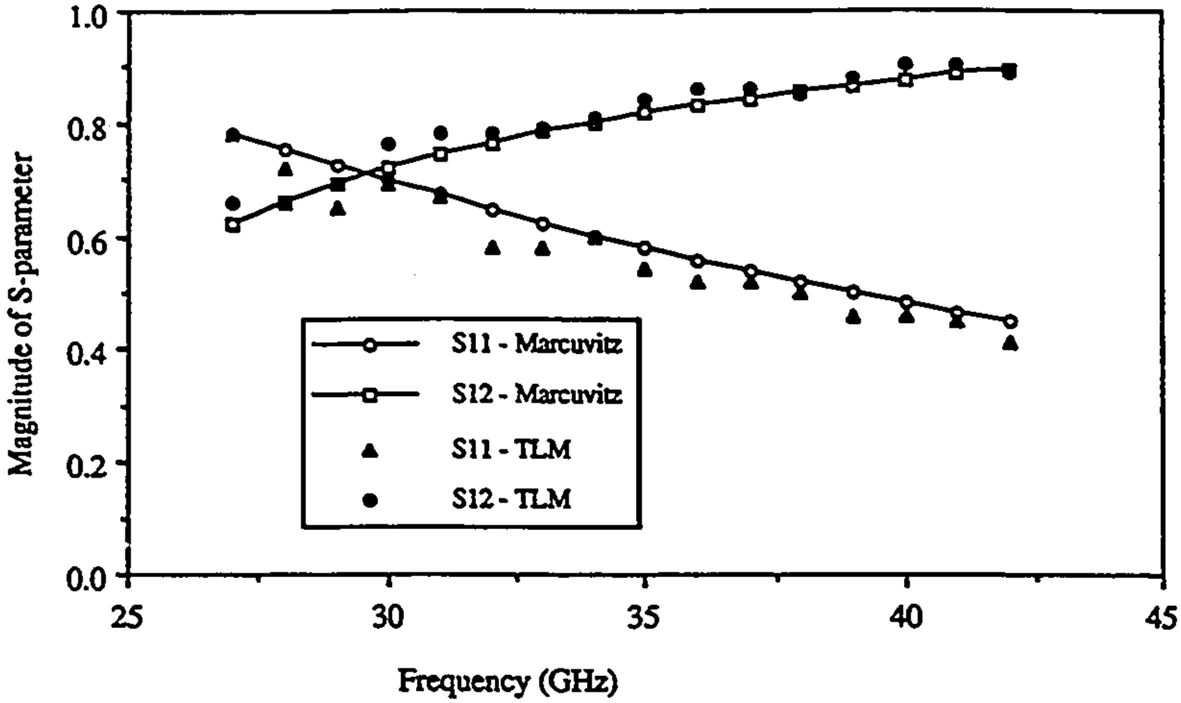

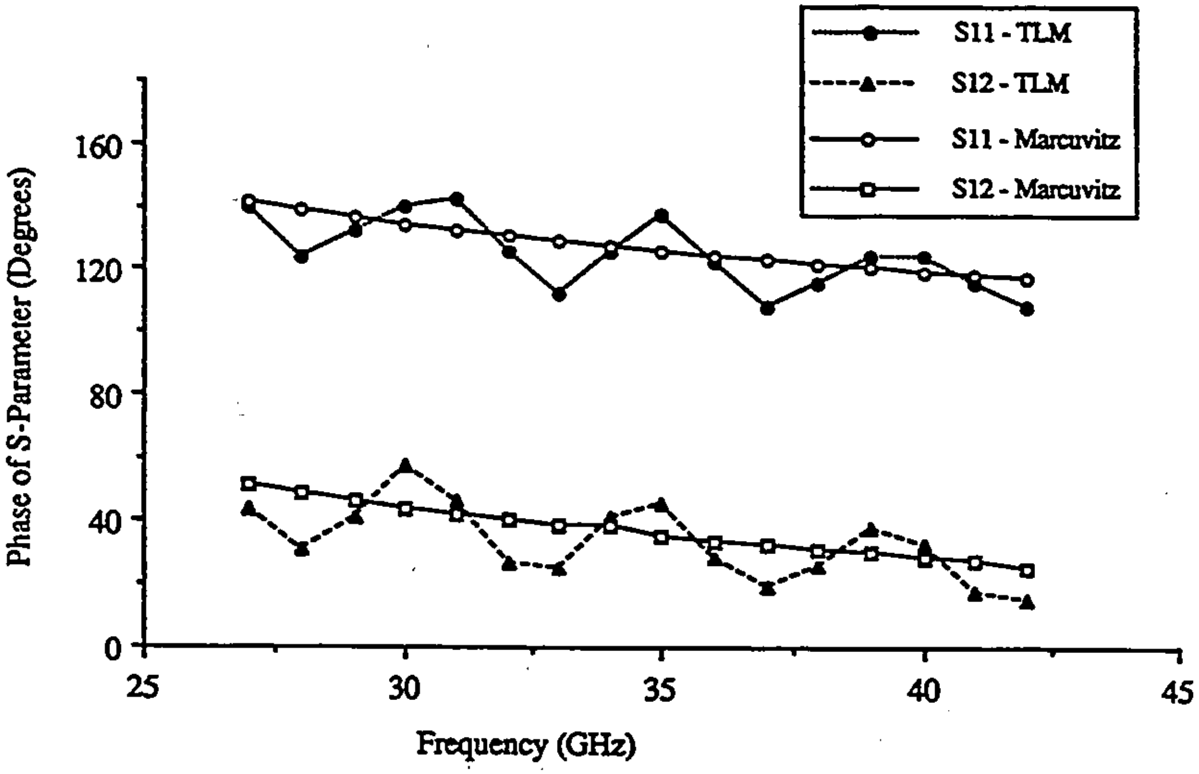

Fig. 6.5 : S-parameters of an Inductive Iris computed with regular Johns Matrix Absorbing boundaries

known that for homogeneous lossy material, the output impulse response value ${}_kA_i'$, for electric and magnetic fields at any node and at any instant $k\Delta t$, is related to the value ${}_kA_i$ in the lossless case as follows [29]:

$$ {}_kA_i' = {}_kA_i \; e^{(-k\alpha\Delta l)} \tag{6.4.1}$$

where α is the attenuation constant of the mesh lines. Thus by merely recalculating the impulse response using different attenuation constants α, different loss conditions can be modeled with a single simulation. Following this argument, the Johns Matrix $J'(k)$ for a long uniform guide with constant loss is related to the Johns Matrix $J(k)$ for a long lossless uniform guide as follows:

$$ J'(k) = J(k) \; e^{(-k\alpha\Delta l)} \tag{6.4.2}$$

However, to minimize reflections over a large bandwidth, the loss must increase slowly along the length of the waveguide. An alternative, but equivalent solution, is to increase α with time. It is found that by exponentially " tapering " the Johns Matrix $J(k)$ of the long uniform guide, this requirement can be met. Hence the tapered Johns Matrix $J'(k)$ can be written as

$$ J'(k) = J(k) \; e^{(-\sum_{k'=1}^{k} \alpha(k'))} \tag{6.4.3}$$

where $\alpha(k')$ is

$$ \alpha(k') = \alpha_1 e^{\left(\frac{(k'-1)}{NI} \ln(\alpha_2/\alpha_1)\right)} \tag{6.4.4}$$

α_1 is the attenuation constant for $k = 1$ (i.e. first iteration) and α_2 the attenuation constant for $k = NI$, the total number of terms in the Johns Matrix. The values of α_1 and

α_2 have been optimized empirically to minimize reflections over the operating bandwidth. The computed reflections of the two opposing absorbing boundaries terminating a $WR28$ waveguide section (about 60 Δl long) are plotted in Fig. 6.4 for different combinations of α_1 and α_2. It can be seen that in some cases, the reflections are less than one percent throughout the operating frequency band.

Using these absorbing boundary conditions, the S-parameters of a symmetrical inductive iris of gap width equal to 3.46 mm in a $WR28$ waveguide have been computed. Results (shown in Fig. 6.6) compare well with those given in [86], and no ripple is detected in either magnitude or phase response. Also, tapering leads to a considerable reduction in the size of the Johns Matrix (from 2000 terms in the regular Johns Matrix to about less than 1100 values in the tapered Johns Matrix). Hence the time taken for the convolution using equations (6.3.1) and (6.3.2) is also considerably reduced.

The algorithm has been applied to compute the S-parameters of some typical 3-D discontinuities. The computed S-parameters of a symmetrical capacitive iris of gap width equal to 1.659 mm in $WR28$ waveguide are compared in Fig. 6.7 with those computed using Marcuvitz's formulas [86]. They compare well. A non-touching axial strip in $WR28$ waveguide (shown in Fig. 6.8) was also analysed. The computed S-parameters are compared in Fig. 6.9 with those computed using the closed-form formulas given in [89]. As described in [89], the non-touching axial strip acts like a series-resonant shunt circuit. The resonant frequency computed with the TLM method is about 36 GHz, being 3 GHz less than that computed using formulas given in [89]. Except for a shift in frequency by 3 GHz, the results are very similar. When the mesh parameter Δl was decreased, there was no appreciable change in results. The grid size used was $(62 \times 32 \times 112)$ and the number of iterations was 3000. The errors associated with the TLM analysis, such

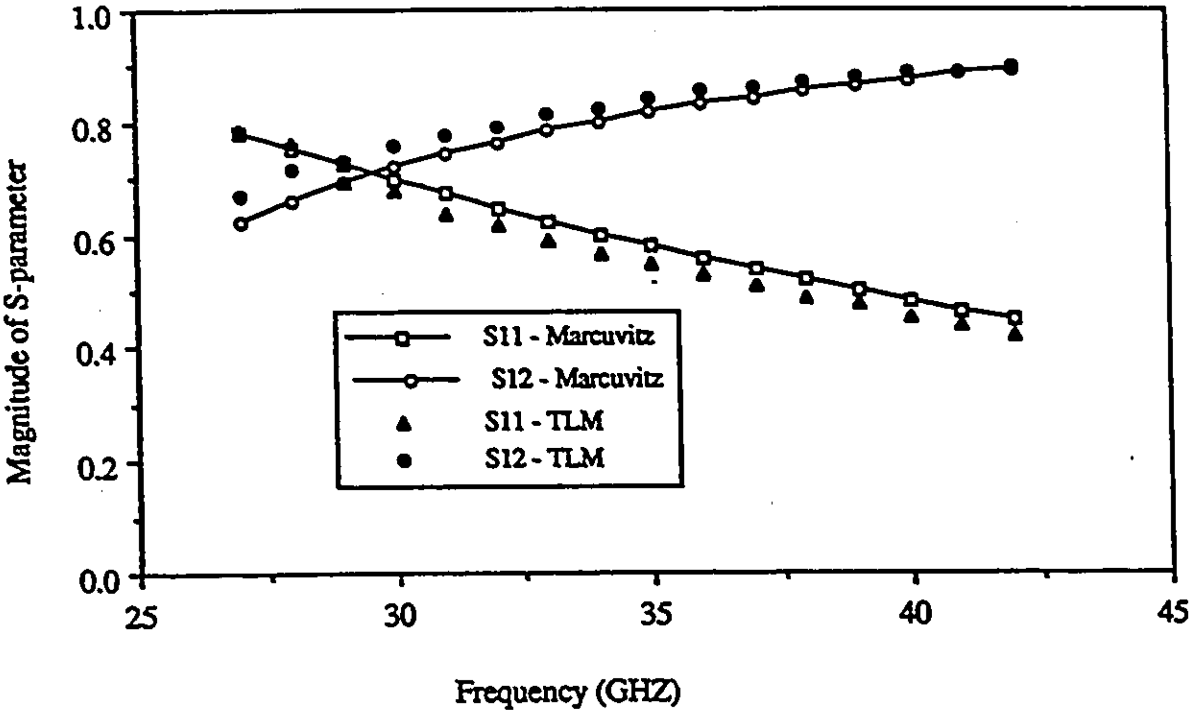

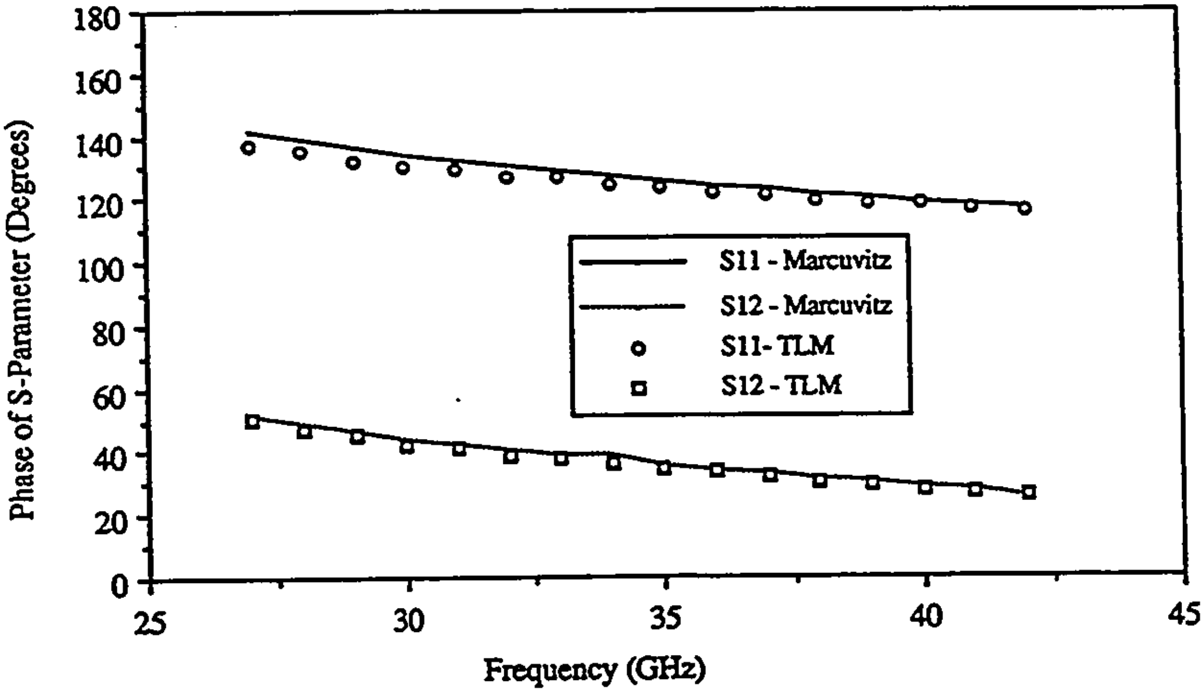

Fig. 6.6 : S-Parameters of an Inductive Iris computed with tapered Johns Matrix Absorbing Boundaries

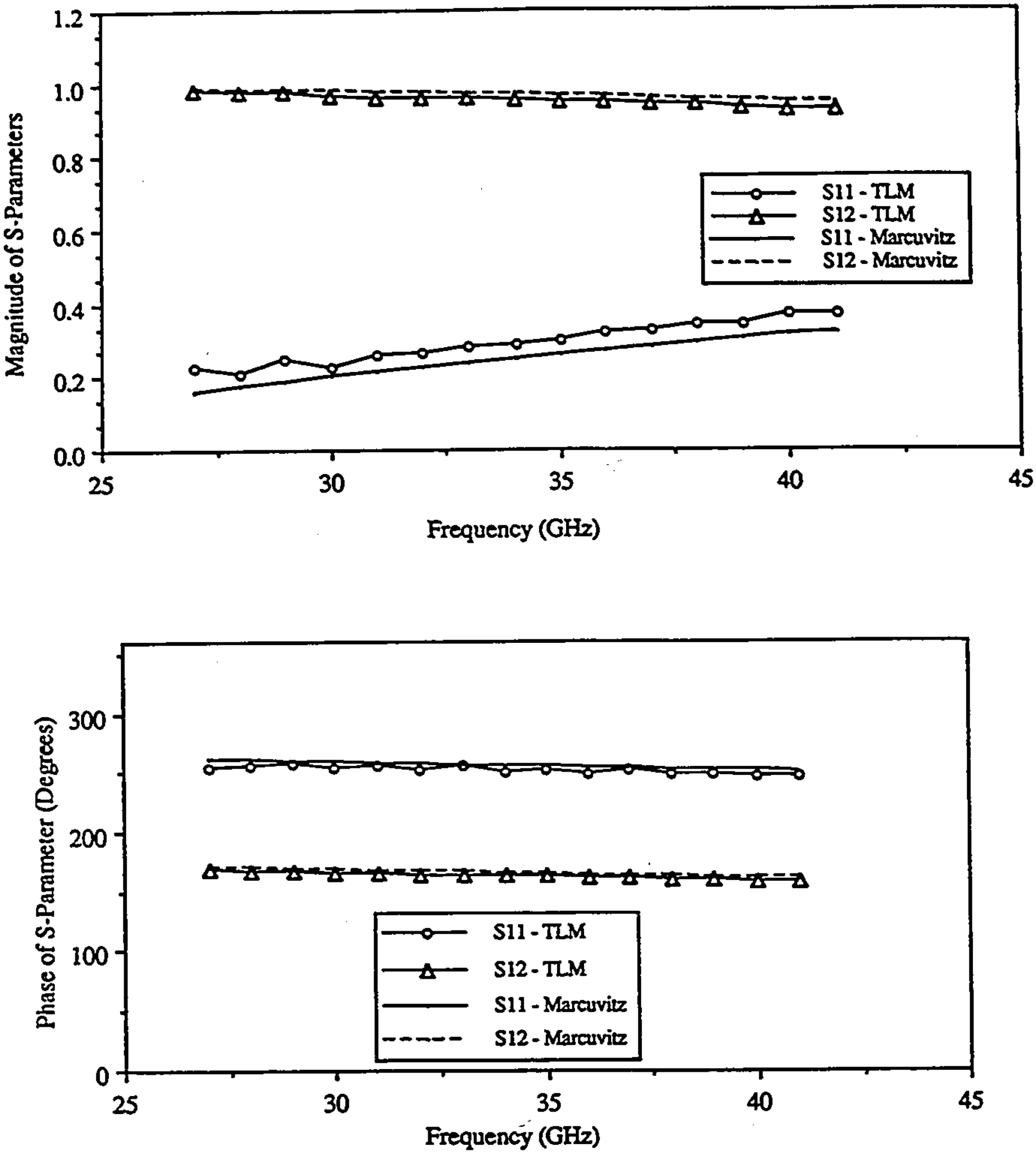

Fig. 6.7 : S-Parameters of a Capacitive Iris Computed with Tapered Johns Matrix Absorbing Boundaries.

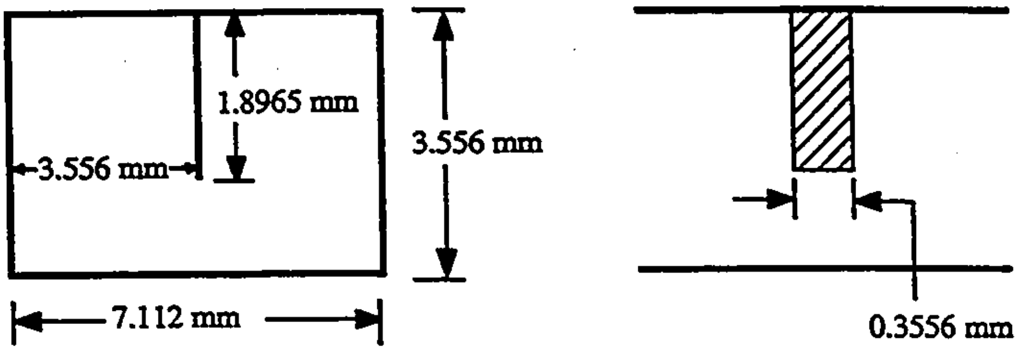

Fig. 6.8 : The axial strip in a rectangular waveguide

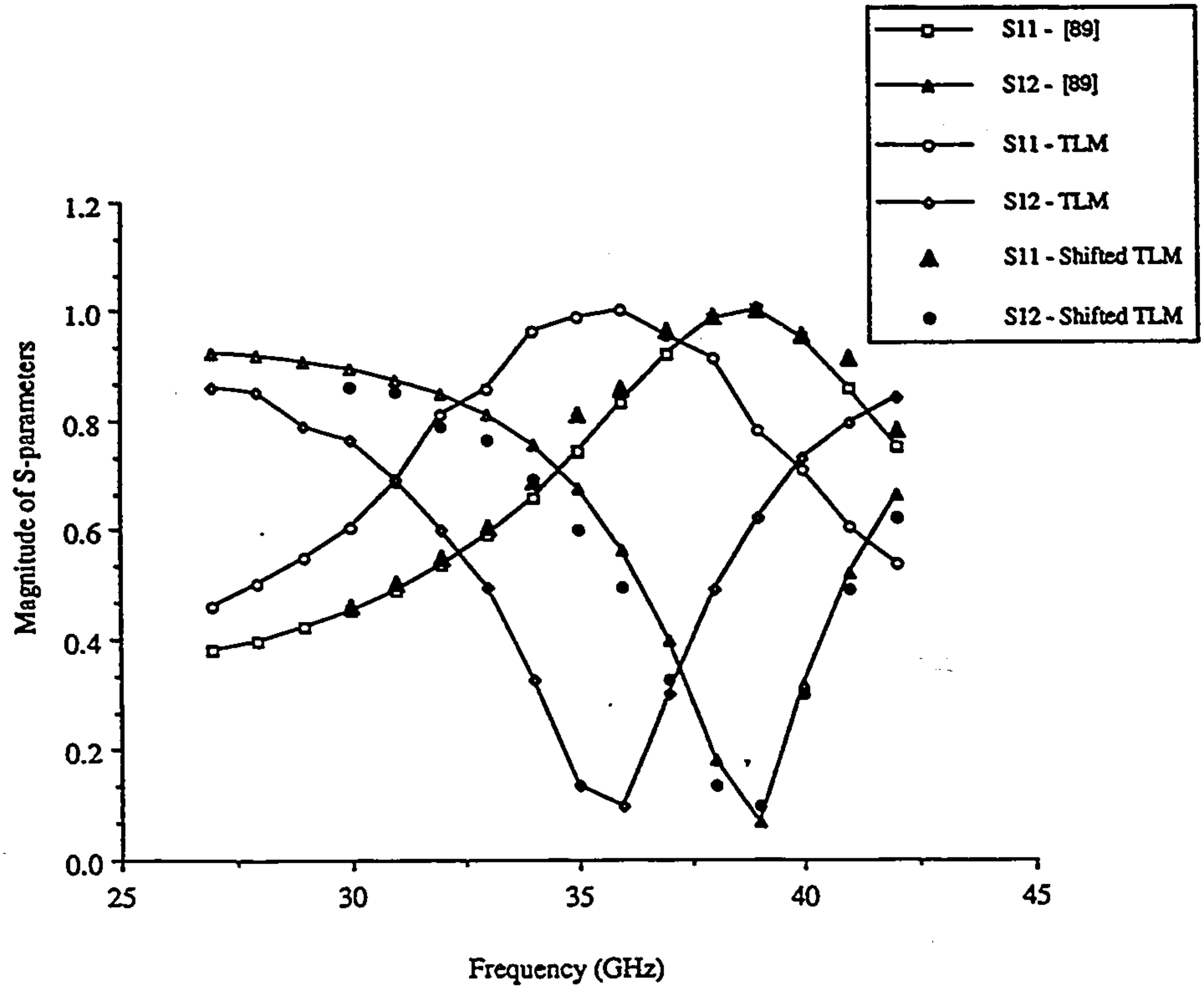
S11 - [89]
S12 - [89]
S11 - TLM
S12 - TLM
S11 - Shifted TLM
S12 - Shifted TLM
Magnitude of S-parameters
1.2
1.0
0.8
0.6
0.4
0.2
0.0
25
30
35
40
45
Frequency (GHz)

Fig. 6.9 (a)

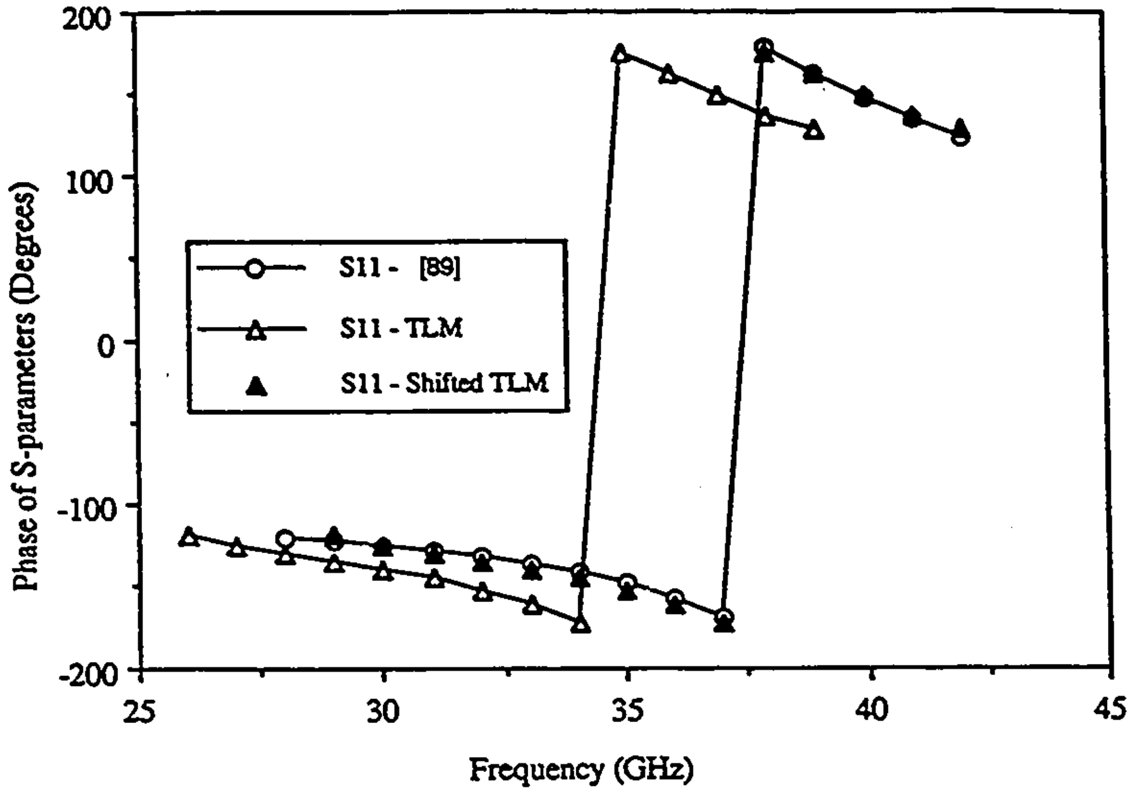

Fig. 6.9 (b)

Fig. 6.9 (a) & (b) : S-Parameters of a non-touching axial strip computed with Tapered Johns Matrix Absorbing Boundaries.

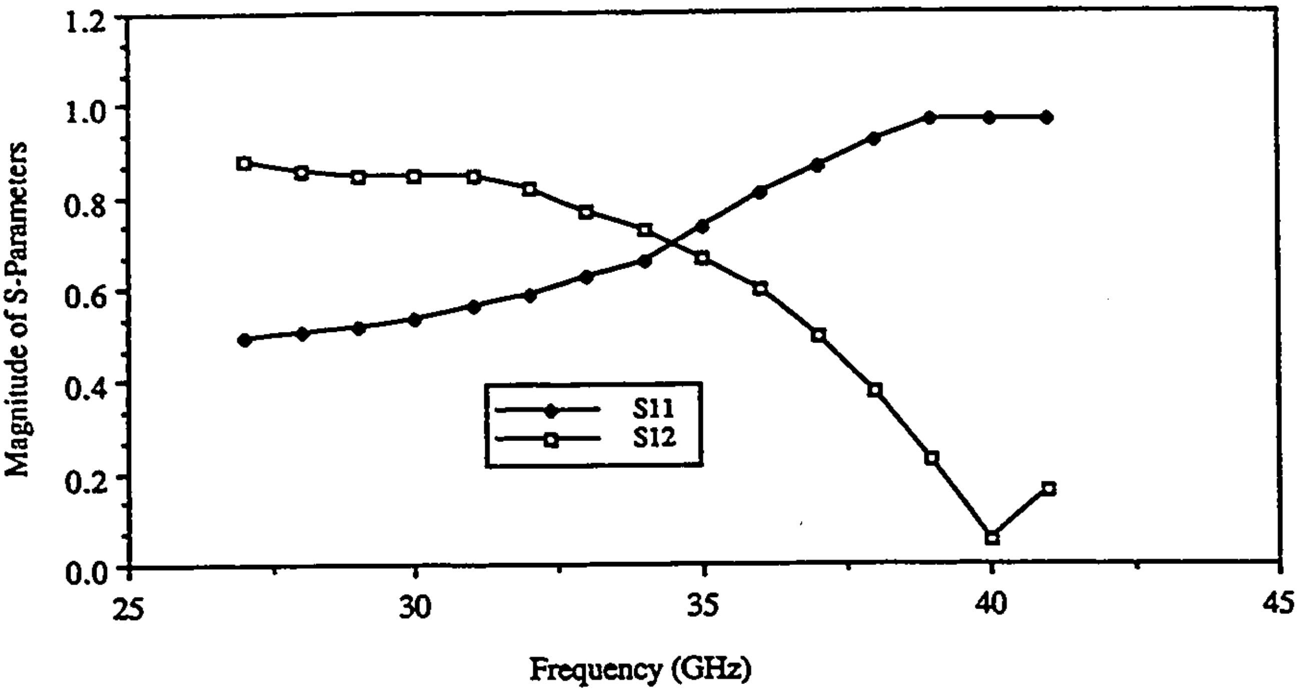

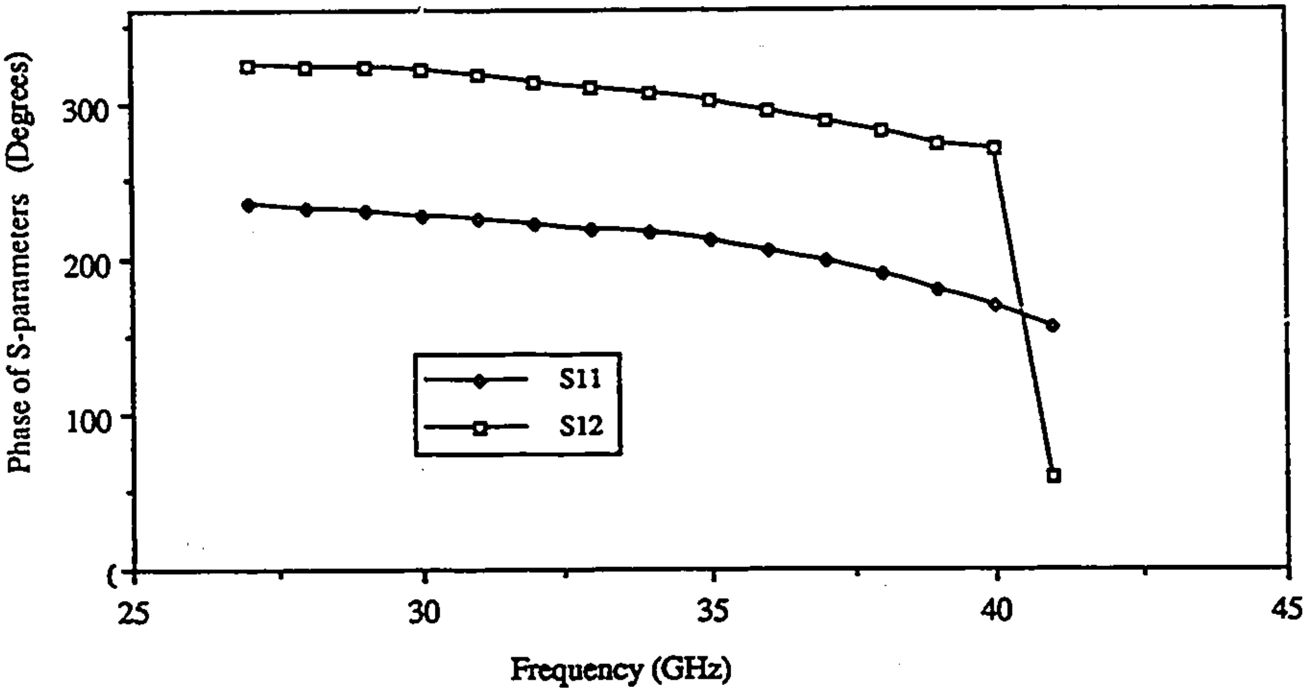

Fig. 6.10 : S-parameters of a metallic post computed with Tapered Johns Matrix Absorbing Boundaries.

as coarseness error, velocity error and truncation error, are negligible for this grid size and number of iterations. Also, with similar grid size and iterations one can accurately predict the loading of the fins in finlines. Hence it is believed that the results obtained in this thesis are accurate. A centered metallic post (square cross-section of dimension 0.36 mm and length equal to 1.64 mm) in *WR*28 waveguide was also analysed. The computed S-parameters are plotted in Fig. 6.10.

6.5 CONCLUSION

In this chapter, the Diakoptics technique has been successfully applied in combination with the 3-D TLM method with symmetrical condensed nodes. Also a very efficient numerical model for wideband non-TEM absorbing boundaries for 3-D TLM, having less than one percent reflections over an entire waveguide operating band, has been developed. This model allows one to extract the scattering parameters of arbitrarily shaped three-dimensional discontinuities in waveguides from a single TLM simulation.

It was found, that by exponentially tapering the Johns matrix (to account for slowly increasing losses as in a practical waveguide matched load) of lossy absorbing boundaries, the number of terms required was only 1100, while 3000 iterations were used to characterize the discontinuity under test. This clearly demonstrates the advantages of Diakoptics, which enables one to compute the overall response of large structures by segmenting them into substructures, and computing their Johns Matrices for the required number of iterations and mesh densities as dictated by the complexity of the fields in each of them.

Chapter VII

DISCUSSION AND CONCLUSIONS

The Finite Element and Transmission Line Matrix (TLM) methods have been enhanced for efficient and thorough analysis of microwave and millimeter-wave structures. The algorithms developed using these techniques may be applied for the analysis of shielded transmission lines and associated discontinuities. Since these programs can accomodate arbitrary geometries, they can be applied to design novel structures with the desired electrical characteristics, or to study second order effects on these characteristics.

A formulation based on a vectorial Finite Element method has been presented to study all aspects of shielded transmission lines of arbitrary cross-section. The main advantage of this formulation is that the field related parameters, such as power density, chatacteristic impedance, and conductor and dielectric losses, are expressed in terms of pre-computed matrices, thus totally avoiding numerical integration and differentiation. Hence, the time taken to compute those parameters which involve spatial integrals and derivatives is negligible when compared to that taken by the eigen-solver. The field distribution for any hybrid mode can be easily plotted. These plots can be used to explain some phenomena such as the effect of mounting grooves, etc. The results obtained with the Finite Element method for some standard structures agree well with the available data. The following are the major original results obtained.

1) The conductor and dielectric losses of bilateral finlines in rectangular waveguide enclosures have been computed.
2) The effect of substrate bending on the dispersion characteristics of bilateral finlines in rectangular waveguide enclosures has been studied.
3) The bilateral finlines in circular waveguide enclosures have been analyzed. The advantages of this structure are easy fabrication and compatibility of the dominant mode with TE_{11} mode of the circular waveguide.
4) A new modified finline structure called " Ridged Finline " has been analyzed. This structure exhibits large monomode bandwidth and reduced dispersion.
5) The conductor and dielectric losses of dielectrically loaded ridged waveguides have been computed.

The Graded Mesh TLM method has also been applied to analyse finlines in circular waveguide enclosures. The results obtained have been compared with those of the Finite Element method and they compare well.

Algorithms which apply the principles of Diakoptics to the TLM method for field partitioning in large structures have been developed. This involves computation of Johns Matrices of substructures. Unlike the traditional [Z], [Y], [ABCD], or [S] matrices, this matrix can account for all the modes over a wide frequency range. Hence this concept can be used for accurate characterization of monolithic microwave integrated circuits of high density or EMI/EMC simulations, where the field interaction between all parts of the structure must be considered. It was found that there was no accumulation of errors (even with single precision computation) while convolving the Johns Matrices, and the impulse values obtained with Diakoptics agree with those of the conventional TLM method to within six decimal places. Hence, it can be concluded that there are no instability problems associated with this approach. Diakoptics lead to considerable reduction in memory and CPU requirement for big structures since it allows numerical preprocessing of those parts of a large electromagnetic structure which remain unchanged during repeated analysis.

Time domain Diakoptics has been applied to simulate wideband non-TEM absorbing boundary conditions. Frequency dispersive boundaries are represented in the time domain by their Johns Matrices. For single- or mono-mode structures, the technique becomes very efficient, because the Johns Matrix is then reduced to a single characteristic impulse function representing the mode reflection coefficient in the time dimension. Two methods of modeling dispersive boundaries have been presented for 2-D problems - one via the Johns Matrix of a long uniform guide and the second via the Johns Matrix of a lossy termination. Since 3-D condensed nodes cannot account for losses, a " Tapered Johns Matrix " has been proposed to eliminate the parasitic reflections from the absorbing boundaries of long uniform guides due to finite space and time discretization. This Tapered Johns Matrix has been obtained by exponentially tapering the impulse response or Johns Matrix of the long uniform guide to simulate slowly increasing losses along the length of the waveguide. This technique results in absorbing boundaries with less than one percent reflections over an entire waveguide operating band. It allows extraction of scattering parameters of arbitrarily shaped discontinuities in waveguides from a single TLM simulation. The results of some typical waveguide discontinuities and components (such as inductive and capacitive irises, E-plane bandpass filter, iris-coupled waveguide filter, metallic post, etc.,) computed with this technique compare well with the available data. Furthermore, it may be noted that, the scattering parameter extraction procedure also yields the dispersion characteristics and the field components.

In conclusion, the work presented in this thesis enables efficient and accurate characterization of microwave and millimeter-wave components. The future potential applications are in the design of monolithic microwave integrated circuits, where numerical fine-tuning of a small substructure can be done. Since the modeling includes the time dimension, high-speed digital circuits can be handled as well. The techniques presented in this thesis also form the basis for an enhanced CAD technique by allowing the generation of multi-dimensional lookup tables for fast interpolation.

REFERENCES

[1] P. Silvester, " TEM wave properties of microstrip transmission lines ", Proc. Inst. Elec. Eng., vol. 115, pp. 43-48, Jan. 1968.

[2] T. G. Bryant and T. A. Weiss, " Parameters of microstrip transmission lines and coupled pairs of microstrip lines ", IEEE Trans. Microwave Theory Tech., vol. MTT-16, pp. 1021-1027, Dec. 1968.

[3] R. Crampagne, M. Ahmadpanah, and T. Guirand, " A simple method for determining the Green's function for a large class of MIC lines having multilayered dielectric structures ", IEEE Trans. Microwave Theory Tech., vol. MTT-26, pp. 82-87, Feb. 1978.

[4] C. Wei, R. Harrington, L. Mautz, and T. Sarkar, " Multiconductor lines in multilayered dielectric media ", IEEE Trans. Microwave Theory Tech., vol. MTT-32, pp. 439-449, April 1984.

[5] R. Chadha and K. C. Gupta, " Segmentation using impedance matrices for analysis of planar microwave circuits ", IEEE Trans. Microwave Theory Tech., vol. MTT-29, pp. 71-74, Jan. 1981.

[6] S. Cohn, " Characteristic impedances of broadside-coupled strip transmission lines ", IRE Trans. vol. MTT-8, pp. 633-637, Nov. 1960.

[7] H. A. Wheeler, " Transmission-line properties of parallel strips separated by a dielectric sheet ", IEEE Trans. Microwave Theory Tech., vol. MTT-13, pp. 172-185, Mar.

1965.

[8] S. K. Koul and B. Bhat, " Generalised analysis of microstrip-like transmission lines and coplanar strips with anisotropic substrates for MIC, electrooptic modulator, and SAW application ", IEEE Trans. Microwave Theory Tech., vol. MTT-31, pp. 1051-1058, Dec. 1983.

[9] Webb, K. J and R. J. Mittra, " Solution of Finline Step-Discontinuity Problem Using the Generalized Variational Technique ", IEEE Trans. Microwave Theory Tech., vol. MTT-33, no. 10, Oct. 1988, pp. 1004-1010.

[10] A. El-Sherbiny, " Exact analysis of shielded microstrip lines and bilateral finlines ", IEEE Trans. Microwave Theory Tech., vol. MTT-29, pp. 669-675, July 1981.

[11] A. Farrar and A. T. Adams, " Computation of propagation constants for the fundamental and higher order modes in microstrip ", IEEE Trans. Microwave Theory Tech., vol. MTT-24, pp. 456-460, July 1976.

[12] T. Itoh and A. S. Herbert, " A generalized spectral domain analysis for coupled suspended microstrip lines with tuning septums ", IEEE Trans. Microwave Theory Tech., vol. MTT-26, pp. 820-826, Oct. 1978.

[13] D. M. Syahkal and J. B. Davies, " Accurate solution of microstrip and coplanar structures for dispersion and for dielectric conductor losses ", IEEE Trans. Microwave Theory Tech., vol. MTT-27, pp. 694-699, July 1979.

[14] L. P. Schmidt and T. Itoh, " Spectral Domain Analysis of dominant and higher modes in finlines", IEEE Trans. Microwave Theory Tech., vol. MTT-28, pp. 981-985, Sept. 1980.

[15] R. Vahldieck and W. J. R. Hoefer," The influence of metallization thickness and mounting grooves on the characteristics of finlines ", in IEEE MTT-S Intl. Microwave Symp. Dig., pp. 182-184.

[16] R. Vahldieck, " Accurate hybrid-mode analysis of various finline configurations including multilayered dielectrics, finite metallization thickness, and substrate holding grooves ", IEEE Trans. Microwave Theory Tech., vol. MTT-32, pp. 1454-1460, Nov. 1984.

[17] T. Kitazawa and R. Mittra, " Analysis of finline with finite thickness", IEEE Trans. Microwave Theory Tech., vol. MTT-32, pp. 1484-1487, Nov. 1984.

[18] J. Bornemann and F. Arndt, " Calculating the characteristic impedance of finlines by Transverse Resonance Method ", IEEE Trans. Microwave Theory Tech., vol. MTT-21, pp. 85-92, Jan. 1986.

[19] R. Sorrentino and T. Itoh, " Transverse Resonance Analysis of Finline Discontinuities ", IEEE Trans. on Microwave Theory Tech., vol. MTT-32, no. 12, Dec. 1984, pp. 1633-1638.

[20] P. Silvester, " High-order polynomial triangular finite elements for potential problems", Int. J. Eng. Sci., vol. 7, pp. 849-861, 1969.

[21] P. Silvester, R. L. Ferrari, " Finite Elements for Electrical Engineers ", Cambridge University Press, Cambridge 1983.

[22] R. F. Harrington, " Field Computation by Moment Methods ", New York, Macmillan, 1968.

[23] C. A. Brebbia, " Boundary Element Method for Engineers ", London : Pentech Press, 1978.

[24] S. Kagami and I. Fukai, " Application of Boundary Element Method to Electromagnetic Field Problems ", IEEE Trans. Microwave Theory Tech., vol. MTT-32, pp. 455-461, April 1984.

[25] A. R. Mitchell and D. F. Griffiths, " The Finite Difference Method in Partial Differential Equations ", New York: Wiley, 1980.

[26] Edgard Schweig and William B. Bridges, " Computer Analysis of Dielectric Waveguides: A Finite-Difference Method ", IEEE Trans. Microwave Theory Tech., vol. MTT-32, May 1984.

[27] P. B. Johns and R. L. Beurle, " Numerical solution of 2-dimensional scattering problems using a transmission-line matrix", Proc. IEE., vol. 118, no. 9, pp. 1203-1208, Sept. 1971.

[28] W. J. R. Hoefer, " The Transmission-Line Matrix Method-Theory and applications ", IEEE Trans. Microwave Theory Tech., vol. MTT-33, pp. 882-893, Oct. 1985.

[29] W. J. R. Hoefer, " The Transmission Line Matrix (TLM) Method ", in T. Itoh : Numerical Techniques for Microwave and Millimeter Wave Passive Structures, New York, 1989, John Wiley & Sons.

[30] P. B. Johns, " Simulation of electromagnetic wave interactions by Transmission - Line Modelling (TLM) ", pp. 597-610, Wave Motion (10) 1988, North-Holland.

[31] K. S. Yee, " Numerical Solution of Initial Boundary Value Problems Involving Maxwell's Equations in Isotropic Media ", IEEE Trans. Antennas Propagation, vol. AP-14, no.3, pp. 302-307, May 1966.

[32] Allen Taflove " Review of the Formulation and Applications of the Finite-Difference Time-Domain Method for Numerical Modeling of Electromagnetic Wave Interactions with Arbitrary Structures ", Wave Motion (10) 1988, pp. 547-582, North-Holland.

[33] P. So, W. J. R. Hoefer and P. Saguet, " CAD of E-plane Circuits with Field-theory Based Lookup Tables and Discontinuity Models ", MTT-S Symposium, May 1988, pp. 335-338.

[34] H. Meliani, D. De Cogan and P. B. Johns, " The use of orthogonal Curvilinear meshes in TLM models ", International Journal of Numerical Modeling : Electronic Networks, Devices and Fields, vol. 1, pp. 221-238, 1988.

[35] M. Fusco, " FD-TD algorithms in Curvilinear coordinates ", IEEE Trans. on Antennas and Propagation, vol. AP-38, Jan. 1990.

[36] J. P. Webb, G. L. Maile, and R. L. Ferrari, " Finite element solution of three-dimensional electromagnetic problems ", IEE Proc., vol. 130, pt. H, no. 2, March 1983.

[37] R. B. Corr and A. Jennings, " A Simultaneous Iteration Algorithm for Symmetric Eigenvalue problems ", Intl. Journal for Numerical methods in Engg., vol. 10, pp. 647-663, 1976.

[38] K. J. Bathe and S. Ramaswamy, " An accelerated Subspace Iteration Method ", J. Comp. Meth. Appl. Mech. Eng., 23, pp. 313-331, 1980.

[39] B. Nour-Omid, B. N. Parlett, and R. L. Taylor, " Lanczos versus Subspace Iteration for solution of eigenvalue problems ", Intl. Journal for Numerical methods in Engg., vol. 19, pp. 859-871, 1983.

[40] M. Papadrakakis and M. Yakoumidakis, " On the preconditioned Conjugate Gradient Method for solving $(A - \lambda B)X = 0$ ", Intl. Journal for Numerical methods in Engg., vol. 24, pp. 1355-1366, 1987.

[41] S. Ahmed and P. Daly, " finite-element methods for inhomogeneous waveguides ", Proc. Inst. Elec. Eng., vol. 116, no. 10, pp. 1661-1664, 1969.

[42] P. Daly, " Finite Element Coupling Matrices", Electron. Lett., vol. 5, pp. 613-615, Nov. 27, 1969.

[43] Z. J. Csendes and P. Silvester, " Numerical solution of dielectric loaded waveguides : I- Finite element analysis ", IEEE Trans. Microwave Theory Tech., vol. MTT-18, pp. 1124-1131, Dec. 1970.

[44] A. Konrad, " High-order triangular finite elements for electromagnetic waves in anisotropic media ", IEEE Trans. Microwave Theory Tech., vol. MTT-25, pp. 353-360, May 1977.

[45 C.Yeh, K. Ha, S. B. Dong, and W. P. Brown, " Single-Mode Optical Waveguides ", Appl. Opt., vol. 18, pp. 1490-1504, May 1979.

[46] M. Hano, " Finite Element Analysis of dielectric loaded waveguides", IEEE Trans. Microwave Theory Tech., vol. MTT-32, pp. 1275-1279, Oct. 1984.

[47] M. Koshiba, K. Hayata, and M.Suzuki, " Improved finite element formulation in terms of the magnetic field vector for dielectric waveguides ", IEEE Trans. Microwave Theory Tech., vol. MTT-33, pp. 227-233, Mar 1985.

[48] T. Angkaew et al., " Finite Element Analysis of Waveguide Modes: A novel approach that eliminates spurious modes", IEEE Trans. Microwave Theory Tech., vol. MTT-35, pp. 117-123, Feb 1987.

[49] P. Daly, " Upper and lower bounds to the characteristic impedance of transmission lines using the finite element method ", COMPEL, vol. 3, no. 2, pp. 65-78, 1984.

[50] Zorica Pantic and Raj Mittra, " Quasi-TEM analysis of microwave transmission lines by the finite element method ", IEEE Trans. on Microwave Theory and Tech., vol. MTT-34, no. 11, November 1986.

[51] S. Akhtarzad and P. B. Johns, " Solution of 6-component electromagnetic fields in three space dimensions and time by the TLM method ", Electron. Lett., vol. 10, pp. 535-537, Dec. 12, 1974.

[52] P. Saguet and E. Pic, " Utilisation d'un nouveau type de noeud dans la me'thode TLM en 3 dimensions, " Electron. Lett., vol. 18, pp. 478-480, May 1982.

[53] P. B. Johns, " A symmetrical condensed node for the TLM method," IEEE Trans. Microwave Theory Tech., vol. MTT-35, pp. 370-377, April 1987.

[54] G. Kron, Diakoptics, MacDonald, London, 1963.

[55] T. Okoshi, Y. Uehara, T. Takeuchi, " The Segmentation Method - An approach to the analysis of Microwave Planar Circuits ", IEEE Trans. Microwave Theory Tech., vol. MTT - 24, pp. 662-668, 1976.

[56] R. Chadha, K. C. Gupta, " Segmentation Method using Impedance Matrices for Analysis of Planar microwave Circuits ", IEEE Trans. Microwave Theory Tech., vol. MTT - 29, pp. 71-74, 1981.

[57] Roberto Sorrentino, " Planar Circuits, Waveguide Models, and Segmentation Method ", IEEE Trans. Microwave Theory Tech., vol. MTT-33, pp. 1057-1066, Oct. 1985.

[58] P. B. Johns, and K. Akhtarzad, " The use of time domain diakoptics in time discrete models of fields ", Int. J. Num. Methods Eng., vol. 17, pp. 1-14, 1981.

[59] P. B. Johns, and K. Akhtarzad, " Time domain approximations in the solution of fields by time domain diakoptics ", Int. J. Num. Methods Eng., vol. 18, pp. 1361-1373, 1982.

[60] W. J. R. Hoefer, " The discrete time domain Green's function or Johns Matrix - A new powerful concept in Transmission Line Modelling (TLM) ", International Journal of Numerical Modeling : Electronic Networks, Devices and Fields, to be appeared in 1990.

[61] D. T. Paris and F. K. Hurd, " Basic Electromagnetic Theory ", McGraw-Hill, Inc., pp. 279, 1969.

[62] G. Kron, " Equivalent circuits to represent the electromagnetic field equations," Phys. Rev., 1943, 64, pp. 126-128.

[63] G. Kron, " Equivalent circuit of the field equations of Maxwell I," Proc. IRE, vol. 32, pp. 289-299, May 1944.

[64] J. R. Whinnery and S. Ramo, " A new approach to the solution of high frequency field problems, ", Proc. IRE, vol. 32, pp. 284-288, May 1944.

[65] P. Saguet and E. Pic, " Le maillage rectangulaire et le changement de maille dans la methode TLM en deux dimensions ", Electronics Letters, vol. 17, no. 7, pp. 277-278, April 2, 1981.

[66] D.A. Al-Mukhtar and J. E. Sitch, " Transmission Line Matrix method with irregular graded space ", IEE Proc., vol. 128, no. 6, Dec. 1981.

[67] R. Allen, A. Mallik and P. B. Johns, " Numerical results for the symmetrical condensed node ", IEEE Trans. Microwave Theory and Techniques, vol. MTT-35, no. 4, April 1987.

[68] K. Akhtarzad and P. B. Johns, " Three-dimensional transmission-line matrix analysis of microstrip resonators ", IEEE Trans. Microwave Theory and Techniques, vol. MTT-23, no. 12, pp. 990-997, 1975.

[69] G. Mariki and C. Yeh, " Dynamic three-dimensional TLM analysis of microstrip lines on anisotropic substrates, IEEE Trans. Microwave Theory and Techniques, vol. MTT-33, no. 9, pp. 789-799.

[70] Y. -C. Shih and W. J. R. Hoefer, " Dominant and second-order mode cutoff frequencies in finlines calculated with a two-dimensional TLM program," IEEE Trans. Microwave Theory and Techniques, vol. MTT-28, pp. 1443-1448, Dec. 1980.

[71] J. E. Sitch and P. B. Johns, " Transmission-line matrix analysis of continuous waveguiding structures using stepped-impedance cavities", Microwaves, Opt. & Acoustics, 1977, 1, (5), pp. 181-184.

[72] P. Saguet and W. J. R. Hoefer, " The modelling of multiaxial discontinuities in quasi-planar structures with the modified TLM method ", International Journal of Numerical Modelling : Electronic Networks, Devices and Fields, vol. 1, 7-17 (1988).

[73] A. T. Villencuve, " Analysis of Slotted Dielectrically Loaded Ridged Waveguide ", IEEE Trans. Microwave Theory Tech., vol. MTT-32, pp. 1302-1310, Oct. 1984.

[74] D. Mirshekar-Syahkal and J. B. Davies, " An accurate unified solution to various finline structures , of phase constant, characteristic impedance, and attenuation, IEEE Trans. Microwave Theory Tech., vol. MTT-30, pp. 1854-1861, Nov. 1982.

[75] Chris Olley and T. Rozzi, " Currents and conduction losses in unilateral finline", IEEE Trans. Microwave Theory and Technique, vol. MTT-36, no.1, January 1988.

[76] R. N. Bates and M.D. Coleman, " Finline For Microwave Integrated Circuits (MICs) at Ka-Band (27-40 GHz) ", IEE Colloquium on Microwave Integrated Circuits Design, No. 1978/26, April 1978.

[77] Robertson. S. D., " The Ultra-Bandwidth Finline Coupler ", Proc. IRE., vol. 43, no. 6, June 1955, pp. 739-741

[78] AEG, Uln, Germany, Private Communications

[79] P. B. Johns, " Ideal transformers and gauge transformations in lumped network models of electromagnetic fields," IEE Proc., vol. 129, pt. A, no. 6, August 1982.

[80] C. R. Brewitt-Taylor and P. B. Johns, " On the construction and numerical solution of transmission line and lumped network models of Maxwell's equations ", International Journal for Numerical Methods in Engineering, vol. 15, pp. 13-30, 1980.

[81] Eswarappa, K. C. Gupta and R. Raghuram, " Mixed boundary semicircular and 120^0 - sectoral microstrip antennas ", AP-S Symposium, June 26-30, 1989, pp. 1688-1691.

[82] G. Mur, " Absorbing boundary conditions for finite-difference approximation of the time-domain electromagnetic field equations," IEEE Trans. Electromagn. Compat., vol. EMC-23, pp. 1073-1077, 1981.

[83] J. Fang and K. K. Mei, " A super-Absorbing Boundary Algorithm for Solving Electromagnetic Problems by Time Domain Finite Difference Method ", AP-S Symposium, June 1988, pp. 472-475.

[84] Jasmin E. Roy and Dennis H. Choi, " The Application of a Simple Absorbing Boundary Algorithm to Cylindrical Waveguide ", AP-S Symposium, San Jose, June 1989, pp. 58-61.

[85] Jasmin E. Roy and Dennis H. Choi, " A Simple Absorbing Boundary Algorithm for the TDFD Method with Arbitrary Incidence Angle", AP-S Symposium, San Jose, June 1989, pp. 54-57.

[86] N. Marcuvitz, " Waveguide Handbook ", Dover Publications Inc., New York, 1965.

[87] Y. Konishi and K. Uenakada, " The design of a bandpass filter with inductive strip planar circuit mounted in waveguide," IEEE Trans. Microwave Theory Tech., vol. MTT-22, pp. 869-873, Oct. 1974.

[88] G. Matthaei, L. Young, and E. M. T. Jones, Microwave Filters, Impedance-Matching Networks and Coupling Structures. New York : McGraw-Hill, 1964.

[89] K. Chang and P. J. Khan, " Equivalent Circuit of a Narrow Axial Strip in Waveguide ", IEEE Trans. on Microwave Theory Tech., pp. 611-615, Sept. 1976.

[90] Eswarappa, George I. Costache and Wolfgang J. R. Hoefer," Finlines in Rectangular and Circular Waveguide Housings Including Substrate Mounting and Bending Effects - Finite Element Analysis ", IEEE Trans. on Micowave Theory Tech, vol. MTT-37, pp. 299 - 306, Feb. 1989.

[91] Eswarappa, George I. Costache and Wolfgang J. R. Hoefer, " Numerical modeling of Generalized Millimeter-Wave Transmission Media with Finite Element and Transmission Line Matrix Methods " , International Journal of Infrared and Millimeter Waves, vol. 10, no. 1, Jan. 1989.

[92] Eswarappa, George I. Costache and Wolfgang J. R. Hoefer, " Application of Finite Element Method for Analysis of Quasi-Planar Transmission Lines ", MIOP , 2 - 4 March 1988, Wiesbaden, West Germany.

[93] Eswarappa, George I. Costache and Wolfgang J. R. Hoefer ," TLM Modeling of Dispersive Wideband Absorbing Boundaries with Time Domain Diakoptics for S-Parameter Extraction ", IEEE Trans. Micowave Theory Techniques, vol. MTT-38, no. 4, pp. 379-386, April 1990.

[94] Eswarappa, Poman So and Wolfgang J. R. Hoefer, " New Procedures for 2-D and 3-D Microwave Circuit Analysis with the TLM Method ", accepted for presentation at 1990 IEEE MTT-S International Microwave Symposium.

[95] Eswarappa and Wolfgang J. R. Hoefer, " Application of Time Domain Diakoptics to 3-D TLM Method with Symmetrical Condensed Node ", accepted for presentation at 1990 IEEE AP-S Symposium.

[96] Poman So, Eswarappa, and Wolfgang J. R. Hoefer, " A Two - Dimensional TLM Microwave Simulator Using New Concepts and Procedures ", IEEE Trans. Micowave Theory Tech, vol. MTT-37, no. 12, pp. 1877-1884, Dec. 1989.